THE ELECTROMAGNETIC CHARACTERISTICS OF A LOOP ANTENNA POSITIONED COAXIALLY ON AN INFINITELY LONG DIELECTRIC CIRCULAR CYLINDER

Walter Douglas Rawle

A thesis presented to the Faculty of Graduate Studies

University of Manitoba

In partial fulfillment of the requirements for the degree

Doctor of Philosophy

ISBN 0-315-76758-8

THE ELECTROMAGNETIC CHARACTERISTICS OF A LOOP ANTENNNA POSITIONED COAXIALLY ON AN INFINITELY LONG DIELECTRIC CIRCULAR CYLINDER

BY

WALTER DOUGLAS RAWLE

A thesis submitted to the Faculty of Graduate Studies of the University of Manitoba in partial fulfillment of the requirements of the degree of

DOCTOR OF PHILOSOPHY

Table of Contents

List of Figures

List of Tables

Acknowledgements

The author wishes to express his deepest gratitude to Dr. L. Shafai for his supervision and tutelage during the course of the program. The author also wishes to thank his many friends and colleagues at the Department of Electrical and Computer Engineering, University of Manitoba, for many helpful discussions.

Financial support was provided by the Natural Sciences and Engineering Research Council of Canada.

Abstract

An analysis of the electromagnetic characteristics of a loop antenna which is positioned coaxially on the surface of an infinitely long dielectric circular cylinder has many applications in the areas of antenna design, fibre-optics, millimeter wave devices, and bioelectromagnetics. Such an analysis, focussing primarily upon input impedance, surface wave behaviour, and radiation characteristics, is the subject of this thesis.

The antenna is modelled with the aid of the thin wire approximation as an $f(\phi)\delta(z)$ electric current distribution situated on the free space - dielectric interface. A Debye potentials based formulation is employed to obtain formal exact expressions for all electromagnetic field components which result from said current distribution. The formulation for the fields is extended to obtain expressions for input impedance and current distribution, surface wave characteristics, and radiation characteristics. The input impedance is evaluated using numerical quadrature and residue theory. The surface wave behaviour is studied with the aid of residue theory. The far field, or radiation characteristics, are studied with the aid of the steepest descent technique.

Numerical results are provided for the three main characteristics of interest and a number of interesting features are shown from these results. In particular, the input impedance of the antenna is shown to consist of two terms, a radiation term and a

surface wave term. Extensive investigation into these terms illustrate the relative impact of each term on the overall behaviour of the loop's input impedance. The field amplitudes of a selected number of surface wave modes are studied. Finally, the radiation characteristics of the antenna are extensively investigated and the extent to which the cylinder affects the radiation from the antenna is thoroughly presented.

Chapter 1

Introduction

Statement of Problem

The installation of a loop antenna coaxially upon a dielectric circular cylinder may be motivated by many applications. For example, the cylinder may provide mechanical support for the loop antenna. Alternatively, the loop antenna may be employed as a surface wave launcher on the cylinder, which is being used as a millimeter-wave waveguide. Further, the cylinder and loop combination may be employed specifically as a radiating element. All of these applications demand a complete and accurate characterization of the current distribution on the loop antenna and the electromagnetic fields resulting from this current distribution. Such a demand establishes the motivation for the research effort represented by this thesis.

Contributions to Research

This thesis presents an analysis of the electromagnetic characteristics of a loop antenna which is positioned coaxially on an infinitely long dielectric circular cylinder. Specifically, the following characteristics are investigated; the input impedance of the antenna and the associated current distribution, the radiation characteristics of the antenna, the propagation velocities and electromagnetic field structure of the hybrid mode surface waves which are excited on the cylinder by the antenna, and, finally, the contributions made to the resistive component of the input impedance by radiation and surface wave excitation.

The antenna is modelled as an $f(\phi)\delta(z)$ electric current distribution situated on the free space - dielectric interface and is under the influence of a rectangular voltage pulse function. A Debye potentials based formulation is employed to obtain exact expressions for all electromagnetic field components resulting from the given current distribution. The thin wire approximation is invoked to obtain the feedpoint current resulting from a 1.0 volt rectangular pulse excitation. From this, the input impedance and current distribution are determined. The radiation characteristics of the loop antenna are obtained through a steepest descent approximation of the tangential electric field expressions for the free space region. The surface wave behaviour is investigated through an evaluation of residue terms which arise in the calculation of the field expressions. Numerical results are presented which illustrate the characteristics of the various parameters of interest. For verification purposes, special cases are compared with results found elsewhere in the literature.

A general analysis of the loop antenna positioned coaxially on a dielectric circular cylinder, to the author's knowledge, has not appeared previously in the literature. Therefore, the research effort presented here is considered to be a fundamental contribution to the discipline of electrical engineering.

Summary of Presentation

The contents of this thesis have been organized into six main chapters, Chapter 2 *Literature Review*, Chapter 3 *Analytical Formulation*, Chapter 4 *Input Impedance and Current Distribution*, Chapter 5 *Surface Wave Characteristics*, Chapter 6 *Radiation Characteristics*, and, Chapter 7 *Conclusions and Recommendations for Future Work*. As implied by its title, Chapter 2 provides a representative overview of the literature pertaining to loop antennas in various environments. The first section deals with the investigations of loop antennas located in free space. Included in this section is an indication of the work performed in the area of transient analysis and the Singularity Expansion Method as applied to loop antennas. The second section reports on the experimental and theoretical work involving loop antennas located in lossy infinite media. The third section details the analysis of loop antennas in the presence of various half spaces. The fourth section is of particular interest in that it reviews the work concerning loop antennas mounted on various cylindrical cores. The fifth section provides a representative overview of efforts directed towards dielectric rod antennas, and the sixth section deals with the analysis of the waveguiding properties of dielectric circular cylinders.

Chapter 3 presents the analytical formulation for this research. First, the devel-

opment of the formal solution for the electromagnetic field components is reviewed. The general evaluation of the electromagnetic field expressions is then discussed. In turn, and with supporting appendices, the evaluations of input impedance, current distribution, radiation characteristics and surface wave characteristics are described.

Chapter 4 provides numerical results for the input impedance and current distribution on the antenna for a variety of situations. Of special interest is the comparison of input impedance results obtained from the present formulation with those obtained elsewhere in the literature, for the case where the dielectric constant of the cylinder is unity.

Chapter 5 provides numerical results for the propagation velocities and electromagnetic field structure of various hybrid mode surface waves which may be excited by loop antennas in the given geometry.

Chapter 6 provides extensive numerical results for the radiation characteristics of the antenna and illustrates the influence of the cylinder's dielectric constant on the shape of the radiation pattern.

Chapter 7 summarizes a number of conclusions which may be taken from this research effort and discusses future directions along which research in this area may follow. Publications resulting from this research work are itemized here.

Chapter 2

Literature Review

Introduction

In analyzing the loop antenna mounted on an infinitely long dielectric circular cylinder, a number of perspectives may be taken. The loop may be considered as the principle radiator of the system, with the rod providing only mechanical support. The loop may be used as a surface wave launcher in applications related to dielectric rod antennas. Or the loop may be employed as an array element in a linear array driven by a dielectric rod waveguide.

To complement the many aspects of the stated problem, a fairly wide review of the literature has been performed. This review highlights the many investigations of loop antennas situated in or next to various media, reports on various efforts in the analysis and design of dielectric rod antennas, and finally, examines the study of surface wave excitation on a dielectric rod. In detail, this chapter begins with a review of the more significant reports of investigations on loop antennas located in

free space. Next, an extension of the free space case is made to investigations of loop antennas located in dissipative media. This is followed by the analysis of loop antennas in so-called half space problems. Of significant importance is the review of available literature on loop antennas mounted coaxially over various infinitely long structures. A synopsis of the work conducted on dielectric rod antennas is provided. And finally, efforts to characterize the guiding properties of various cylinder geometries are explored.

Loop Antennas in Free Space

It appears that Storer [1] was the first investigator to provide extensive numerical data for the input impedance of a loop antenna. His analysis involved the Fourier expansion of not only the current distribution on the loop itself, but also the free space Green's function which serves as the kernel in the integral equation which describes the current distribution. The input impedance for the loop was then described in terms of an infinite series. Storer reported in his paper that Hallen also arrived at this infinite series for the impedance of the loop. A numerical difficulty, however, prevented Hallen from providing useful results. The numerical difficulty proved to be a term in the series which becomes very large. Hallen thought that this term represented a singularity. Storer contended that the term was finite. From this discussion, Storer decided to circumvent the problem by explicitly evaluating the first four terms of the series and then represent the remaining summation as an integral. An extensive collection of numerical data was developed from this formulation for a variety of loop geometries and numerous graphs for the input

impedance presented. A number of experimental observations were made to verify the formulation.

T.T. Wu took exception to the techniques employed by Storer and published a detailed account of the theory of the loop antenna [2]. From the exact integral equations for the current distribution on the wire loop, the simplified one-dimensional integral equation was obtained. A Fourier transform for the current distribution was then employed. The integrals were then simplified with the aid of Bessel function relations. Finally, an equation for the input impedance of the loop was presented which involves taking the limit as the azimuthal co-ordinate approaches the origin. Wu stated that his formulation would provide better results than those obtained by Storer but, unfortunately, he did not provide any numerical results to substantiate his claim.

Rao [3] investigated the radiation characteristics of a loop antenna which was loaded with a terminating resistor located at a position diametrically opposite to the feed point. The value of the terminating resistor was set equal to the feedpoint impedance. The current on the loop was presumed to have travelling wave nature where the propagation constant of the current wave was taken to be a free space value. The far field electric field components were then determined from a standard magnetic vector potential formulation. Experimental results were compared with predicted results and, on a relative basis, there was good agreement.

Martins [4] presented a short paper on the derivation of closed form expressions for the vector potential functions and, hence, the field components, resulting from sinusoidal, co-sinusoidal, and travelling wave current distributions on loop antennas

of arbitrary size. Large distance approximations were made in the free space Green's function. These approximations allow the integrals for the vector components to be cast in a form which may be represented by a Bessel function of the first kind. The resulting closed form expressions are now very popular and may be found in many textbooks.

In a subsequent paper, Martins [5] evaluated the integral expressions for the magnetic vector potential without employing any approximations. The evaluation of the integrals in this case involved an expansion of the free space Green's function into an infinite series of spherical Bessel functions. The resulting expressions for the vector potential then consisted of this infinite series which must be evaluated term by term.

Lindsay [6] followed Martin's work with another analysis of the far field radiation characteristics of a loop antenna located in free space. Again, the analysis followed the standard magnetic vector potential formulation. An interesting aspect of this paper was the method used to determine the current distribution on the loop. Lindsay considered the loop to be a section of lossy open wire transmission line which had been deformed from a straight line to a loop. Therefore, $\mathrm{I}(s) = \mathrm{I}_L \cosh \gamma R\phi$ where γ is the propagation constant of the wave along the wire line and $R\phi$ is the circumferential distance. There was no discussion concerning the actual value of γ. However, Lindsay did present a theoretical-experimental comparison, which indicated that the shape of the radiation pattern predicted was in good agreement with the shape of the experimentally obtained pattern. It should be noted, however, that only three cuts were taken in the measurement of the patterns, indicating that

the experimental data may be insufficient to yield definitive conclusions.

Imrie [7] presented an interesting note on the evaluation of the vector potential integrals for loop antennas which have sinusoidal current distributions. Instead of using a Fourier series expansion for the integrand, which in turn will yield Bessel function representations for the field patterns, he used a power series expansion for the integrand. Equations for the radiation resistance of a loop antenna, developed from this particular approach, are presented in the paper.

Redlich [8] presented a short paper on using numerical integration techniques to evaluate vector potential expressions for the prediction of the radiation resistance of a loop antenna of arbitrary radius. The expression for the radiation resistance involved the integration of Bessel functions over a finite interval. Experimental and numerical results were compared and good agreement was observed.

Shockley [9] reported an interesting analysis of the electric and magnetic fields resulting from a loop antenna. In this analysis, the antenna was posed as a boundary value problem in spherical co-ordinates with the radial components of the magnetic vector potential described as follows:

$$\mathcal{F}_{r_I} = \sum_{n=0}^{\infty} a_n P_n(\cos\theta) \mathrm{H}_n^{(2)}(kr) \ldots\ldots r > a$$

$$\mathcal{F}_{r_{II}} = \sum_{n=0}^{\infty} b_n P_n(\cos\theta) \mathrm{J}_n(kr) \ldots\ldots r < a$$

The radial component of the magnetic vector potential, $\mathrm{A}_r = 0$ for both regions. At $r = a$, the current distribution $\mathcal{K} = \hat{a}_\phi \frac{\mathrm{I}}{a} \delta(\theta - \frac{\pi}{2})$. From these expressions, the electric and magnetic fields were determined in the usual manner.

K.K. Mei [10] presented a discussion on the numerical evaluation of Hallen's

integral equation for wire antennas by what is now generally referred to as the moment method. Hallen's integral equation was cast into a form more suitable for the evaluation of circular and helical wire geometries. Numerical results were provided for loop antennas to illustrate the usefulness and accuracy of the numerical techniques described.

Baghdasarian and Angelakos [11] reported on the numerical evaluation of an integral equation for the current distribution on a circular loop antenna. The technique essentially replaced the integral operators with equivalent Riemann sum operators which resulted in a set of linear equations. The equations could then be solved to yield the current distribution on the loop. Again, the author presented numerical and experimental results for loop antennas with C/λ ratios of 1.5 and 3.0.

Shockley, Glekas, and Mott [12] presented another short paper describing the evaluation of current distributions on loop antennas which were driven at four equally spaced points on their periphery. The motivation for this investigation came from a need to establish a method which would improve the uniformity of the current distribution on the loop. In this investigation, the current distribution was measured by probing the magnetic field in the immediate vicinity of the loop.

Rao [13] presented a paper on the radiation characteristics of large loop antennas. The loops considered had an electrical circumference of 1.5, 2.0, and 2.5 wavelengths. Numerical results, based upon Storer's analysis, were provided along with some experimental observations. The purpose of this investigation was to confirm that Storer's analysis was valid for large loop antennas.

Conventionally, engineers presume that the standing wave current distribution on a loop may be decomposed into two travelling wave components where the propagation constant of the travelling waves is equal to the free space propagation constant. Realizing that this may not always be the case, Prasad and Das [14] investigated the far field radiation characteristics of a loop antenna with a travelling wave current distribution. The propagation constant of this travelling wave was, in general, not equal to the free space value. The equations for the radiation characteristics were developed from the standard magnetic vector potential formulation. Numerical results were provided to illustrate the E_θ, E_ϕ, and antenna directivity dependance upon the current distribution's propagation constant.

Iizuka [15] considered the analysis of a loop antenna which was multiply- loaded with lumped circuit elements. He extended Storer's analysis, through superposition, to the case where this antenna was modelled as a loop antenna which was excited by multiple generators. Multiple resistive loads were then included as an extension to this model using the compensation theorem. The currents associated with each load were determined by the solution of a system of linear equations. Various case studies were presented where both theoretical and experimental values for the loop's input impedance were determined.

In a subsequent paper, Iizuka, La Russa, and Dunne [16] presented the results of an experimental analysis for the far field radiation characteristics of loop antennas which were loaded at one point with an arbitrary lumped impedance. The results were presented, in part, to verify the numerical results presented in a previous paper. Additional experimental observations were made of the input impedance of these

antennas. The results of the experiments indicated that changes in the reactive part of the lumped impedance had a more significant impact upon the current distribution than would changes in the resistive part of the lumped impedance.

King [17] considered an interesting variation on the standard series fed loop antenna. He proposed a shunt feed for the loop. His analysis of this feed arrangement was based upon circuit concepts which transformed the shunt section into a folded dipole, the ends of which were then connected to the rest of the antenna. From this model, the current distribution was determined. King provided equations for the current distribution, feedpoint impedance, and the far field radiation characteristics for this antenna.

Lin [18] investigated the current distribution on a loop antenna which exhibits an impedance boundary condition on the wire surface. He developed a second order partial differential equation for the resulting current distribution on the loop, based upon the internal impedance concepts employed previously in linear antenna analysis. Current distributions predicted by Lin's technique were compared to current distributions obtained from a standard integral equation formulation which employed this boundary condition. Good agreement between the two techniques was observed.

Gonzalez and Huerta [19] presented simplified closed form expressions for the near fields produced by a loop antenna. He considered the case of constant current distribution and the case of the two-term current distribution. The expressions were cast in terms of an integral which had been previously tabulated. Numerical results for the evaluation of this integral were presented. However, results for the

field distribution were not provided.

As a variation upon King's report on the shunt fed loop antennas, Tsukiji [20] investigated the input impedance and radiation characteristics of a center line fed circular loop antenna. His analysis employed a numerical solution to Hallen's integral equation where the current distribution was expanded with Lagrangian interpolation polynomials. Numerical and experimental results were presented for the input impedance, far field radiation characteristics, and the power gain of the antenna.

Richtscheid [21] presented a short paper on the evaluation of the radiation resistance of a loop antenna which carries a sinusoidal current distribution. The expressions used for the evaluation were derived from the Poynting vector approach. Electric field components were obtained from the magnetic vector potential. The field quantities were then integrated over the Poincare sphere to obtain the real power leaving the antenna. The radiation resistance was then computed from the power leaving the antenna and the enforced current distribution. Numerical results were provided for the radiation resistance of loop antennas with electrical circumferences ranging from 1 to 10 wavelengths.

Chang [22] reported on an evaluation of field components resulting from a loop antenna. He adopted the approach employed by Storer to obtain the original integral equation for the current distribution. He did not expand the Green's function in a Fourier series as had been done previously. He simply evaluated the integral equation numerically. He observed that acceptable results could be obtained by using the first three terms of the current distribution.

Adachi [23] considered the evaluation of the feedpoint impedance of a loop antenna by the induced EMF method. A closed form expression was given for the impedance of an n wavelength loop and it was verified by numerical example.

Adekola [24] presented a tutorial review paper on the analysis of the electromagnetic fields and power radiated from circular loop antennas which carry both standing wave and travelling wave current distributions. The analysis follows the standard magnetic vector potential formulation. An interesting feature of this paper is that series representations for the Bessel functions, which are otherwise stated as is in other papers, are employed directly in the final solutions for the field expressions. From these series solutions, various simplifying approximations are directly reported. The paper concludes with a discussion on the various practical applications of the loop antenna.

Awadella and Sharshar [25] present simplified closed form expressions for the input impedance of a loop antenna. These expressions appear to be valid for thin wire loops of radius up to 0.5 wavelengths. The equation for the resistive part of the input impedance is actually obtained by fitting an empirical equation to data obtained from a moment method solution. The equation obtained for the reactive portion of the input impedance is obtained from a transmission line model for the loop. Awadella presented numerical results which indicated that the simplified equations would yield reasonably accurate results for the resistive portion of the input impedance for loops of radius up to 0.5 wavelength, and for the reactive portion of the input impedance for loops of radius up to 0.8 wavelengths.

The time dependant characteristics of loop antennas have also been of some in-

terest to investigators. Langenburg [26] presented a short discussion on the analysis of the transient field response of the loop antenna. Essentially, the determination of the field quantities resulting from a time dependant current distribution on the loop is reported. The solution to the problem involves the Laplace transformation of the wave equation for the magnetic vector potential, solving for the field variables resulting from the transformed current distributions in the s domain, and finally obtaining the desired results through Fast Fourier Transform techniques. A discussion on the transformability of the current distribution function and its effect on the numerical convergence of the solution was presented. Finally, numerical results were provided to illustrate the transient response of a small loop (radius 0.1 meters) antenna to a step input function.

The Singularity Expansion Method has seen application to the transient response of loop antennas and the modelling of such antennas by lumped element circuits. Blackburn and Wilton [27] presented an analysis of an impedance loaded loop antenna based upon the singularity expansion method. This technique casts the solutions for the field components into a sum of residues in the Laplace s domain. The required results are obtained by performing an inverse Laplace transform on the series. Numerical results were provided in this paper which illustrated the effects of impedance loading on the locations of the poles in the s plane.

Streable and Pearson [28] presented a novel paper on the modelling of thin dipole and circular loop antennas by lumped element passive circuits. These circuits aided in the evaluation of the transient input response of the loop under a variety of conditions. The synthesis procedure for the equivalent circuits is based upon the

characterization of the loop using the singularity expansion method. Various approximations regarding the number of poles employed in the series were discussed. Also, reference was made to the requirement that the residues obtained from the SEM analysis must be positive real in order to obtain a physically realizable equivalent circuit. Equivalent circuits were constructed for two different antennas. The transient input impedance response of those two circuits was measured and the results were compared to results obtained from a time domain thin wire antenna analysis package. The comparisons validated the equivalent circuit method.

King and Schmidt [29] presented theoretical and experimental results for the transient input response of a linear and a circular loop antenna. The main contribution to this response was reported to be the input impedance of an infinitely long wire antenna fed against an infinite ground plane for an excitation frequency which corresponded to the highest spectral component of the input pulse. Simple relations for the input response were obtained which indicated that the reactive component of the response was essentially independant of the pulse width, but that the resistive component of the response was a slowly varying function of the pulse width. Experimental investigations of the transient response of a linear antenna and a loop antenna were performed using a time domain reflectometry technique and these investigations confirmed the theoretical expectations.

Clark and Tauritz [30] presented a short paper containing numerical results for the radar cross section of a loop antenna which is loaded with a single lumped impedance element. The numerical results were based upon an analysis performed by Harrington. Their paper indicated that the radar cross section of the loop

could be optimized by adjusting the reactive portion of the lumped element. He introduced this as the optimum susceptance load.

Abo-Zena and Beam [31] presented a short paper detailing the numerical results for the current distribution and radiation fields of a loop antenna which is excited by a band-limited rectangular voltage pulse. The current distributions were determined using a moment method solution and were taken to be a superposition of responses to the spectral components of a periodic pulse train. The travelling wave nature of the current distribution was explored by adjusting the voltage generator's internal impedance. A change in this impedance was seen to have a significant impact upon the radiated fields.

Thiele [32] presented a short paper on the radar cross section of open circular loop antennas. The RCS of the loop was first predicted using two different moment method techniques, the first employing a subsection expansion and the second employing a modal expansion. The numerical results were compared to experimental observations to verify the approach. The investigation illustrated an interesting resonance condition which occurs as the radius of the loop decreases, bringing the ends of the open loop closer together.

Landt and Miller [33] presented numerical results for the current distribution on a large loop antenna which results from a Gaussian type input voltage pulse. The results were obtained from a time domain moment method program for thin wire structures. The numerical results were experimentally verified by comparing the inductance of the loop to the steady state numerical result.

Michalski and Pearson [34] reported on a technique for the evaluation of a loop

antenna's response to a time dependant incident plane wave. The technique, again based upon the singularity expansion method, involved the synthesis of an equivalent circuit model for the loop under the given excitation conditions. Numerical results were given to illustrate the effects of truncating the residue series, obtained from the SEM analysis, upon the input impedance and the short circuit current for a loop antenna which was excited by an incident plane wave which had a Gaussian time history. The data obtained from evaluating the equivalent circuit's response was compared to data obtained from a traditional frequency domain - Fourier transform moment method solution. The results re-affirmed the benefits of using the SEM technique to analyze problems of this nature.

In concluding this section, attention is drawn to an interesting paper presented by Whiteside and King [35] on an application of the circular loop antenna. They discussed using a small loop antenna as a probe element for the measurement of magnetic field strength. Their analysis of the loop for this application emphasized the fact that induced currents on the antenna result from both electric and magnetic fields and that, if caution is not exercised, extreme errors in field measurement will be obtained. Probe sensitivity parameters K_b and K_e (magnetic and electric) were derived from circuit concepts. The authors employed Storer's results for the input impedance of certain loop antennas in evaluating the sensitivity parameters. Additionally, it was shown that greater accuracy in magnetic field measurement could be obtained by a single or double loading of the loop. Greater accuracy implied a reduced sensitivity to the electric field. Experimental results confirmed that the loaded loops of radius less than 0.001 wavelengths were suitable as probes

for a magnetic field.

The sensitivity of the probe current to the electric field will also create problems in the application of radio direction finding. In this area, the undesired response is referred to as the 'antenna effect'. The electric field in the plane of the loop is the cause of error. Experimentally, the antenna effect may be evaluated by observing the current induced on the loop, possibly with the aid of a radio receiver, and then rotating the loop in its own plane. If the current changes, then the loop is responding to the electric field also and, under these conditions, corrective action must be taken.

Loop Antennas in Lossy Media

There has been considerable interest in the electromagnetic characteristics of loop antennas which are immersed in lossy materials. This interest appears to be mainly motivated by applications in the areas of submarine communications, mining communications, and geophysical exploration. Originally, experimental investigations were dominant in the literature. These were closely followed by analytical investigations by Wait and others.

Smith [36] presented a description of an experimental investigation of the radiation characteristics of bare and insulated loop antennas situated in a dissipative medium, in this case, tap water. Tests were performed on a bare loop, a loop insulated in a toroidal shell, and a loop insulated in a spherical shell. The experiments indicated that, while the shape of the insulating shell had little impact upon the results, if the loop was electrically small in the insulating medium but not electrically

small in the dissipative medium, its radiation characteristics would be significantly different from a similar loop positioned in the same medium but without insulation.

King, Harrison, and Tingley [37] appear to be the first investigators to report a theoretical analysis of the characteristics of loop antennas located in lossy media. Their paper, which numerically evaluated the admittance of the loop, was based upon T.T. Wu's analysis for the loop in free space. For the problem at hand, the intrinsic impedance and wavenumber for the lossy medium were substituted into the previous formulation. The results obtained indicated that accurate predictions for the loop's admittance could be computed when using twenty terms in the Fourier series. The twenty term criteria appeared valid for loops of electrical circumference ranging up to 2.5 wavelengths. Supplementary comparisons were also made with results obtained from Storer's formulation, where an appropriate substitution of the medium's parameters had been made. The supplementary results showed that, while there was excellent agreement between the two formulations for conductance computations, there was significant disagreement for the susceptance.

In a subsequent paper, King et al [38] present further numerical results from the evaluation of the current distribution on a loop antenna under these conditions. Of particular interest were the results provided for the evaluation of nine terms in the Fourier series. As expected, an increase in the number of evaluated terms provided a significant improvement for the prediction of the imaginary component of the current distribution. This improvement was observed for loops with radii ranging from 0.5 to 2.5 wavelengths.

Iizuka [39] reported experimental results for the input impedance, current dis-

tribution, and near field characteristics of a loop antenna which is located in a lossy medium. In this case, the medium was a tank filled with an electrolytic solution. Measurements were performed on a number of loop antennas where the loop radius was changed in each trial. Each antenna was subsequently tested in a variety of solutions where the dielectric constant and loss tangent of the solution was changed for each test. The current distributions were measured using a small magnetic probe while the near field characteristics were obtained with the aid of a monopole antenna. The experimental results were in good agreement with theoretical results presented by King and others.

Galejs [40] presented a theoretical analysis for the admittance of a loop antenna situated in a lossy medium. The loop was modelled as a flat ring in a cylindrical region with the tangential field components positioned along the ρ and ϕ co-ordinates. The field expressions were derived in a manner similar to that of a loop antenna positioned co-planar to an infinite half space. The outermost cylindrical region was assumed to be perfectly conducting and of very large radius so as to create a denumerably infinite set of transverse eigenvalues for the wave equation solutions. The admittance was obtained using a variational expression with the current distribution on the loop represented by the first two terms of a Fourier cosine series. Numerical results from this formulation agree well with those alreading reported in the literature for the small loop case. However, as the loop radius was increased, deviations in the susceptance became significant. The author suggested that the inclusion of more terms in the current distribution expansion would remedy this difficulty.

Chen and King [41] presented an analysis of the input impedance of a small circular loop antenna located in a dissipative medium. The approach taken in this paper was a modified Storer formulation. In considering a small loop, only the first three terms of the Fourier expansion were computed. A comparison of numerical values for the first term and the second term indicated that, for this problem, the uniform current distribution assumption was valid for loops of electrical circumference less than 0.3 wavelengths. Further, it was observed from the computations that the input susceptance of the small loop was virtually independant of the loop circumference.

Benning [42] presented simple closed form expressions for the input impedance of a loop antenna located in a lossy medium and carrying a constant current distribution. These equations were cast in terms of tabulated elliptic integrals and, because of the assumed current distribution, would be valid for only small loop antennas.

Lee and Smith [43] reported on the experimental investigation of the input admittance of both bare and insulated linear and circular loop antennas which were immersed in moist sand. The investigation was motivated by the need to characterize insulated antennas located in lossy media where the dielectric constant of the lossy media was approximately equal to that of the insulation. Measurements were made for a variety of dielectric conditions. The experimental results were compared to numerical results obtained from a modified Wu analysis for the bare loop antenna and to numerical results obtained from Smith's analysis for the insulated loop antenna. All comparisons yielded satisfactory results.

Finally, Smith [44] presented an accurate closed form expression for the input admittance of a small loop antenna located in a lossy medium. Previously reported expressions for the input admittance, in which the current distribution was approximated by the first two terms of a Fourier series expansion and where certain approximations had been made in the computation of these terms, yielded poor results for the loop's input conductance, especially for the case of high loss in the medium. The present equation provides a more accurate prediction for the loop input conductance and is verified by comparison with results obtained from a twenty term computation.

Loop Antennas in the Presence of a Half Space

The analysis of loop antennas in the presence of both lossy and perfectly conducting half spaces has been of considerable interest both from the perspectives mentioned in the previous section and from the perspective of the high frequency or short wave communications system. At communications frequencies in the 3 to 30 MHz range, all practical antennas are electrically close to the earth. In the analysis of such communications antennas, the earth is modelled as a lossy infinite lower half space. For antennas which are operated against a large ground screen, this screen is modelled as a perfectly conducting lower half space.

Row [45] appears to be one of the first investigators to consider the loop antenna in such an environment. He presented an analysis of the receiving properties of a small loop antenna which is buried in a lossy half space. His analysis begins from the work presented by Chen and King and is essentially an investigation into the

relative amplitudes of the first and second terms in the Fourier representation for the current distribution. The second term contributes the so-called antenna effect observed in radio direction finding applications. The author extends the previous formulation to the problem involving half space geometry by simply determining how deep the loop must be buried before the extension becomes valid. This depth is determined through comparison to work performed by Galejs. Effective heights are then computed to relate the open circuit voltages at the terminals of the loop to the applied incident electric fields. Space factor equations are derived to illustrate the azimuthal dependance of the open circuit voltage to the incident field location. Finally, the paper ends with a discussion on the significance of the higher order terms in the current distribution.

Galejs [46] investigated the input resistance of a small loop antenna placed co-planar to a lossy ground plane. The analysis follows the Sommerfeld approach. Small argument approximations are applied to the integrands of the field equations to obtain numerical results for the input resistance. Computations are performed for both an assumed current distribution and for an assumed two term current distribution. The results presented in this paper agree favourably with results obtained from a variational approach to the problem considered earlier by Galejs.

Wait has shown considerable involvement with this problem. In his first paper on the subject [47], he presented a rigorous analysis of a loop antenna mounted co-planar at a short distance above the conducting earth. The analysis followed the classical Sommerfeld approach. The radiation resistance was determined through the Poynting vector formulation. The integrals involved in computing the power

flow were subjected to a series of approximations which yielded simple closed form expressions for the radiation resistance. Further approximations were made for loops which are located directly above the interface. Numerical results were provided to illustrate the ratio of the loop's radiation resistance over the earth to that of free space as a function of antenna height above ground.

Wait [48] then presented a short paper on the radiation from a small loop buried in the earth. The loop was modelled as a vertical magnetic dipole and the field expressions were obtained using the classical Sommerfeld formulation. In conclusion, a simple expression was provided for the additional attenuation imposed upon the dipole's far field due to immersion in the conducting medium.

An analysis of the input impedance of a small loop antenna positioned over a lossy half space was considered by Wait and Spies [49]. Again the formulation followed the classical Sommerfeld approach. Of interest in this paper is the use of Bessel function small argument approximations to reduce the Sommerfeld integrals to closed form expressions involving complete elliptic integrals. Graphical results illustrated the dependance of the loop impedance upon the loop height above the interface.

Following this, Wait and Spies [50] presented a short paper on the evaluation of sub-surface electromagnetic fields resulting from an electrically small loop antenna located on or slightly above the interface. Again the analysis was based upon the classical Sommerfeld formulation. The resulting integrals were evaluated numerically, employing interval division and twelve point Gaussian quadrature techniques, and results for the radial and vertical components of the magnetic field were pre-

sented in graphical form.

Finally, Wait and Spies [51] reported on the investigation of the electromagnetic fields resulting from a small loop antenna which is buried in the lower layer of a two layer dissipative half space. The analysis provided Sommerfeld type integral representations for the electric and magnetic field components for the upper half space region. The integrals for the magnetic field components were evaluated numerically and graphical results for the ratio between the radial and vertical components of the magnetic field were presented.

Shvarts and Kaganskiy [52],[53] reported on a theoretical analysis of a loop antenna placed horizontally above a lossy half space. The application of this analysis was to a communications system employing inductively coupled loops operating at very low frequencies. The analysis again employed the classical Sommerfeld technique. The fields were determined from numerically integrating the expressions for E_ϕ, H_r, and H_z around the branch cuts. Although the authors indicated the existance of singularities in the integrand, there was no mention of surface wave excitation or coupling. The numerical results were compared to an empirical relation which had been determined from experimental observation and good agreement was obtained.

An and Smith [54] presented a detailed theoretical and experimental investigation of a loop antenna positioned near a planar interface. The analysis was based upon solutions to the wave equation in spherical co-ordinates. Extensive mathematical detail was provided to show how the general spherical co-ordinate solutions may be approximated to provide the more well-known Sommerfeld type solutions. Both

the transmitting and receiving characteristics of the antenna were studied. For the transmitting case, the current distribution, input impedance, and radiation characteristics of the antenna were numerically evaluated. For the receiving case, the terminal voltage of the loop was evaluated for various polarizations of plane wave incidence. Experimental results were obtained for the near field characteristics and input impedance of the loop by a time domain admittance technique.

Chang [55] provided an analysis of the admittance of a loop antenna positioned co-planar above a multiply-layered dissipative half space. The analysis employed image theory and an integral equation was formulated for the modal components of the current distribution on the loop. The primary contribution was evaluated via the Wu approach and the secondary contribution, which was represented in Sommerfeld form, was evaluated numerically. Twenty terms were again considered in the Fourier expansion for the current distribution. Numerical results were presented which indicated an oscillatory dependance of the loop's input impedance upon its height above the interface.

Moorthy [56] reported on the analysis of a loop antenna of arbitrary radius located over an infinite lossy half space. The analysis employed the primary and secondary contributions obtained through plane wave reflection co-efficents. Aside from this feature, the analysis followed the classical Sommerfeld formulation. Special limiting cases for a perfectly conducting lower half space and a free space lower half space were considered. Graphical results presented illustrate the dependance of the loop's input admittance on both the conductivity of the lower half space and the loop's separation from the interface.

Vogler [57] presented a short paper outlining some approximate expressions for the input impedances of small loop and dipole antennas located near the ground. Graphical results are presented to illustrate the dependance of the antenna's input impedance upon different ground parameters.

To conclude this section, Shoamenesh and Shafai [58] presented graphical results for the gain and input impedance of a loop antenna located over a perfectly conducting ground plane. Although no analytical details were provided in the discussion, the authors concluded from the graphical data that optimum spacings between loop and ground plane may be determined for gain enhancement.

Loop Antennas Mounted on Cylindrical Cores

Of particular interest to the present problem of a loop antenna situated over an infinitely long dielectric circular cylinder is the work reported on the topic of loop antennas mounted on cylindrical cores. It appears that Pavlov [59] was the first investigator to examine a loop antenna mounted in such a fashion. He reported on an investigation of a small loop antenna situated coaxially on the surface of an infinitely long circular ferrite rod. The entire structure was then immersed in a conducting medium. A uniform current distribution on the loop was assumed. The approach taken in the analysis was to formulate equations for the magnetic vector potential components separately for the loop without the core and then the core without the loop. The equations were then combined for the total magnetic vector potential resulting from a loop and core with loop radius set equal to core radius. In the discussion on the evaluation of the field expressions, it was noted that there

would be contributions to the resulting fields from both a space wave, which may be obtained through an integral operation with a deformed contour, and a surface wave which could be obtained by evaluating the residues of the integrand at the appropriate singularities.

Numerical results were provided for the propagation velocities of surface waves for a number of physical parameters. Graphical results were presented for the radiation characteristics for the structure under similar physical parameters. In concluding the paper, a discussion on the input impedance of the loop was presented. This parameter was obtained by integrating the resulting magnetic field in the permeable core to obtain the voltage induced at the loop terminals. This voltage was divided by the magnitude of the assumed current distribution to obtain the input impedance. It was interesting to note that this impedance was essentially dependant upon the surface wave characteristics, under the conditions cited, and that the space wave presented only a negligible contribution to the real part of this impedance.

Islam [60] presented an analysis of a loop antenna mounted coaxially over an infinitely long circular cylinder. The radius of the loop was larger than the radius of the cylinder so that the geometry presented a three region problem. Further, the current distribution on the loop was considered uniform thereby permitting consideration of only the first term in the Fourier series expansion for the distribution. The analysis, employing components of the magnetic vector potential, followed the standard Fourier integral transform approach with the transformation taken with respect to the axial co-ordinate. Simplified closed form expressions were obtained

by using, first the small argument approximations for the Bessel functions found in the integrand, and second Weyrich's formula for the Hankel function integral. The expressions obtained through the simplification of the analysis were similar to those obtained by simplifying the magnetic vector potential formulation for loops in free space. The field analysis was followed by an examination of the radiation resistance of the loop as situated above. This parameter was obtained through a numerical evaluation of the Poynting integral for the fields over a cylindrical boundary. The numerical results presented indicate that the radiation resistance for the loop situated coaxially above the cylinder as discussed, is almost linearly dependant upon the permeability of the cylinder.

The appendix of this paper provided a brief analysis of a circular loop antenna positioned coaxially over a prolate spheroid. An expression was provided for the ϕ component of the magnetic vector potential. Of interest here is the assumption made by Islam that the wave functions are orthogonal in this geometry. In a subsequent communication, Wait [61] discussed this point with Islam. Islam, in turn, suggested that the mode cross coupling term could be considered negligible for loops of small radius when situated in this geometry.

Burton, King, and Wu [62] reported on the analysis of a loop antenna mounted over a circular core. The analysis presented in this paper was essentially an extension of Islam's earlier work. The electric fields produced by loops situated over cores of varying permittivity and conductivity were investigated. A number of experiments were performed to validate the numerical results. The results of the experimental investigation were further employed through scaling so that they could

be used in the investigation of large loop antennas operating at very low frequencies. The results of this last analysis were considered applicable to the area of surface-subsurface communications.

Dielectric Rod Antennas

The dielectric rod antenna has received considerable attention over the past thirty years. It has many advantages, cost and weight being just two of many. Conventionally, the dielectric rod is excited by a circular waveguide. However, there have been reports of dielectric rods being excited by small loop and annular slot antennas. There have also been reports of using small wire segments as elements in a linear array which is excited by a dielectric rod waveguide. With these reports as motivation, a review of the literature pertaining to significant developments in the area of dielectric rod antennas has been undertaken.

Horton, Karal, and McKinney appear to be the first to investigate the radiation characteristics of a dielectric rod antenna. In their first paper [63], they reported on a theoretical and experimental investigation of the radiation from a dielectric rod excited with the TM_{01} surface wave. Surface equivalent currents were obtained from the presumed field distribution along the cylinder. These equivalent currents were taken over the surface of the rod only and no consideration was given to the waveguide feed. Predicted radiation patterns were compared to experimental results. Horton et al claimed that the experimental and theoretical results agreed only under one special condition. This condition was that the radius of the surface over which they assumed the equivalent currents to exist had to be approximately

65 percent less than the radius of the rod under investigation.

In a subsequent paper, Horton and McKinney [64] reported on the results of an experimental investigation of the radiation and gain characteristics of a dielectric rod antenna. A series of rods were constructed with variations in the dielectric constant, length, radius, and taper. The salient observation of this study was that, while the length of the rod controlled the number of sidelobes observed in the radiation pattern, the diameter of the rod dictated the sidelobe amplitudes. The rods were fed with a circular waveguide in which either the TM_{11} or TE_{11} waveguide mode would be established. It was found that both waveguide modes would excite the HE_{11} surface wave mode on the cylinder. Experiments were conducted to compare the patterns of antennas which were excited in the two modes and there were no differences observed.

McKinney [65] extended the work reported in the previous paper by performing an experimental investigation of the radiation characteristics of a series of dielectric rod antennas which would operate under the TE_{01} and TM_{01} surface wave conditions. The patterns obtained in this investigation were similar to results reported in the first paper by Horton and McKinney. McKinney indicated the existance of the TE_{02} and TM_{02} surface waves also but these waves did not have any significant impact upon the results obtained.

Brown and Spector [66] discussed the radiation characteristics of end fire antennas, specifically the yagi and circular dielectric rod. The primary radiation mechanism for the dielectric rod was conjectured to be the aperture plane field distribution at the end of the rod. Secondary radiation occured from the rod feed

if the transfer of waveguide incident power to rod surface wave was not complete. A numerical evaluation of the radiation characteristics for a dielectric rod was performed with an aperture distribution derived from the surface wave field structure. From this evaluation, it was noted that the beamwidth of the radiation pattern decreased as the rod radius decreased. Secondary radiation from the feed was then also included in the computations. The results obtained from these subsequent computations compared favourably with results obtained from other investigators.

Duncan and DuHamel [67] reported on the development of a linear array antenna which consisted of a set of small wire elements excited by a dielectric rod waveguide, HE_{11} mode. This antenna and its design technique are similar to a slotted waveguide array. A novel experimental method for determining the element admittance was reported. In this method, the wire element was positioned on a dielectric image line. The standing wave pattern was then probed through a slot in the image line's ground plane. After the element admittance was determined and the propagation velocity for the surface wave computed, standard array design techniques were employed to determine the element locations along the structure for a given desired radiation pattern. The paper concluded with remarks on the construction of three of these arrays and the radiation patterns of each were discussed.

DuHamel and Duncan [68] formulated a launching efficiency parameter for various loops and slots which might be used to excite surface waves along a dielectric cylinder. The formulation, which was based upon the reciprocity theorem, related the launching efficiency of the loop or slot to its impedance as a scatterer on the cylinder. The scattering impedance was obtained experimentally by a method sim-

ilar to the one used by Duncan as indicated above. Numerical results were provided for the launching efficiencies of a straight wire, loop, straight slot and annular slot as a function of surface wave propagation velocity and launcher physical dimensions. It was interesting to note that, in the experiments performed on the loop launcher, the optimum radius of the loop was approximately one half the radius of the cylinder.

Angulo and Chang presented two papers on their work in the area of dielectric rod antennas. In their first paper [69], they reported on an analysis of an infinitely long dielectric cylinder covered by a semi-infinitely long circular waveguide. This model was employed to study the radiation characteristics of a dielectric rod antenna. The objective of this investigation was to predict the reflected power sent back down the circular waveguide, the transmitted power carried by surface waves along the dielectric rod, and the power radiated as a space wave. The radiation occurs because of the discontinuity along the structure. Final expressions for these quantities were presented and numerical results provided from evaluations for certain physical parameters.

In their second paper [70], Angulo and Chang employed a variational expression for the surface wave terminal admittance located at the end of a semi-infinite dielectric rod. The investigation was motivated by an interest in the amount of power reflected as surface wave from an abrupt junction on a dielectric cylinder. The formulation proceeded by obtaining field expressions for regions on both sides of the junction. The continuity of the electric and magnetic fields at the junction was employed in a variational expression. One trial field was explored, the field of a TM_{01}

surface wave, and graphical results were provided for the terminal admittance.

Duncan [71] presented a comprehensive investigation of TM_{01} surface wave excitation on an infinitely long dielectric circular cylinder. Specifically, he investigated the efficiency with which this surface wave could be excited when using a magnetic current ring as a launcher. The radius of the current ring was set to a value less than the radius of the rod so that the current ring appears imbedded within the dielectric rod. The author provided a complete account of the solution for the ϕ component of the magnetic field including a discussion on the inclusion of the launcher as a boundary condition in the problem. The inverse Fourier transform operator, which is a required step in the solution, was cast in terms of a contour integral. The evaluation of this integral in the complex plane was reviewed. The residues from the singularities of the integrand were identified as the surface wave contributions to the total field. It was indicated that the evaluation of the integral around the branch cut, which is seen in solutions to problems of this type, would yield the so-called radiation field. The branch cut integration was further approximated by the technique of steepest descent to provide closed form expressions for the far field radiation characteristics of the structure. Poynting integrals were employed to calculate the power in the radiation field and the surface wave. A comparison of the two provided an excitation efficiency factor for the magnetic current ring. An extensive experimental program was conducted to verify the theoretical results. In the experiments, a dielectric rod was mounted against an annular slot antenna on one end and a short circuiting plate on the other end. The annular slot was fed with a coaxial transition so that the ϕ independance could be maintained.

Additionally, a small polystyrene ring was positioned in the transition so that the susceptance of the slot could be tuned out. The magnitude of the surface wave was then determined by measuring the reflected wave on the coaxial line connected to the transition. The experimental and theoretical results consistently agreed to within ten percent. Additional experimental investigations were conducted where the size of the terminating ground plane and the slot ground plane were varied. These parameters had no effect on the final results.

Chu and Kilcoyne [72] presented a short note on the excitation of a dielectric rod antenna with a helix. It was observed that the field configuration for two HE_{11} surface wave modes in time quadrature was similar to the field configuration of a helical antenna operating in axial mode. Preliminary experimental results for the axial ratio and beamwidth for this type of antenna were presented.

McLean and Williams [73] reported on an experimental investigation of the radiation characteristics of dielectric rod antennas of different lengths and radius. The objective of this investigation was to identify the antenna's bandwidth with respect to power gain. Additionally, a new type of feed was introduced which, the authors contend, produces a wider bandwidth than the conventional cup and probe feed originally introduced by Kiely [74]. The two significant conclusions that arise from this study are that, first, the new feed essentially doubles the bandwidth of the dielectric rod antenna and, second, as the radius of the rod decreases, the radiation characteristics of the structure, that is, rod plus feed, take on the radiation characteristics of the feed alone.

James [75] provided a detailed discussion on the radiation mechanism of the

dielectric rod antenna. His analysis supports the work reported by Brown and Spector who postulated the dielectric rod antenna as a two element end fire radiator, the first element being the surface wave launcher and the second element being the aperture plane at the free end of the rod. Subsequently, the appproaches taken by Horton and McKinney, Bouix, and Fradin, which modelled the antenna as a leaky wave structure, were discounted. James developed equations for the radiated electric field components based upon the vector Kirchoff integral. It is important to note that the equivalent sources employed in the radiation integrals are located at the two elements indicated above. The alleged failure of the previous theories lies in the fact that the vector nature of the fields was not included in the analysis, thus leading the previous investigators to the incorrent conclusion that energy radiates from the sides of the cylinder. James then presented an extensive comparison of numerical results obtained from his analysis to previously reported experimental results. The paper concludes with some practical considerations concerning the tapered dielectric rod antenna.

In a subsequent short paper, Andersen [76] disputed the claim made by James that the radiation integrals involved in his analysis of the dielectric rod antenna should be taken only over carefully selected surfaces, those surfaces being ones over which appropriate equivalent current distributions are found. Andersen suggested that the radiation integrals should be taken over all surfaces of the antenna. Those surfaces which do not hold appropriate equivalent current distributions would not contribute to the radiation pattern. In response to this, James [77] showed that the formal evaluation of the radiation integral over certain surfaces would not yield a

zero result. The integral over these particular surfaces would in fact be improper. James then re-stated his original contention and the matter was dropped.

James also received criticism from Kleinburg [78] for remarks made in the original paper on the dielectric rod. Kleinburg brought forward two points for consideration. First, the field expressions presented by James for the surface wave may be extended to the case of general azimuthal dependance. Second, he suggested that the method employed by Duncan could be used to evaluate the launching efficiency for the feed and thus incorporate this into the analysis of the dielectric rod. This second suggestion would alleviate the requirement to guess at the percentage amount of power which is being radiated by the feed and provide for a more accurate estimate of the interaction between the feed and aperture plane radiation patterns. James accepted the first suggestion without hesitation but was somewhat sceptical of the accuracy with which measurements could be made.

In concluding this interesting exchange in the literature, James presented a final note on the analysis of the dielectric rod [79]. He re-emphasized his ideas presented in the original analysis. However, of special interest, he alluded to a new item which, until this time, had not been considered. He postulated the existance of a leaky wave field structure in the vicinity of the feed. Although not discussed in detail, his remarks concerning such a field structure are significant.

In previous reports on the analysis of radiation characteristics for dielectric rod antennas, the feed radiation pattern was taken to be an amplitude reduced version of the pattern resulting from the feed antenna located by itself in free space. The inclusion of the rod was considered to have negligible impact upon the feed's radi-

ation pattern. Blakey [80] provided a refinement to this approach. He developed an amplitude and phase correction factor which accommodated the presence of the dielectric rod. This correction was based upon a geometrical optics interpretation of the plane wave spectral representation for the field components. Numerical results were presented for the correction factors but no experimental validation was provided.

Hastings [81] presented a short paper describing how a dielectric rod may be loaded with an axially located wire to reduce its scattering cross section. The technique described has been applied to antenna structures where scattering off the dielectric support rods negatively affected the radiation characteristics of the antenna itself. Design equations were given, based upon static circuit parameters, and preliminary numerical results, confirmed by experimental observations, were presented.

Smits [82] provided a short application note which outlined the use of a choke at the feed of a dielectric rod antenna to reduce far out sidelobes in the radiation pattern. Experimental results were reported which indicated that the choke provides greater than 20 dB far out sidelobe suppression for an aluminum oxide dielectric rod antenna employed as a seeker in a missle application.

Neumann [83] reported on the development of simplified design equations for a dielectric rod antenna which are derived from Brown and Spector's results. Equations for the transverse field extent, directive gain, and half power beamwidth were provided. Numerical results, obtained from these equations, were compared to experimental results. An interesting point was found in the experimental procedure.

The radiation from the feed was blocked by irises so that the radiation pattern from the terminal end only could be observed.

Yaghjian and Kornhauser [84] adopted an interesting perspective in their analysis of the dielectric rod antenna. Their investigation was concerned with the near and far field structure associated with a dielectric rod excited by the HE_{11} surface wave. Their analysis is interesting because the antenna is modelled inside a large circular waveguide. This approach leads to a denumerably infinite set of transverse eigenvalues instead of the normal continuous spectra. To attain free space conditions, the radius of the waveguide is set to infinity. Modal solutions for fields on both sides of the discontinuity, the free end of the dielectric rod, were formulated. The associated expansion co-efficients were evaluated through a power orthogonality relation and a numerical procedure. The evaluation of the co-efficients for the fields in the forward half space then led to computation of the far field characteristics and radiation efficiency. The analysis presented in this paper was validated through comparisons with previously published results.

In a second paper on the subject, Blakey [85] reported on the experimental evaluation of the radiation characteristics of a composite dielectric rod antenna. This cylindrical dielectric structure was constructed from polystyrene with embedded teflon annular segments. Under certain conditions, this new antenna displayed narrower main beam lobe and sidelobe structure that did a uniform dielectric rod under the same conditions. Blakey suggested that the improved performance might arise from the annular segment structure's affect upon the direct radiation from the feed.

Blakey [86] subsequently proposed a scattering theory approach for the evaluation of the radiation characteristics of certain dielectric rod antennas which are excited by TM_{01} surface waves. An integral equation relating incident and scattered fields on a dielectric structure was specialized to the geometry involved. An angular spectra representation for the scattered field was then introduced into the integral equation. The integration over the surface of the cylinder was performed through a change in the order of integration with respect to the spectral variable, resulting in spectral representations for the scattered fields. These spectral representations were numerically evaluated to obtain the desired results. The numerical data was then compared to previously published results for validation.

Gupta and Bahl [87] presented an overview of the design considerations for leaky wave antennas of arbitrary geometry. Of particular interest were the two methods used for the evaluation of the leaky wave radiation characteristics of such antenna, the steepest descent method and the Kirchoff integral method. The steepest descent method employs wave equation solutions in transformed space, solves the expansion co-efficients through the boundary conditions, and then applies the steepest descent approximation to the Fourier integrals to obtain the far field radiation characteristics for the antenna. The Kirchoff integral method establishes an equivalent current distribution on the surface of the cylinder and computes the radiation characteristics with the appropriate integral expression. The Kirchoff integral method requires a priori knowledge of the leaky wave pole location, this pole describes the propagation constants for the leaky wave, whereas the steepest descent technique does not. Additionally, the Kirchoff integral technique may handle only one propagating

mode at a time where the steepest descent technique can handle all modes simultaneously. This discussion is of particular significance to the investigation of the loop antenna on a dielectric cylinder because, as will be seen later, there is debate in the literature on the significance of the leaky wave pole locations on the steepest descent approximations to the field equations. Gupta and Bahl infer that the steepest descent technique is the method of choice. They provide closed form equations for the leaky wave radiation patterns, beamwidths, sidelobe levels, radiation efficiency, and pattern - scan frequency dependance for the general class of leaky wave structures.

Ittipiboon, Shafai, and Bridges [88] present an experimental investigation of a short dielectric rod antenna which is intended to be used as a feed for a paraboloidal reflector. Results were presented for the E and H plane radiation characteristics, from which the pattern beamwidth was determined. Associated cross-polarization patterns were also provided. Ittipiboon et al suggest that an experimental optimization of this antenna would make its performance comparable to a corrugated conical horn for the intended applications and that it may be manufactured at a fraction of the cost.

Vasil'yev, Sedel'nikova, and Seregina [89] considered the non-symmetrical excitation of a dielectric rod by an electric dipole source positioned perpendicular to the rod axis. An integral equation approach was employed to determine the equivalent magnetic current distribution on the rod surface, and from these distributions, the radiation characteristics were obtained. Through this analysis, Vasil'yev et al were able to identify the currents associated with the incident and reflected surface waves and the currents associated with radiation at the discontinuities. From the vari-

ous currents, partial radiation patterns were computed. The currents which most significantly affect the radiation pattern were identified. The partial patterns were then superposed to obtain the final results.

Finally, Kishk and Shafai [90] reported on a numerical investigation of the radiation characteristics of a short dielectric rod antenna. The analysis was performed with the aid of a moment method solution to a set of integral equations. Results for co- and cross- polar radiation characteristics for a number of antenna parameters were presented.

Guiding Properties of Circular Dielectric Rods

An important aspect in the analysis of the loop antenna situated coaxially on a dielectric cylinder is the generation of surface waves. These waves will have a significant impact upon the input impedance of the loop, and to a lesser extent, upon the low angle radiation characteristics of the loop. Because of their significance to the stated problem, a review of the literature relevant to the topic of surface waves on dielectric cylinders is appropriate.

Elsasser [91] and Chandler [92] appear to be the first investigators to consider the circular dielectric cylinder as a device for guiding electromagntic energy. Elsasser developed the by now well known transcendental eigenvalue equation for the propagation constant of the guided wave:

$$\left[\frac{\epsilon_r \mathrm{J}'_m(\mathrm{p})}{\mathrm{p}\mathrm{J}_m(\mathrm{p})} + \frac{\mathrm{K}'_m(\mathrm{q})}{\mathrm{q}\mathrm{K}_m(\mathrm{q})}\right]\left[\frac{\mathrm{J}'_m(\mathrm{p})}{\mathrm{p}\mathrm{J}_m(\mathrm{p})} + \frac{\mathrm{K}'_m(\mathrm{q})}{\mathrm{q}\mathrm{K}_m(\mathrm{q})}\right] = \left[\frac{m\beta}{k_o}\left(\frac{\mathrm{p}^2+\mathrm{q}^2}{\mathrm{p}^2\mathrm{q}^2}\right)\right]^2$$

where $\mathrm{p} = \sqrt{k_i^2 - \beta^2}\ a$; $\mathrm{q} = \sqrt{\beta^2 - k_o^2}\ a$; k_i is the wavenumber in the dielectric

material, k_o is the free space wavenumber, β is the propagation constant of the guided wave, a is the radius of the dielectric cylinder, $J_m(\bullet)$ and $K_m(\bullet)$ are Bessel functions of the first and modified second kind respectively, and the prime denotes differentiation with respect to the argument of the function.

Elsasser obtained this equation by enforcing the appropriate boundary conditions and the wave equation solution separability conditions on the eigenfunction solutions for the geometry involved. Such eigenfunction solutions may be found, for example, in Schelkenoff [93]. From this equation, Elsasser computed propagation constants for the TE_{01}, TM_{01}, and HE_{11} waves travelling on cylinders of various radii. These numerical results indicated two things. First, that the TE_{01} and TM_{01} waves could not propagate on rods which had a radius smaller than a certain critical value, a cutoff radius. Second, the HE_{11} wave, or dipole surface wave would propagate on rods of arbitrarily small radius. There appeared to be no cutoff radius for the HE_{11} wave. These results have found many applications in the areas of fibre-optic cables and dielectric rod antennas. Elsasser's numerical results have since been published in graphical form [94],[95].

Elsasser also derived an equation to predict the attenuation of a surface wave as it propagates along a cylinder where the attenuation is due to dielectric loss. This equation was derived from the Poynting vector components which describe power flow in the axial direction.

Chandler performed a number of experiments to verify Elsasser's computations. He deployed a section of dielectric rod in an open frame and configured the apparatus as a resonant cavity. The determination of resonant frequency and cavity Q

provided the required information to evaluate the propagation constant and the attenuation of the wave on the dielectric rod. It was interesting to note that Chandler used a rectangular waveguide operating in TE_{01} mode to launch the surface wave onto the dielectric rod.

Clarricoats [96] and Gillespie [97] considered the propagation of energy along a dielectric cylinder using a slightly different formulation. Clarricoats extended the analysis by including the non free space permeability of the dielectric material. He also employed the Hankel function, second kind, with imaginary argument, to describe the field's radial distribution in the external region. In previous formulations, the modified Bessel function, second kind, real argument, had been employed. He presented a graphical solution for the propagation constants of the HE_{11} surface wave under various conditions and he evaluated the relative difference in power flow between the interior and exterior regions of the guide. This last investigation was based upon a Poynting vector approach and the results indicated that the ratio of power flow inside the rod to power flow outside the rod decreased to zero as the rod radius decreased to zero, for the HE_{11} wave. For other guided waves, the ratio was found to be finite for all values of rod radius. Gillespie added an interesting point to the discussion by indicating that in some situations, at certain radial distances from the guide axis, the power flow would be negative, or backwards. He contended, however, that the total power flow would be positive, as expected.

Many investigators have evaluated the eigenvalue equation for particular applications. However, it appears that a complete study of this equation has not been undertaken, especially for the case of a dielectric cylinder with high dielectric

constant.

Biernson and Kinsley [98] employed the dielectric waveguide as a model for the retinal cone of the human eye. They reported that previous investigators had employed this model to explain the phenomenon of colour blindness. It had been suggested that certain optical frequencies are below the cut-off frequency for surface wave propagation along the retinal cones. Thus, the colours associated with these frequencies are not perceived by the human mechanism. In their investigation, Biernson and Kinsley determined the propagation velocities for the twelve lowest order surface wave modes for conditions of low dielectric constant. Although originally intended for biomedical applications, they suggested that the results may be of some value to the antenna community. These results were presented in terms of a normalized frequency parameter which could, in general, be useful. However, the highest dielectric constant considered was 1.5. The numerical data was obtained from Elsasser's eigenvalue equation. This equation was also simplified to yield expressions for the cut-off frequency for certain rod dimensions. These simplified equations came under the scrutiny of Diament and Schlesinger [99], who claimed that the equations were not valid for cases where the dielectric constant was a realistic value. Biernson and Kinsley responded to these comments by indicating that their data had been obtained from the exact equations and that, although there may have been a small error in the text, the final results were valid.

Layburn [100] provided graphical results for the propagation velocity and group delay for low order modes on a dielectric waveguide. The application in this instance was to fibre-optic cable. Layburn employed a slightly different formulation for the

problem which yielded results in an argument which was normalized with respect to the dielectric constant of the rod. Unfortunately, again results were provided for only low dielectric constant materials. The equation for the group delay was obtained by simply differentiating both sides of the eigenvalue equation with respect to the free space wavenumber. Although no numerical data was reported, Layburn indicated that the present results could be used to predict group delay due to multi-mode propagation.

From the analysis of surface wave propagation on a dielectric rod, attention turned to the more general problem of the continuous mode spectrum for the dielectric rod. This principle incorporates both radiation and surface wave propagation into one general formulation. Specifically, any radiation which occurs from the rod is said to be the result of a continuum of radiation modes which propagate with a velocity greater than the free space propagation velocity. They are said to be so-called fast waves. The trapped waves which travel along the rod are said to be characterized by a discrete set of surface wave modes which propagate with a velocity less than the free space propagation velocity. These are said to be the so-called slow waves.

Snyder [101] provided a detailed discussion on the continuous mode spectrum of the circular dielectric rod. His analysis dealt with the scattering of oblique incidence plane waves from such a rod. His formulation provided wave equation solutions for both the internal and external regions of the rod. The external region solution contained both the incident and scattered field as a combination of standing and outward travelling wave solutions. He carefully delineated the various spectral

regions where discrete surface modes, propagating continuous modes and cut-off continuous modes could exist. He further suggested that individual radiating modes could be excited by controlling the angle of oblique incidence of the plane wave excitation. He concluded his discussion by providing some approximate equations, intended for fibre-optic applications, which would facilitate the computation of the field quantities.

Yip [102] provided an extensive report on the launching of the HE_{11} surface wave mode by a point electric dipole transversely oriented on the cylinder axis of an infinitely long dielectric cylinder. The utility of this paper lies in the detailed and explicit statement of the method of solution for problems of this nature. The non-homogeneous wave equations were solved by first obtaining a Fourier transform along the axial co-ordinate and a Fourier series along the azimuthal co-ordinate. Evaluation of the fields involved an integration around the branch cut and evaluation of the residues at the surface wave poles. Yip made reference to the saddle point technique as a means to evaluate the branch cut integral. However, the saddle point technique was not used in this paper. Yip evaluated the radiation resistance through a determination of the space wave power. The space wave power was determined through a Poynting vector integration over the infinitely long radial surface. By including the Fourier transformed field expressions in the Poynting integral, Yip was then able to obtain a simplified expression for the radiated power through Parseval's theorem. The integrand of this simplified expression provided an indication of the power per unit solid angle which is radiated through the Poynting surface. Thus, it was this integrand which was numerically evaluated by Yip to

obtain the radiation characteristics of the structure under consideration. From this investigation, the amplitude and power of the surface wave was determined, and an evaluation of the radiation characteristics of the structure was obtained. In conclusion, Yip computed the launching efficiency of the surface wave by relating the power in the surface wave to the power in the space wave plus surface wave.

In a subsequent paper, Yip [103] determined the launching efficiency of the HE_{11} mode on a dielectric tube. The formulation employed in this paper was identical to that of the previous paper except for the accommodation of three regions instead of two. Of particular interest in this paper, however, was the detailed discussion concerning the evaluation of the residues of the surface wave poles. In the previous paper, it was simply stated that the residues were obtained. In this paper, the residues were obtained analytically by L'Hopital's rule and the eigenvalue equation for the surface wave modes.

Further to the discussion on the continuous mode spectrum for the dielectric rod, reports on the developments in the search for the so-called leaky wave poles have appeared. While many investigators have employed the modal representations reviewed so far, concern has been raised regarding the possibility of complex solutions, that is, solutions involving a complex variable, for the eigenvalue equation. The concern is raised because of the fact that these poles may be crossed when simplifying field expressions in the far field region with the steepest descent technique. Originally the idea of a leaky wave pole or single leaky wave mode was used in the analysis of so-called leaky wave antennas. Such antennas were essentially closed wave guiding structures which were perturbed with perforated boundaries. The ax-

ial propagation velocity for the waveguide mode was presented as a complex number so that both the phase constant and the attenuation of the wave as it leaked from the guide could be characterized in the axial direction. It has been suggested that the leaky wave solutions for open waveguide systems may provide additional contributions to the radiation pattern over limited angular sectors. Although it appears that no evaluation of the leaky wave pole contribution for a particular geometry has been reported, there has been some success in locating the pole locations in the complex plane.

Arnbak [104] and James [105] appear to be the first investigators to report numerical results for complex solutions to the eigenvalue equation for the dielectric cylinder. Arnbak considered the zero order surface wave mode only. For this condition, he examined the split dispersion equations in the region of small argument for the Hankel functions involved. This was the region of greatest interest. He employed small argument approximations for the cylinder functions and obtained a simplified expression from which the leaky wave pole locations could be identified. He briefly considered also the influence of losses on the positions of the poles in the complex plane. Arnbak suggested that a surface wave would be transformed into a leaky wave as the excitation frequency of the field was decreased.

James further considered complex solutions to the eigenvalue equation. Of significance was his investigation of the symmetry involved in the complex solutions. In summary, he reported that pairs of complex solutions could be found to the eigenvalue equation where the individual solutions were in adjacent quadrants of the complex plane. He further indicated that the eigenvalue equation would take

on a form containing first and second order Hankel functions, a form which is also seen in the integration of the branch cut integral. This work may suggest that the residues from the individual leaky wave poles may eliminate each other, leaving the original steepest descent contribution as the only term which will yield the radiation field.

Additional work on the location of complex solutions has been reported by Veselov and Rayevskiy [106],[107]. In their first paper, a mathematical theorem is provided by which the existance of a complex solution to the wave equation may be proven. Of greater interest is the method by which they obtained the complex solutions, which was the subject of the second paper. The eigenvalue equation was recast in the form of a quadratic equation in terms of:

$$P(\alpha, a) = \frac{\mathrm{J}'_n(\alpha, a)}{\mathrm{J}_n(\alpha, a)}$$

Solutions for $P(\alpha, a)$ were determined by solving the resultant quadratic equations and then determining α from $P(\alpha, a)$. Numerical results were provided which indicated the trajectory of α in the complex plane under the influence of various factors.

To conclude this section, attention is drawn to the work of King and Schlesinger on a structure referred to as the dielectric image line. A dielectric image line is an open guiding structure which consists of a half round dielectric rod mounted on a ground plane. The electromagnetic field structure of the HE_{11} surface wave is observed to be the same for both conventional dielectric rods and image lines. The image line provides some experimental advantage in the observation of such field

structures and, therefore, deserves mention in this discussion.

King and Schlesinger [108] and Schlesinger and King [109] appear to be the first investigators to consider the propagation of surface waves along a dielectric image line. They employed Elsasser's eigenvalue equation to determine the propagation velocity for the HE_{11} surface wave. Of particular interest was the attenuation per unit length observed on this type of line. King and Schlesinger investigated loss due to the dielectric material, ohmic loss due to the ground plane, and radiation loss. Theoretical evaluations for the dielectric and ohmic loss were performed using a technique similar to that reported by Elsasser, while the radiation loss due to perturbations on the line was evaluated experimentally.

The outstanding result of these investigations was that the ohmic loss was insignificant compared to the dielectric loss, even for the case of when the ground plane was composed of nichrome plate.

Chapter 3

Analytical Formulation

Introduction

The electromagnetic characteristics of a loop antenna positioned coaxially on the surface of an infinitely long dielectric circular cylinder may be divided into three main categories: radiation, surface wave, and input impedance. The evaluation of these characteristics requires an analysis of the electromagnetic fields which result from the current distribution on the loop. This chapter outlines the formulation employed for the analysis of these fields and the various extensions required to evaluate the characteristics of interest.

Formulation and Solution of Equations for the Fields

Figure 3.01 illustrates the loop antenna positioned coaxially on the infinitely long dielectric circular cylinder. The cylinder is denoted as Region I, with radius $\rho = a$, dielectric constant ϵ_i, extending from $-\infty$ to ∞ along the z axis. Region II is free

space. The antenna's current distribution, $f(\phi)\delta(z)$, is shown at $\rho = a,\ z = 0$, in the cylindrical co-ordinate system (ρ, ϕ, z). Superimposed upon the cylindrical co-ordinate system is the spherical co-ordinate system (r, θ, ϕ) which is used in the evaluation of the loop's radiation characteristics. A harmonic time dependance of the form $e^{j\omega t}$ is assumed.

The antenna itself is modelled using the thin wire approximation [110]. This approximation presumes that the antenna current exists only along the axis of the conductor. The radius of the conductor, therefore, becomes an important parameter in evaluating antenna characteristics. A common technique for specifying loop conductor radius is the loop antenna parameter Ω. $\Omega = 2\ln(2\pi a/b)$. The loop antenna radius a and conductor radius b are shown in Figure 3.01

The loop antenna is excited by a rectangular pulse function, 1.0 volt amplitude. The angular extent of this function is 5 degrees from -2.5 to 2.5 along the circumference of the loop. The length of the function is obtained by translating the angular extent along the circle at $\rho = a$. From the applied voltage and pulse function length, the ϕ component of the electric field which excites the antenna, is determined. The feedpoint details are also shown in Figure 3.01.

As indicated previously, the first step required in the evaluation of the antenna's various characteristics is the determination of the electromagnetic fields resulting from the current distribution on the loop. There are many different approaches to the formulation of equations for this type of problem. All of them, in general, lead to the formulation of a wave equation for functions which describe the actual fields under consideration or potential functions from which the field expressions

may be obtained. Illustrative examples of three different approaches found in the literature are Yip [102], who formulated scalar wave equations directly in terms of the axial components of the electric and magnetic field vectors $\mathbf{E}$ and $\mathbf{H}$, Harrington [111], who formulated scalar wave equations in terms of the axial components of the electric and magnetic vector potentials $\mathbf{A}$ and $\mathbf{F}$, and Wait [95], who formulated scalar wave equations in terms of the axial components of the Hertz electric and magnetic vector potentials $\mathbf{\Pi}$ and $\mathbf{\Pi}^*$. In this last case, the axial components are known as the scalar Debye potentials U and V. The formulation approach employed for this research effort follows Wait.

The vector wave equation for the Hertz vector potentials may be obtained directly from Maxwell's equations. By defining the electric Hertz vector as follows:

$$\mathbf{H} = (\sigma + j\omega\epsilon)\ curl\ \mathbf{\Pi} \tag{3.1}$$

the following homogeneous vector wave equation may be obtained:

$$curl\ curl\ \mathbf{\Pi} - grad\ div\ \mathbf{\Pi} + \gamma^2 \mathbf{\Pi} = 0 \tag{3.2}$$

where $\gamma^2 = j\omega\mu\,(\sigma + j\omega\epsilon)$. Similar equations are available for $\mathbf{\Pi}^*$.

The scalar Debye potentials are defined as follows:

$$\mathbf{\Pi} = (0, 0, U) \tag{3.3}$$

$$\mathbf{\Pi}^* = (0, 0, V)$$

From this definition, it may be seen that the scalar potential functions U and

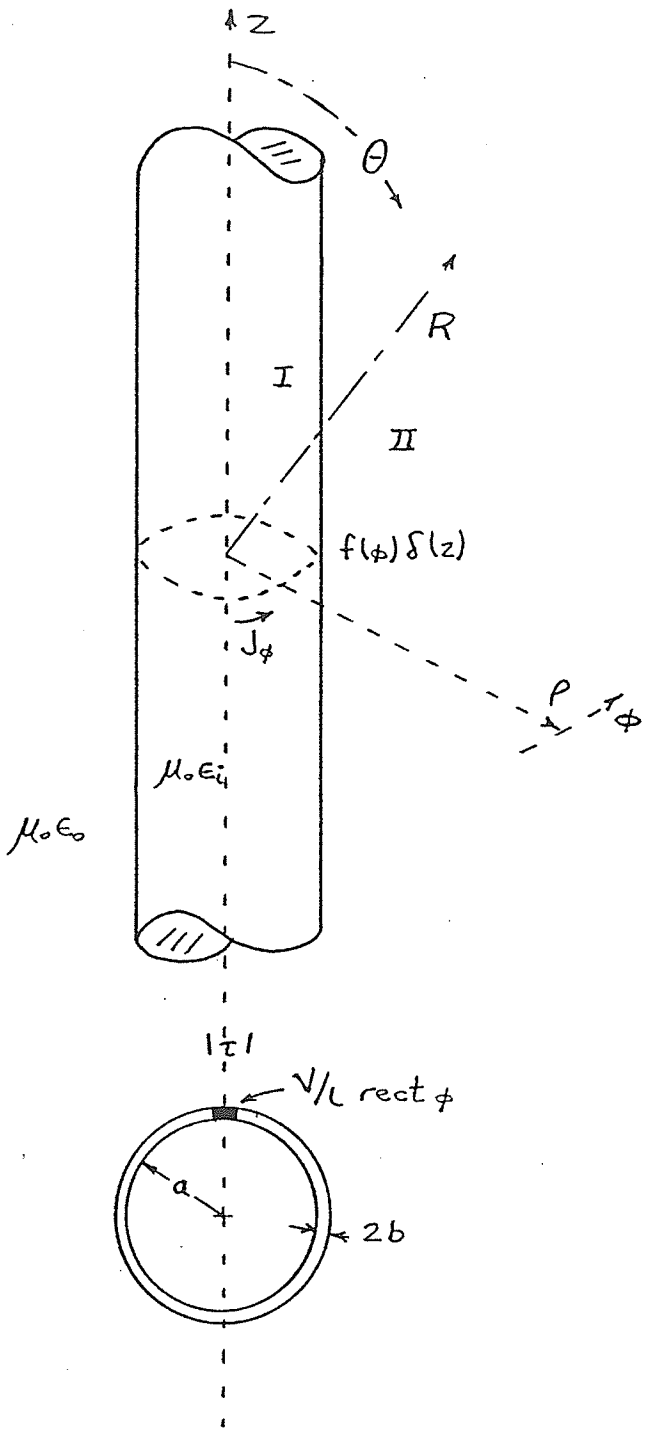

Figure 3.01 Problem Geometry

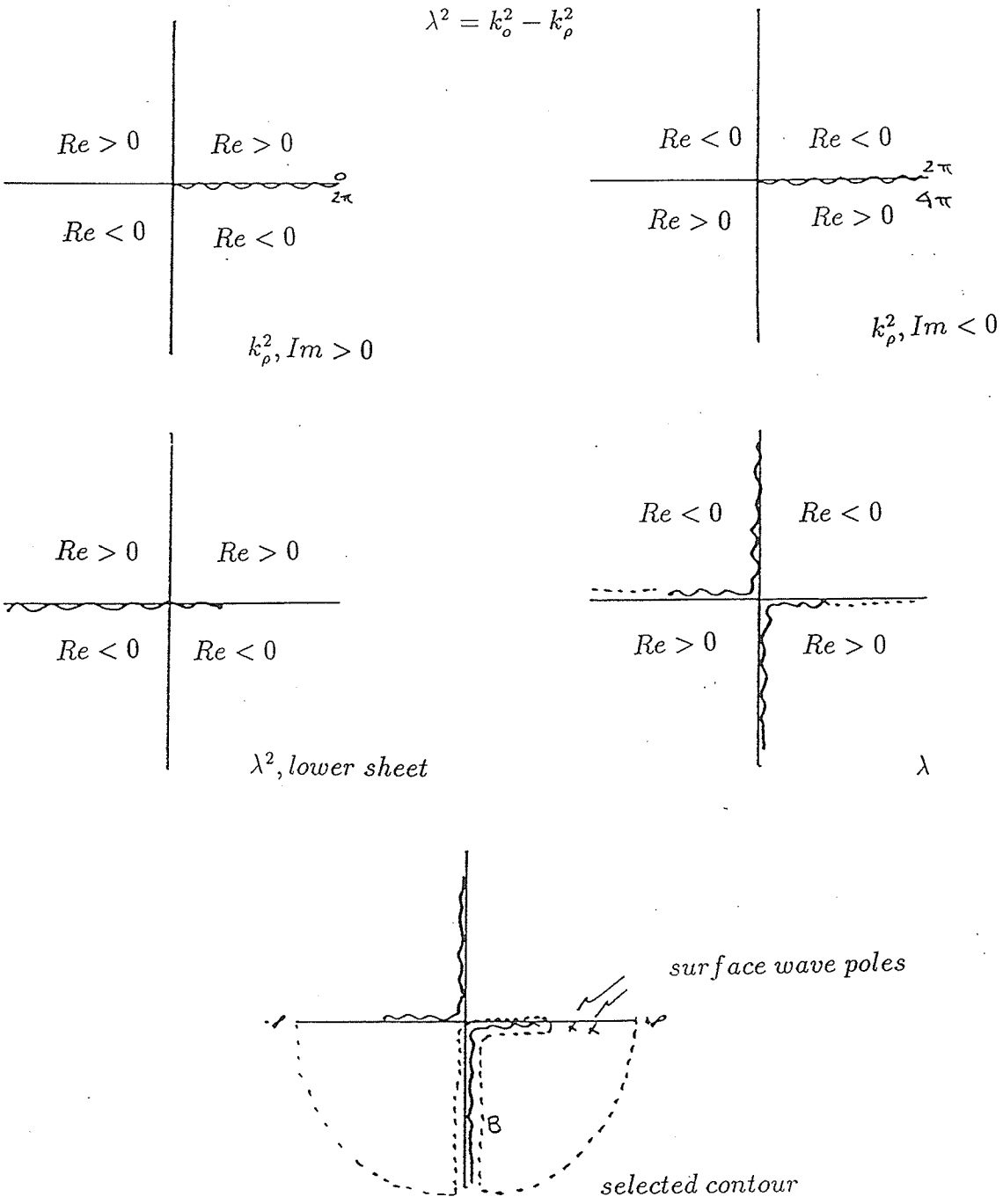

$\int_{-\infty}^{\infty}(\cdot)d\lambda = -2\pi j Res[f, z_i] - \int_B(\cdot)d\lambda$

Figure 3.02 Contour mapping for Integral Evaluation

V satisfy the following scalar homogeneous wave equation for a lossless medium:

$$\left(\nabla^2 + k^2\right) \begin{matrix} U \\ V \end{matrix} = 0 \tag{3.4}$$

where

$$\nabla^2 = \frac{1}{\rho}\frac{\partial}{\partial\rho}\left(\rho\frac{\partial}{\partial\rho}\right) + \frac{1}{\rho^2}\frac{\partial^2}{\partial\phi^2} + \frac{\partial^2}{\partial z^2}$$

and $k^2 = \omega^2\mu\epsilon$.

From the above definitions and the following:

$$\mathbf{E} = \left(-\gamma^2 + grad\ div\ \right)\mathbf{\Pi} - j\omega\mu\ curl\ \mathbf{\Pi}^* \tag{3.5}$$

$$\mathbf{H} = \left(-\gamma^2 + grad\ div\ \right)\mathbf{\Pi}^* + (\sigma + j\omega\epsilon)\ curl\ \mathbf{\Pi} \tag{3.6}$$

a set of equations may be obtained which relate the electric and magnetic field components to the Debye potentials:

$$E_\rho = \frac{\partial^2 U}{\partial\rho\partial z} - \frac{j\omega\mu}{\rho}\frac{\partial V}{\partial\phi} \tag{3.7}$$

$$H_\rho = \frac{\partial^2 V}{\partial\rho\partial z} + \frac{j\omega\epsilon}{\rho}\frac{\partial U}{\partial\phi}$$

$$E_\phi = \frac{1}{\rho}\frac{\partial^2 U}{\partial\phi\partial z} + j\omega\mu\frac{\partial V}{\partial\rho}$$

$$H_\phi = \frac{1}{\rho}\frac{\partial^2 V}{\partial\phi\partial z} - j\omega\epsilon\frac{\partial U}{\partial\rho}$$

$$E_z = \left(k^2 + \frac{\partial^2}{\partial z^2}\right)U$$

$$H_z = \left(k^2 + \frac{\partial^2}{\partial z^2}\right)V$$

From these relations, the potential U may be referred to as the *transverse magnetic* potential and V may be referred to as the *transverse electric* potential.

Solutions for the potential functions are obtained for Region I and Region II, shown in Figure 3.01, by Fourier transforming the wave equations with respect to the axial and azimuthal co-ordinates z and ϕ. The transform with respect to z produces a continuum of eigenvalues. The transform with respect to ϕ produces a denumerably infinite set of eigenvalues because of the periodicity of the structure. This procedure of transforming wave equations with respect to co-ordinates which describe surfaces of separation is very general and may be seen in the solution of many wave equation problems involving open geometries.

A general two dimensional transform pair [112] may be introduced which facilitates the solution of the problem:

$$f(\phi, z) = \sum_{m=-\infty}^{\infty} e^{-jm\phi} \int_{-\infty}^{\infty} g_m(\lambda) e^{-j\lambda z} d\lambda \tag{3.8}$$

$$g_m(\lambda) = \frac{1}{4\pi^2} \int_0^{2\pi} \int_{-\infty}^{\infty} f(\phi, z) e^{j\lambda z} e^{jm\phi} dz d\phi$$

The resulting transformed wave equations for the scalar potentials will be in the form of Bessel's differential equation. Appropriate cylinder functions must be chosen to meet the boundary conditions imposed upon the radial co-ordinate solution. The boundary conditions are, in Region I, the field should appear to be of a standing wave nature and must be finite at $\rho = 0$. In Region II, the field should appear to be of an outward travelling wave nature and must tend to zero as $\rho \to \infty$.

From these considerations, general solutions for the Debye potentials in Region I and Region II may be written as follows:

$$U_I = \sum_{m=-\infty}^{\infty} e^{-jm\phi} \int_{-\infty}^{\infty} A_m^e(\lambda) \mathrm{J}_m(\sqrt{k_i^2 - \lambda^2}\rho) e^{-j\lambda z} d\lambda \tag{3.9}$$

$$V_I = \sum_{m=-\infty}^{\infty} e^{-jm\phi} \int_{-\infty}^{\infty} A_m^h(\lambda) \mathrm{J}_m(\sqrt{k_i^2 - \lambda^2}\rho) e^{-j\lambda z} d\lambda \tag{3.10}$$

$$U_{II} = \sum_{m=-\infty}^{\infty} e^{-jm\phi} \int_{-\infty}^{\infty} B_m^e(\lambda) \mathrm{H}_m^{(2)}(\sqrt{k_o^2 - \lambda^2}\rho) e^{-j\lambda z} d\lambda \tag{3.11}$$

$$V_{II} = \sum_{m=-\infty}^{\infty} e^{-jm\phi} \int_{-\infty}^{\infty} B_m^h(\lambda) \mathrm{H}_m^{(2)}(\sqrt{k_o^2 - \lambda^2}\rho) e^{-j\lambda z} d\lambda \tag{3.12}$$

where U_I and U_{II} are the transverse magnetic potential functions for Region I and Region II respectively. V_I and V_{II} are the transverse electric potential functions for Region I and Region II respectively. The expansion co-efficients $A_m^e(\lambda)$, $A_m^h(\lambda)$, $B_m^e(\lambda)$, and $B_m^h(\lambda)$ are determined from appropriate boundary conditions at $\rho = a$. The superscripts e and h on the co-efficients re-emphasize the connection between each co-efficient and its corresponding potential function. The co-efficients associated with the transverse magnetic potential function U are identified with the superscript e indicating that they are related to the axial component of the electric field. Similarly, the co-efficients associated with the transverse electric potential function V are identified with the superscript h indicating that they are related to the axial component of the magnetic field. $\mathrm{J}_m(\bullet)$ represents Bessel function first kind, $\mathrm{H}_m^{(2)}(\bullet)$ represents Hankel function second kind, k_i and k_o are the wavenumbers for Region I and Region II respectively, and m and λ are the transformation variables associated with the ϕ and z co-ordinates respectively.

Further to the discussion concerning the selection of appropriate cylinder functions to meet the required boundary conditions on the radial co-ordinate, attention must be drawn to the arguments of the Hankel functions which appear in the ex-

pressions for the potential functions, and therefore the expressions for the electromagnetic fields, for Region II. The term $\sqrt{k_o^2 - \lambda^2}$ establishes these arguments as multiple branch complex valued functions of λ where λ itself is also considered to be a complex variable. The radiation boundary condition on the radial co-ordinate is maintained when the Hankel function argument remains on the lower half of its complex plane. A transformation of this restriction to the integration variable λ readily shows that the contour for the integrals in the potential functions must lie on the lower sheet of the double sheet Riemann surface which represents the complex plane for the variable λ. Singularities will be observed along the real axis in the interval defined by $k_i > |\lambda| \geq k_o$. The nature of these singularities is the subject of the investigation of surface wave behaviour. They are mentioned here, however, because of their role in establishing the integration contour.

A recognition of the singularities and branch cuts for the Riemann surfaces in the λ domain leads to two approaches for the evaluation of the Fourier integrals associated with the potential functions and field expressions. The first approach is to integrate along the real λ axis from $-\infty$ to ∞. This involves the determination of the Cauchy Principle Value CPV of the integral and the residue contributions arising from the surface wave singularities. Since the evaluation of the CPV is performed, in general, through numerical quadrature, an estimate of the *tail contribution*, the value of the integral from some large value to infinity, is also required. The second approach involves the transformation of the integration contour along the real λ axis to an integration contour around the branch cuts plus a summation of residues occuring from the singularities. This transformation is accomplished

under Jordan's lemma. The contour is closed in the lower half of the λ complex plane, for $z > 0$, to ensure convergence of the integral as λ approaches infinity. Tamir and Oliner [113],[114] refer to the evaluation of such integrals by this technique as the spectral representation approach. Note that in the second approach a calculation of the integral's CPV is not required. However, a tail contribution estimate is still needed. Figure 3.02 provides a graphical step-by-step development of the integration contour, starting with the restricted Hankel argument domain and leading through to the two approaches discussed here.

For this research effort, the first approach proved to be of greater advantage. As will be seen, the cylinder functions become exponential in behaviour, for $|\lambda| > k_i$ along the real λ axis. This leads to easier calculation and tail contribution estimation. In the second approach, the cylinder functions remain oscillating for large argument values. This leads to greater difficulties in calculating the integrals.

From the solutions for the potential functions, and the foregoing discussion concerning the selection of appropriate integration contour, equations may be obtained for all field components in Region I and Region II:

$$E_{\rho_I} = \sum_{m=-\infty}^{\infty} e^{-jm\phi} \int_{-\infty}^{\infty} \left[A_m^e(\lambda)\Omega_{01} - A_m^h(\lambda)\Omega_{02} \right] e^{-j\lambda z} d\lambda \tag{3.13}$$

$$E_{\rho_{II}} = \sum_{m=-\infty}^{\infty} e^{-jm\phi} \int_{-\infty}^{\infty} \left[B_m^e(\lambda)\Omega_{03} - B_m^h(\lambda)\Omega_{04} \right] e^{-j\lambda z} d\lambda$$

$$H_{\rho_I} = \sum_{m=-\infty}^{\infty} e^{-jm\phi} \int_{-\infty}^{\infty} \left[A_m^h(\lambda)\Omega_{05} + A_m^e(\lambda)\Omega_{06} \right] e^{-j\lambda z} d\lambda$$

$$H_{\rho_{II}} = \sum_{m=-\infty}^{\infty} e^{-jm\phi} \int_{-\infty}^{\infty} \left[B_m^h(\lambda)\Omega_{07} + B_m^e(\lambda)\Omega_{08} \right] e^{-j\lambda z} d\lambda$$

$$E_{\phi_I} = \sum_{m=-\infty}^{\infty} e^{-jm\phi} \int_{-\infty}^{\infty} \left[A_m^h(\lambda)\Omega_{09} - A_m^e(\lambda)\Omega_{10} \right] e^{-j\lambda z} d\lambda$$

$$E_{\phi_{II}} = \sum_{m=-\infty}^{\infty} e^{-jm\phi} \int_{-\infty}^{\infty} \left[B_m^h(\lambda)\Omega_{11} - B_m^e(\lambda)\Omega_{12} \right] e^{-j\lambda z} d\lambda$$

$$H_{\phi_I} = \sum_{m=-\infty}^{\infty} e^{-jm\phi} \int_{-\infty}^{\infty} \left[A_m^e(\lambda)\Omega_{13} - A_m^h(\lambda)\Omega_{14} \right] e^{-j\lambda z} d\lambda$$

$$H_{\phi_{II}} = \sum_{m=-\infty}^{\infty} e^{-jm\phi} \int_{-\infty}^{\infty} \left[B_m^e(\lambda)\Omega_{15} - B_m^h(\lambda)\Omega_{16} \right] e^{-j\lambda z} d\lambda$$

$$E_{z_I} = \sum_{m=-\infty}^{\infty} e^{-jm\phi} \int_{-\infty}^{\infty} A_m^e(\lambda)\Omega_{17} e^{-j\lambda z} d\lambda$$

$$E_{z_{II}} = \sum_{m=-\infty}^{\infty} e^{-jm\phi} \int_{-\infty}^{\infty} B_m^e(\lambda)\Omega_{18} e^{-j\lambda z} d\lambda$$

$$H_{z_I} = \sum_{m=-\infty}^{\infty} e^{-jm\phi} \int_{-\infty}^{\infty} A_m^h(\lambda)\Omega_{17} e^{-j\lambda z} d\lambda$$

$$H_{z_{II}} = \sum_{m=-\infty}^{\infty} e^{-jm\phi} \int_{-\infty}^{\infty} B_m^h(\lambda)\Omega_{18} e^{-j\lambda z} d\lambda$$

As indicated earlier, the expansion co-efficients are determined from the boundary conditions at $\rho = a$. Specifically, the tangential components of the electric field are continuous across the boundary. The axial component of the magnetic field is discontinuous across the boundary by an amount equal to the ϕ component of the surface current distribution on the boundary, which, in this investigation, is the current distribution on the loop antenna.

$$E_{\phi_I} = E_{\phi_{II}} \tag{3.14}$$

$$E_{z_I} = E_{z_{II}}$$

$$H_{\phi_I} = H_{\phi_{II}}$$

$$H_{z_I} - H_{z_{II}} = J_\phi$$

The vector nature of J_ϕ, the current distribution on the loop, is indicated in Figure 3.01.

To facilitate the solution of the expansion co-efficients, a transformed representation for the surface current is introduced:

$$J_\phi(\phi,z) = \sum_{m=-\infty}^{\infty} e^{-jm\phi} \int_{-\infty}^{\infty} \kappa_m(\lambda) e^{-j\lambda z} d\lambda \tag{3.15}$$

$$\kappa_m(\lambda) = \frac{1}{4\pi^2} \int_0^{2\pi} \int_{-\infty}^{\infty} J_\phi(\phi,z) e^{jm\phi} e^{j\lambda z} dz d\phi$$

For the boundary conditions to hold for all values of ϕ and z, the following equations must be satisfield at $\rho = a$.

$$A_m^h(\lambda)\Omega_{09} - A_m^e(\lambda)\Omega_{10} = B_m^h(\lambda)\Omega_{11} - B_m^e(\lambda)\Omega_{12} \tag{3.16}$$

$$A_m^e(\lambda)\Omega_{17} = B_m^h(\lambda)\Omega_{18}$$

$$A_m^e(\lambda)\Omega_{13} - A_m^h(\lambda)\Omega_{14} = B_m^e(\lambda)\Omega_{15} - B_m^h(\lambda)\Omega_{16}$$

$$A_m^h(\lambda)\Omega_{17} - B_m^h(\lambda)\Omega_{18} = \kappa_m(\lambda)$$

As indicated earlier, the current distribution is presumed to be of the form $f(\phi)\delta(z)$. This removes the λ dependance from the variable κ_m.

From this set of simultaneous equations, solutions for the expansion co-efficients may be found as follows:

$$A_m^e(\lambda) = \frac{j\omega\mu_o\kappa_m\Psi_2\left[\Psi_3\Psi_6 - \Psi_4\Psi_5\right]}{\Delta} \tag{3.17}$$

$$A_m^h(\lambda) = \frac{\kappa_m\left[\Psi_6\left(\Psi_2\Psi_4 - \Psi_1\Psi_6\right) - k_o^2\Psi_5\left(\epsilon_r\Psi_2\Psi_3 - \Psi_1\Psi_5\right)\right]}{\Delta}$$

$$B_m^e(\lambda) = \frac{j\omega\mu_o\kappa_m\Psi_1\left[\Psi_3\Psi_6 - \Psi_4\Psi_5\right]}{\Delta}$$

$$B_m^h(\lambda) = \frac{\kappa_m\left[\Psi_4\left(\Psi_2\Psi_4 - \Psi_1\Psi_6\right) - k_o^2\Psi_3\left(\epsilon_r\Psi_2\Psi_3 - \Psi_1\Psi_5\right)\right]}{\Delta}$$

where

$$\Delta = k_o^2 \left[\epsilon_r \Psi_2 \Psi_3 - \Psi_1 \Psi_5\right] \left[\Psi_2 \Psi_3 - \Psi_1 \Psi_5\right] + \left[\Psi_2 \Psi_4 - \Psi_1 \Psi_6\right] \left[\Psi_1 \Psi_6 - \Psi_2 \Psi_4\right]$$

For $k_o \geq \lambda$

$$\begin{aligned}
\Psi_1 &= (k_i^2 - \lambda^2) \mathrm{J}_m(\sqrt{k_i^2 - \lambda^2}a) \\
\Psi_2 &= (k_o^2 - \lambda^2) \mathrm{H}_m^{(2)}(\sqrt{k_o^2 - \lambda^2}a) \\
\Psi_3 &= \frac{1}{2}\sqrt{k_i^2 - \lambda^2} \left[\mathrm{J}_{m-1}(\sqrt{k_i^2 - \lambda^2}a) - \mathrm{J}_{m+1}(\sqrt{k_i^2 - \lambda^2}a)\right] \\
\Psi_4 &= \frac{m\lambda}{a} \mathrm{J}_m(\sqrt{k_i^2 - \lambda^2}a) \\
\Psi_5 &= \frac{1}{2}\sqrt{k_o^2 - \lambda^2} \left[\mathrm{H}_{m-1}^{(2)}(\sqrt{k_o^2 - \lambda^2}a) - \mathrm{H}_{m+1}^{(2)}(\sqrt{k_o^2 - \lambda^2}a)\right] \\
\Psi_6 &= \frac{m\lambda}{a} \mathrm{H}_m^{(2)}(\sqrt{k_o^2 - \lambda^2}a) \\
\Omega_{01} &= \Omega_{05} = \frac{-j\lambda}{2}\sqrt{k_i^2 - \lambda^2} \left[\mathrm{J}_{m-1}(\sqrt{k_i^2 - \lambda^2}\rho) - \mathrm{J}_{m+1}(\sqrt{k_i^2 - \lambda^2}\rho)\right] \\
\Omega_{02} &= \frac{\omega\mu_o m}{\rho} \mathrm{J}_m(\sqrt{k_i^2 - \lambda^2}\rho) \\
\Omega_{03} &= \Omega_{07} = \frac{-j\lambda}{2}\sqrt{k_o^2 - \lambda^2} \left[\mathrm{H}_{m-1}^{(2)}(\sqrt{k_o^2 - \lambda^2}\rho) - \mathrm{H}_{m+1}^{(2)}(\sqrt{k_o^2 - \lambda^2}\rho)\right] \\
\Omega_{04} &= \frac{\omega\mu_o m}{\rho} \mathrm{H}_m^{(2)}(\sqrt{k_o^2 - \lambda^2}\rho) \\
\Omega_{06} &= \frac{\omega\epsilon_i m}{\rho} \mathrm{J}_m(\sqrt{k_i^2 - \lambda^2}\rho) \\
\Omega_{08} &= \frac{\omega\epsilon_o m}{\rho} \mathrm{H}_m^{(2)}(\sqrt{k_o^2 - \lambda^2}\rho) \\
\Omega_{09} &= \frac{j\omega\mu_o}{2}\sqrt{k_i^2 - \lambda^2} \left[\mathrm{J}_{m-1}(\sqrt{k_i^2 - \lambda^2}\rho) - \mathrm{J}_{m+1}(\sqrt{k_i^2 - \lambda^2}\rho)\right] \\
\Omega_{10} &= \Omega_{14} = \frac{m\lambda}{\rho} \mathrm{J}_m(\sqrt{k_i^2 - \lambda^2}\rho) \\
\Omega_{11} &= \frac{j\omega\mu_o}{2}\sqrt{k_o^2 - \lambda^2} \left[\mathrm{H}_{m-1}^{(2)}(\sqrt{k_o^2 - \lambda^2}\rho) - \mathrm{H}_{m+1}^{(2)}(\sqrt{k_o^2 - \lambda^2}\rho)\right] \\
\Omega_{12} &= \Omega_{16} = \frac{m\lambda}{\rho} \mathrm{H}_m^{(2)}(\sqrt{k_o^2 - \lambda^2}\rho) \\
\Omega_{13} &= \frac{-j\omega\epsilon_i}{2}\sqrt{k_i^2 - \lambda^2} \left[\mathrm{J}_{m-1}(\sqrt{k_i^2 - \lambda^2}\rho) - \mathrm{J}_{m+1}(\sqrt{k_i^2 - \lambda^2}\rho)\right]
\end{aligned}$$

$$\Omega_{15} = \frac{-j\omega\epsilon_o}{2}\sqrt{k_o^2-\lambda^2}\left[\mathrm{H}^{(2)}_{m-1}(\sqrt{k_o^2-\lambda^2}\rho) - \mathrm{H}_{m+1}(\sqrt{k_o^2-\lambda^2}\rho)\right]$$

$$\Omega_{17} = (k_i^2-\lambda^2)\mathrm{J}_m(\sqrt{k_i^2-\lambda^2}\rho)$$

$$\Omega_{18} = (k_o^2-\lambda^2)\mathrm{H}^{(2)}_m(\sqrt{k_o^2-\lambda^2}\rho)$$

For $\lambda > k_o$, terms which contain Hankel functions, second kind, are modified as follows:

$$\Psi_2 = -\frac{2}{\pi}j^{m+1}(\lambda^2-k_o^2)\mathrm{K}_m(\sqrt{\lambda^2-k_o^2}a)$$

$$\Psi_5 = -\frac{1}{\pi}j^{m+1}\sqrt{\lambda^2-k_o^2}\left[\mathrm{K}_{m-1}(\sqrt{\lambda^2-k_o^2}a) + \mathrm{K}_{m+1}(\sqrt{\lambda^2-k_o^2}a)\right]$$

$$\Psi_6 = j^{m+1}\frac{2m\lambda}{\pi a}\mathrm{K}_m(\sqrt{\lambda^2-k_o^2}a)$$

$$\Omega_{03} = \Omega_{07} = -\frac{\lambda}{\pi}j^m\sqrt{\lambda^2-k_o^2}\left[\mathrm{K}_{m-1}(\sqrt{\lambda^2-k_o^2}\rho) + \mathrm{K}_{m+1}(\sqrt{\lambda^2-k_o^2}\rho)\right]$$

$$\Omega_{04} = j^{m+1}\frac{2m\omega\mu_o}{\pi\rho}\mathrm{K}_m(\sqrt{\lambda^2-k_o^2}\rho)$$

$$\Omega_{08} = j^{m+1}\frac{2m\omega\epsilon_o}{\pi\rho}\mathrm{K}_m(\sqrt{\lambda^2-k_o^2}\rho)$$

$$\Omega_{11} = \frac{\omega\mu_o}{\pi}j^m\sqrt{\lambda^2-k_o^2}\left[\mathrm{K}_{m-1}(\sqrt{\lambda^2-k_o^2}\rho) + \mathrm{K}_{m+1}(\sqrt{\lambda^2-k_o^2}\rho)\right]$$

$$\Omega_{12} = \Omega_{16} = j^{m+1}\frac{2m\lambda}{\pi\rho}\mathrm{K}_m(\sqrt{\lambda^2-k_o^2}\rho)$$

$$\Omega_{15} = -\frac{\omega\epsilon_o}{\pi}j^m\sqrt{\lambda^2-k_o^2}\left[\mathrm{K}_{m-1}(\sqrt{\lambda^2-k_o^2}\rho) + \mathrm{K}_{m+1}(\sqrt{\lambda^2-k_o^2}\rho)\right]$$

$$\Omega_{18} = -\frac{2}{\pi}j^{m+1}(\lambda^2-k_o^2)\mathrm{K}_m(\sqrt{\lambda^2-k_o^2}\rho)$$

For $\lambda > k_i$, terms which contain Bessel functions, first kind, are modified as follows:

$$\Psi_1 = j^m(-1)^{m+1}(\lambda^2-k_i^2)\mathrm{I}_m(\sqrt{\lambda^2-k_i^2}a)$$

$$\Psi_3 = \frac{1}{2}j^m(-1)^m\sqrt{\lambda^2-k_i^2}\left[\mathrm{I}_{m-1}(\sqrt{\lambda^2-k_i^2}a) + \mathrm{I}_{m+1}(\sqrt{\lambda^2-k_i^2}a)\right]$$

$$\Psi_4 = \frac{m\lambda}{a}j^m(-1)^m\mathrm{I}_m\sqrt{\lambda^2-k_i^2}a)$$

$$\Omega_{01} = \Omega_{05} = \frac{\lambda}{2}j^{m+1}(-1)^{m+1}\sqrt{\lambda^2-k_i^2}\left[\mathrm{I}_{m-1}(\sqrt{\lambda^2-k_i^2}\rho) + \mathrm{I}_{m+1}(\sqrt{\lambda^2-k_i^2}\rho)\right]$$

$$
\begin{aligned}
\Omega_{02} &= \frac{m\omega\mu_o}{\rho} j^m (-1)^m \mathrm{I}_m(\sqrt{\lambda^2 - k_i^2}\rho) \\
\Omega_{06} &= \frac{m\omega\epsilon_i}{\rho} j^m (-1)^m \mathrm{I}_m(\sqrt{\lambda^2 - k_i^2}\rho) \\
\Omega_{09} &= \frac{\omega\mu_o}{2} j^{m+1} (-1)^m \sqrt{\lambda^2 - k_i^2} \left[\mathrm{I}_{m-1}(\sqrt{\lambda^2 - k_i^2}\rho) + \mathrm{I}_{m+1}(\sqrt{\lambda^2 - k_i^2}\rho) \right] \\
\Omega_{10} &= \Omega_{14} = \frac{m\lambda}{\rho} j^m (-1)^m \mathrm{I}_m(\sqrt{\lambda^2 - k_i^2}\rho) \\
\Omega_{13} &= \frac{\omega\epsilon_i}{2} j^{m+1} (-1)^{m+1} \sqrt{\lambda^2 - k_i^2} \left[\mathrm{I}_{m-1}(\sqrt{\lambda^2 - k_i^2}\rho) + \mathrm{I}_{m+1}(\sqrt{\lambda^2 - k_i^2}\rho) \right] \\
\Omega_{17} &= j^m (-1)^{m+1} (\lambda^2 - k_i^2) \mathrm{I}_m(\sqrt{\lambda^2 - k_i^2}\rho)
\end{aligned}
$$

$\mathrm{I}_m(\bullet)$ and $\mathrm{K}_m(\bullet)$ are modified Bessel functions, first and second kind, respectively.

Input Impedance and Current Distribution

The calculation of input impedance and current distribution for the loop antenna follows a general integral equation procedure. An equation is formulated which relates the ϕ component of the electric field to the ϕ directed current distribution on the antenna. The equation for $E_{\phi_{II}}$ from (3.13), at $z = 0$, is employed:

$$
E_{\phi_{II}} = \sum_{m=-\infty}^{\infty} e^{-jm\phi} \int_{-\infty}^{\infty} \left[B_m^h(\lambda)\Omega_{11} - B_m^e(\lambda)\Omega_{12} \right] d\lambda \tag{3.18}
$$

As may be seen in (3.17), the λ independant variable κ_m appears in both terms $B_m^h(\lambda)$ and $B_m^e(\lambda)$. This term may be taken outside the integral to obtain a generalized expression:

$$
E_{\phi_{II}} = \sum_{m=-\infty}^{\infty} e^{-jm\phi} \kappa_m \int_{-\infty}^{\infty} \mathcal{I}(\lambda) d\lambda \tag{3.19}
$$

This expression may now be employed to relate the electric field on the surface of the antenna's conductor to the current on the central axis of the antenna's conductor.

Further, the electric field may be represented as a Fourier series:

$$E_\phi(\phi) = \sum_{m=-\infty}^{\infty} \chi_m e^{-jm\phi} \tag{3.20}$$

$$\chi_m = \frac{1}{2\pi}\int_0^{2\pi} E_\phi(\phi) e^{jm\phi} d\phi$$

Equation (3.20) then becomes:

$$\sum_{m=-\infty}^{\infty} \chi_m e^{-jm\phi} = \sum_{m=-\infty}^{\infty} \kappa_m \mathcal{Z}_m e^{-jm\phi} \tag{3.21}$$

The well known orthogonality of these functions in ϕ allows the introduction of the modal parameters χ_m as modal voltage, κ_m as modal current, and $\mathcal{Z}_m$ as modal impedance. These parameters are related as follows:

$$\kappa_m = \frac{\chi_m}{\mathcal{Z}_m} \tag{3.22}$$

where $\mathcal{Z}_m = \int_{-\infty}^{\infty} \mathcal{I}(\lambda) d\lambda$ as shown in (3.19). For the present investigation, a 1.0 volt rectangular pulse function was taken as the antenna's excitation. Therefore:

$$E_\phi(\phi) = \frac{\mathcal{V}}{l} rect(\phi) \tag{3.23}$$

where $\mathcal{V}$ is the 1.0 volt excitation, l is the length of the rectangular function, and the rectangular function itself is taken from $\phi = -2.5°$ to $+2.5°$, as shown in Figure 3.01. The modal voltage for the present investigation may be defined as follows:

$$\begin{aligned} \chi_m &= \tfrac{\tau}{2\pi l} \qquad m = 0 \\ \chi_m &= \tfrac{\sin m(\frac{\tau}{2})}{lm\pi} \qquad m \neq 0 \end{aligned} \tag{3.24}$$

where τ is the angular extent of the function, 0.0873 radians.

From the preceeding discussion, the modal current amplitudes, κ_m, as determined in (3.22), may now be used to compute the current distribution on the loop

through (3.15). The input impedance for the antenna is determined simply:

$$\mathcal{Z}_{in} = \left.\frac{\mathcal{V}}{J_\phi}\right|_{\phi=0} \tag{3.25}$$

The evaluation of the modal impedance terms $\mathcal{Z}_m$ requires careful consideration. As indicated previously, singularities exist along the integration contour between $|\lambda| = k_o$ and $|\lambda| = k_i$. These singularities result from the excitation of hybrid mode surface waves. The integral may be written in the form:

$$\mathcal{Z}_m = P.V. \int_{-\infty}^{\infty} \mathcal{I}(\lambda) d\lambda \quad \pm \quad j\pi Res\left[\mathcal{I}(\lambda), \lambda_o\right] \tag{3.26}$$

where the plus sign on the residue term is taken for $\lambda < 0$ and the minus sign for $\lambda > 0$. $\mathcal{I}$ is defined in (3.19). The selection of the plus/minus sign results from the sense in which the pole is circled on the integration contour. This detail is shown in Figure 3.02. λ_o represents the singularity due to the surface wave and *P.V.* represents Cauchy Principle Value. The locations of the singularities between k_o and k_i may be obtained through the solution of the eigenvalue equation represented by the term Δ in (3.17). By setting $\Delta = 0$, an equation, originally presented by Elsasser [91], may be obtained. Solutions for this equation represent the propagation velocities of the various hybrid mode surface waves. Cutoff conditions for these waves have been studied by Biernson and Kinsley [98]. The cutoff conditions are as follows:

$$\begin{array}{lll} \mathrm{TE}_{0m}/\mathrm{TM}_{0m} & \mathrm{J}_0(\alpha_m) = 0 & \\ \mathrm{EH}_{nm} & \mathrm{J}_n(\alpha_m) = 0 & \alpha_m > 0 \\ \mathrm{HE}_{1m} & \mathrm{J}_1(\alpha_m) = 0 & \\ \mathrm{HE}_{nm} & \mathrm{J}_{n-2}(\alpha_m) = 0 \quad n \geq 2, & \alpha_m > 0 \end{array} \tag{3.27}$$

where the α_m are the eigenvalues of the associated Bessel functions. Note that the HE_{11} surface wave is presumed to have a zero cutoff condition implying that it may be excited on an infinitely small dielectric cylinder.

The evaluation of the residue term is easily accomplished with the aid of L'Hopital's rule and may be written as follows:

$$Res\left[\mathcal{I}(\lambda), \lambda_o\right] = \left.\frac{N(\lambda)}{D'(\lambda)}\right|_{\lambda=\lambda_o} \tag{3.28}$$

where $N(\lambda)$ and $D(\lambda)$ are the numerator and denominator of the modal impedance kernal. The prime indicates differentiation with respect to λ.

The denominator of the modal impedance kernal is the term Δ described above. Its derivative with respect to λ may be obtained through successive applications of the chain rule.

$$D'(\lambda) = k_o^2(\xi_1\xi_2 + \xi_3\xi_4) + \xi_5\xi_6 + \xi_7\xi_8 \tag{3.29}$$

where

$$\begin{aligned}
\xi_1 &= \epsilon_r\Psi_2\Psi_3 - \Psi_1\Psi_5 \\
\xi_2 &= \Psi_2\Psi_3' + \Psi_2'\Psi_3 - \Psi_1\Psi_5' - \Psi_1'\Psi_5 \\
\xi_3 &= \epsilon_r\Psi_2\Psi_3' + \epsilon_r\Psi_2'\Psi_3 - \Psi_1\Psi_5' - \Psi_1'\Psi_5 \\
\xi_4 &= \Psi_2\Psi_3 - \Psi_1\Psi_5 \\
\xi_5 &= \Psi_2\Psi_4 - \Psi_1\Psi_6 \\
\xi_6 &= \Psi_1\Psi_6' + \Psi_1'\Psi_6 - \Psi_2\Psi_4' - \Psi_2'\Psi_4 \\
\xi_7 &= \Psi_2\Psi_4' + \Psi_2'\Psi_4 - \Psi_1\Psi_6' - \Psi_1'\Psi_6 \\
\xi_8 &= \Psi_1\Psi_6 - \Psi_2\Psi_4
\end{aligned}$$

where the prime indicates differentiation with respect to λ. The terms $\Psi_i,\ i = 1 \ldots 6$ may be found in (3.17). The derivatives of these terms with respect to λ are required only for the region $k_o < |\lambda| < k_i$ and may be written as follows:

$$\begin{aligned}
\Psi_1' &= -\frac{\lambda a}{2}\sqrt{k_i^2-\lambda^2}\left[\mathrm{J}_{m-1}(\sqrt{k_i^2-\lambda^2}a) - \mathrm{J}_{m+1}(\sqrt{k_i^2-\lambda^2}a)\right] - 2\lambda \mathrm{J}_m(\sqrt{k_i^2-\lambda^2}a) \\
\Psi_2' &= j^{m+1}\frac{\lambda a}{\pi}\sqrt{\lambda^2-k_o^2}\left[\mathrm{K}_{m-1}(\sqrt{\lambda^2-k_o^2}a) + \mathrm{K}_{m+1}(\sqrt{\lambda^2-k_o^2}a)\right] \\
&\quad -\frac{2\lambda}{\pi}\mathrm{K}_m(\sqrt{\lambda^2-k_o^2}a) \\
\Psi_3' &= \frac{\lambda a}{4}\left[2\mathrm{J}_m(\sqrt{k_i^2-\lambda^2}a) - \mathrm{J}_{m-2}(\sqrt{k_i^2-\lambda^2}a) - \mathrm{J}_{m+2}(\sqrt{k_i^2-\lambda^2}a)\right] \\
&\quad -\frac{\lambda}{2\sqrt{k_i^2-\lambda^2}}\left[\mathrm{J}_{m-1}(\sqrt{k_i^2-\lambda^2}a) - \mathrm{J}_{m+1}(\sqrt{k_i^2-\lambda^2}a)\right] \\
\Psi_4' &= \frac{m}{a}\left[\mathrm{J}_m(\sqrt{k_i^2-\lambda^2}a) - \frac{a\lambda^2}{2\sqrt{k_i^2-\lambda^2}}\left[\mathrm{J}_{m-1}(\sqrt{k_i^2-\lambda^2}a) - \mathrm{J}_{m+1}(\sqrt{k_i^2-\lambda^2}a)\right]\right] \\
\Psi_5' &= \frac{1}{\pi}j^{m+1}\left[\frac{a\lambda}{2}\left[2\mathrm{K}_m(\sqrt{\lambda^2-k_o^2}a) + \mathrm{K}_{m-2}(\sqrt{\lambda^2-k_o^2}a) + \mathrm{K}_{m+2}(\sqrt{\lambda^2-k_o^2}a)\right]\right. \\
&\quad \left. -\frac{\lambda}{\sqrt{\lambda^2-k_o^2}}\left[\mathrm{K}_{m-1}(\sqrt{\lambda^2-k_o^2}a) + \mathrm{K}_{m+1}(\sqrt{\lambda^2-k_o^2}a)\right]\right] \\
\Psi_6' &= j^{m+1}\frac{2m}{\pi a}\left[\mathrm{K}_m(\sqrt{\lambda^2-k_o^2}a)\right. \\
&\quad \left. -\frac{a\lambda^2}{2\sqrt{\lambda^2-k_o^2}}\left[\mathrm{K}_{m-1}(\sqrt{\lambda^2-k_o^2}a) + \mathrm{K}_{m+1}(\sqrt{\lambda^2-k_o^2}a)\right]\right]
\end{aligned}$$

The convergence of the modal impedance integral is verified by obtaining a large argument approximation, or tail contribution, for the *P.V.* (See Appendix A). The tail contribution may be seen to take the form

$$\mathcal{Z}_{m,tail} = \mathcal{T}\int_{-\infty}^{\infty}\frac{e^{-\lambda(\rho-a)}}{\lambda}d\lambda \tag{3.30}$$

where

$$\mathcal{T} = \frac{\omega\mu_o}{\sqrt{\rho a}}\left[\frac{-ja}{2} + \frac{jm^2}{(\epsilon_r+1)k_o^2\rho}\right]$$

This is the well known exponential integral. Tabulated values for this function appear in the literature [115]. It is interesting to note the location of the term $(\rho - a)$ in the above equation. The thickness of the loop conductor establishes the rate of convergence of the modal impedance kernel as $\lambda \to \infty$.

The contribution made by surface wave excitation and space wave radiation to the real component of the loop's input impedance is of interest in this research. The real component of the *P.V.* result represents the contribution made by the space wave radiation and the residue result represents the contribution made by surface wave excitation.

In discussing surface wave excitation, it is interesting to note that an expansion of the modal impedance kernel, for $m = 0$, verifies that the antenna is not capable of exciting the zero order transverse magnetic modes TM_{0m}. For arbitrary m, the modal impedance kernel may be expanded as follows:

$$\mathcal{I}(\lambda) = \frac{j\omega\mu_o \left[\zeta_1 \left[\Psi_4(\Psi_2\Psi_4 - \Psi_1\Psi_6) - k_o^2\Psi_3(\epsilon_r\Psi_2\Psi_3 - \Psi_1\Psi_5)\right] - \zeta_2\Psi_1\left[\Psi_3\Psi_6 - \Psi_4\Psi_5\right]\right]}{\Delta} \tag{3.31}$$

where

$$\begin{aligned} \zeta_1 &= \frac{1}{2}\sqrt{k_o^2 - \lambda^2}\left[\mathrm{H}_{m-1}^{(2)}(\sqrt{k_o^2 - \lambda^2}\rho) - \mathrm{H}_{m+1}^{(2)}(\sqrt{k_o^2 - \lambda^2}\rho)\right] \\ \zeta_2 &= \frac{m\lambda}{\rho}\mathrm{H}_m^{(2)}(\sqrt{k_o^2 - \lambda^2}\rho) \end{aligned}$$

and the other terms are defined in (3.17). For $m = 0$, the terms Ψ_4, Ψ_6 and ζ_2 are equal to zero. Therefore, (3.31) becomes:

$$\mathcal{I}(\lambda) = \frac{-j\omega\mu_o\zeta_1 k_o^2\Psi_3(\epsilon_r\Psi_2\Psi_3 - \Psi_1\Psi_5)}{k_o^2(\epsilon_r\Psi_2\Psi_3 - \Psi_1\Psi_5)(\Psi_2\Psi_3 - \Psi_1\Psi_5)} \tag{3.32}$$

which may be further reduced to

$$\mathcal{I}(\lambda) = \frac{-j\omega\mu_o\zeta_1\Psi_3}{\Psi_2\Psi_3 - \Psi_1\Psi_5} \tag{3.33}$$

The denominator of (3.33) may be readily cast into the eigenvalue equation for the transverse electric TE_{0m} modes, as seen in [95]. This result may be verified by examining the zero order field structure in the vicinity of the antenna. The z and ρ components of the magnetic field and the ϕ component of the electric field will exist due to the given current distribution. These field components comprise a transverse electric propagating wave. The existance of the z component of the magnetic field eliminates a transverse magnetic travelling wave.

For the special case of determining the input impedance of the antenna when the cylinder's dielectric constant $\epsilon_r = 1.0$, the free space condition, a simplification of the modal impedance kernel provides a slightly improved algorithm with respect to computation time. This simplification again comes from the expansion of the modal impedance kernel and the invocation of a Wronskian relation in its denominator. When $\epsilon_r = 1.0$, (3.31) becomes:

$$\mathcal{I}(\lambda) = \frac{j\omega\mu_o\left[\zeta_1\left[\Psi_4(\Psi_2\Psi_4 - \Psi_1\Psi_6) - k_o^2\Psi_3(\Psi_2\Psi_3 - \Psi_1\Psi_5)\right] - \zeta_2\Psi_1\left[\Psi_3\Psi_6 - \Psi_4\Psi_5\right]\right]}{\Delta} \tag{3.34}$$

where Δ is modified as follows:

$$\Delta = k_o^2\left[\Psi_2\Psi_3 - \Psi_1\Psi_5\right]^2 - \left[\Psi_2\Psi_4 - \Psi_1\Psi_6\right]^2$$

Through the use of the Wronskian [115]:

$$\mathrm{J}_{m-1}(\bullet)\mathrm{H}_m^{(2)}(\bullet) - \mathrm{J}_m(\bullet)\mathrm{H}_{m-1}^{(2)}(\bullet) = \frac{j2}{\pi z}$$

the following reductions are obtained:

$$\begin{aligned}
[\Psi_2\Psi_4 - \Psi_1\Psi_6] &= 0 \\
[\Psi_2\Psi_3 - \Psi_1\Psi_5] &= \frac{j2(k_o^2 - \lambda^2)}{\pi a} \\
[\Psi_3\Psi_6 - \Psi_4\Psi_5] &= \frac{j2m\lambda}{\pi a^2}
\end{aligned}$$

A substitution of the above reductions into (3.34) yields a *free space* modal impedance kernel:

$$\mathcal{I}(\lambda)_{free\ space} = \frac{-\pi a\omega\mu_o \left[k_o^2\zeta_1\Psi_3(k_o^2 - \lambda^2) + \frac{m\lambda}{a}\zeta_2\Psi_1\right]}{2k_o^2(k_o^2 - \lambda^2)^2} \tag{3.35}$$

Surface Wave Characteristics

The electromagnetic fields resulting from the current distribution on the antenna consist of two major components. The first component is related to radiation and its associated near field structure. The second component is related to surface wave excitation. As with the modal impedance calculations, which essentially considered the ϕ vector component of the electric field in Region II, these two components are readily identified in the calculation of the fields. The first component arises from a calculation of the *C.P.V.* of the field expression and the second component arises from the evaluation of the residues from the field expressions when $\Delta = 0$.

The surface wave fields may be evaluated from a generalized expression for the residue term:

$$\mathcal{F}_{surface} = -2\pi j \sum_{m=-M}^{M} e^{-jm\phi} \sum_{p=0}^{P} \frac{N(\lambda)}{D'(\lambda)}\bigg|_{\lambda=\lambda_{m,p}} \tag{3.36}$$

where $\mathcal{F}_{surface}$ represents the total electromagnetic surface wave field vector component under consideration. $\mathcal{F}_{surface}$ is the sum of the fields resulting from the

excitation of all $m \times p$ surface waves which can exist for the given geometry. $N(\lambda)$ and $D(\lambda)$ are the associated numerator and denominator of the field expression. The prime denotes differentiation with respect to λ. $\lambda_{m,p}$ denotes the particular surface wave pole at which the residue is calculated. Cutoff conditions for surface waves under given geometries are provided in (3.27). These cutoff conditions establish values for M and P.

Surface wave power may be determined through an evaluation of the Poynting vector over a cross-sectional plane at $z = z_o$.

$$P_{surface} = \frac{1}{2} Re \left[\int_0^{2\pi} \int_0^a (E_{\rho_I} H^*_{\phi_I} - E_{\phi_I} H^*_{\rho_I}) \rho d\rho d\phi \quad + \right. \tag{3.37}$$

$$\left. \int_0^{2\pi} \int_a^{\infty} (E_{\rho_{II}} H^*_{\phi_{II}} - E_{\phi_{II}} H^*_{\rho_{II}}) \rho d\rho d\phi \right]$$

where E_{ρ_I}, $E_{\rho_{II}}$, E_{ϕ_I}, $E_{\phi_{II}}$, H_{ρ_I}, $H_{\rho_{II}}$, H_{ϕ_I}, and $H_{\phi_{II}}$ are the surface wave field components for Region I and Region II, obtained from (3.36). Re denotes real part of a complex variable and the asterisk denotes complex conjugate.

Radiation Characteristics

The radiation characteristics of a loop antenna mounted on an infinitely long dielectric circular cylinder are determined from the Region II field components. Further, since E_z, E_ϕ, H_z, and H_ϕ contribute to radial power propagation, they are the only components which require consideration.

Far field equations are obtained using a technique commonly referred to as the method of steepest descent or saddle point method. This technique is employed in an approximate sense to determine the θ and ϕ spherical co-ordinate components of

the radiated electric and magnetic fields from the cylindrical co-ordinate tangential field expressions.

Appendix B contains a full development for the far field equations. The equations themselves are presented here:

$$E_{\theta_{II}} = \frac{-2jk_o^2 \sin\theta e^{-jk_oR}}{R} \sum_{m=-\infty}^{\infty} B_m^e(k_o \cos\theta) e^{-jm(\phi-\frac{\pi}{2})} \tag{3.38}$$

$$H_{\theta_{II}} = \frac{-2jk_o^2 \sin\theta e^{-jk_oR}}{R} \sum_{m=-\infty}^{\infty} B_m^h(k_o \cos\theta) e^{-jm(\phi-\frac{\pi}{2})} \tag{3.39}$$

$$E_{\phi_{II}} = \frac{2jk_o e^{-jk_oR}}{R} \sum_{m=-\infty}^{\infty} \left[\omega\mu_o B_m^h(k_o\cos\theta)\sin\theta - \frac{m\cos\theta}{R\sin\theta} B_m^e(k_o\cos\theta)\right] e^{-jm(\phi-\frac{\pi}{2})} \tag{3.40}$$

$$H_{\phi_{II}} = \frac{-2jk_o e^{-jk_oR}}{R} \sum_{m=-\infty}^{\infty} \left[\omega\epsilon_o B_m^e(k_o\cos\theta)\sin\theta - \frac{m\cos\theta}{R\sin\theta} B_m^h(k_o\cos\theta)\right] e^{-jm(\phi-\frac{\pi}{2})} \tag{3.41}$$

Chapter 4

Input Impedance and Current Distribution

The input impedance and current distribution characteristics for a number of loop antenna geometries have been evaluated from the formulation presented in Chapter 3. For each case of cylinder dielectric constant, $\epsilon_r = 1.0$, 2.56, 5.6, and 9.0, two sets of input impedance data were computed. The first data set was for loop parameter $\Omega = 10$ and the second data set was for loop parameter $\Omega = 12$. Because of the extensive computer time required for the modal impedance calculations, only twenty values of input impedance were obtained for each data set, over a range of normalized loop circumference C/λ_o from 0.1 to 2.0.

The evaluation of the loop antenna's input impedance involved a four stage process. First, all eigenvalues for the surface wave modes were determined from (3.17) $\Delta = 0$ through a direct search technique. Next, for a given geometry, modal impedance terms were calculated from (3.21). Twenty terms of the Fourier series

expansion in ϕ, $-19 < m < 19$, were calculated for each data point in order to verify convergence. Twenty terms proved to be more than satisfactory as will be seen in the following results. As indicated by (3.36), the modal impedance terms were calculated in two parts. The Cauchy Principle Value was evaluated using Simpson's rule numerical quadrature. The upper limit for the numerical evaluation of the CPV was determined with the aid of (3.30). An arbitrarily large value of λ was selected which would yield a negligible tail contribution. This value was then used in an evaluation of the integrand for confirmation. After confirmation, the upper limit was employed in the actual calculation of the modal impedance term. An approximation to the value of the CPV integral in the vicinity of a singularity was obtained by first finding values of λ which effectively straddled the singularity and then using these values of λ in a trapezoidal rule numerical quadrature. Note that these values of λ did not, in general, correspond to the sample points generated by the Simpson's rule procedure. Therefore, this small modification was employed. Other numerical quadrature techniques were tested for the evaluation of the CPV. However, these alternate methods, such as the Gauss method, did not prove to be of any great advantage. Because of this, the well proven Simpson technique was employed for all calculations.

Appropriate eigenvalue results were then employed to calculate residue contributions to the modal impedance terms, through (3.28). Complete modal impedance values were then employed in (3.22), along with (3.24), to obtain modal current amplitudes. The current distribution on the antenna was obtained through (3.15) and the input impedance through (3.25).

Figure 4.01 illustrates the input impedance of a loop antenna in free space $\epsilon_r = 1.0$. Twenty data points are provided for each of the two cases $\Omega = 10$ and $\Omega = 12$, over a range of normalized circumference C/λ_o of 0.1 to 2.0. The impedance results are displayed as separate resistive and reactive components following a convention employed by Smith. The results from the present formulation are compared to results published by Smith [116]. Excellent agreement is observed between the two cases. The dashed lines on both the resistance and reactance curves indicate the presumed general behaviour of the input impedance for the given geometries. This presumed behaviour has been interpolated from the present data and the previously available results. Note that the plus and minus signs on the reactance curves indicate the inductive and capacitive nature of the input impedance reactive component. One anti-resonant point is observed at approximately $C/\lambda_o = 0.5$.

Figures 4.02, 4.03, and 4.04 illustrate the input impedance of loop antennas situated on dielectric cylinders where the dielectric constant $\epsilon_r = 2.56$, 5.6, and 9.0, respectively. Again, for each figure, twenty data points are provided for each of the two cases $\Omega = 10$ and $\Omega = 12$ over a range of normalized circumference C/λ_o of 0.1 to 2.0. The dashed lines on the resistance and reactance curves indicate the presumed behaviour of the input impedance for the geometries presented. This general behaviour is interpolated from the given data points and the results observed in Figure 4.01. The plus and minus signs on the reactance curves indicate the inductive and capacitive nature of the input impedance reactive component over the specified regions. Note that two anti-resonant points are observed in Figures 4.02 and 4.03, while three anti-resonant points are observed in Figure 4.04.

Figures 4.01, 4.02, 4.03, and 4.04 exhibit some interesting features which should be noted. First, the increase in dielectric constant obviously increases the electrical size of the loop antenna. This can be inferred from the increase in the number of anti-resonant points observed for a given geometry. Secondly, an impact upon the resistive component of the input impedance is observed as the dielectric constant increases. In Figure 4.01, the variation in resistance, excluding the anti-resonant point, is relatively small. However, as the dielectric constant is increased, larger variations in the resistance are observed. This increased variation in resistance is assumed to be the combined result of cylinder influence upon the radiation characteristics of the antenna and surface wave excitation.

The impact of surface wave excitation on the resistive component of the input impedance is an item of interest which arises from the present results. To observe this clearly, comparisons are made between the contribution to the resistive part of the modal impedance term made by radiation, the real part of the CPV, and by surface wave excitation, the residue. These comparisons are illustrated in Figures 4.05, 4.06, 4.07, and 4.08. The data for these figures was extracted from the input impedance results presented earlier. Figure 4.05 illustrates the radiation contribution made when $\epsilon_r = 1.0$. Obviously, no surface wave activity is present under these conditions so this figure provides a baseline for the subsequent results. It is interesting to note the shape of the curve in this figure and the degree to which each modal term contributes to the final imput impedance result. These results may be related to the small variation in the resistance of the loop antenna as seen in Figure 4.01. Figure 4.06 illustrates the radiation contribution made when $\epsilon_r = 2.56$ and

the surface wave contribution made by the HE_{11} mode. The HE_{11} mode is the only mode which may be excited under these conditions. Cut-off condition verification may be performed through (3.27).

The behaviour of the HE_{11} mode contribution is interesting in that it exhibits behaviour similar to behaviour seen in results obtained by Duncan [97]. Specifically, the shape of the curve for the HE_{11} mode is identical to a curve obtained by Duncan which illustrated the excitation of the HE_{11} mode on a dielectric cylinder, as a function of rod radius. The variability in the radiation contribution may be associated with behaviour, shown in Figure 4.02, for the resistance of the loop antenna under this geometry. Figure 4.07 illustrates the radiation contribution made when $\epsilon_r = 5.6$ and the surface wave contributions provided by the TE_{01}, HE_{11}, EH_{11}, HE_{12}, and HE_{21} modes. Equation (3.33) verifies that the $TE_{0,m}$ modes can not be excited by the loop antenna. Again, the variability of the radiation contribution may be associated with the resistance behaviour shown in Figure 4.03. The surface wave contributions exhibit behaviour discussed earlier. Finally, Figure 4.08 illustrates the radiation contribution made when $\epsilon_r = 9.0$ and the surface wave contributions provided by the TE_{01}, TE_{02}, HE_{11}, EH_{11}, HE_{12}, HE_{21}, EH_{21} and HE_{31} modes. Again, the highly variable radiation contribution may be associated with resistance behaviour seen in Figure 4.04. Note that only the first four terms 0, 1, 2, and 3, were employed in the analysis of the radiation contribution. Only four terms were necessary because the highest surface wave mode which can be excited is the HE_{31} mode, and the objective of Figures 4.05 to 4.08 is to compare the radiation contribution and surface wave contribution to the real part of the modal impedance

term.

The identification of all surface wave modes which may be excited under a given geometry is very important to the determination of the antenna's input impedance. As indicated above, surface wave data is required for both the CPV calculation and the residue calculation. Tables 4.01 to 4.08 identify all surface wave modes which may exist under the conditions discussed in Figures 4.01 to 4.08. Each table provides specific information on the dielectric constant of the cylinder ϵ_r, the azimuthal mode number m, the normalized loop circumference C/λ_o at which the surface wave mode is observed, the normalized propagation velocity β/β_o for the particular observation, and on the identity of the particular surface wave observed $S/W\ MODE$. Table 4.01 provides the necessary information for the fourteen occurrences of surface wave excitation which appear for $\epsilon_r = 2.56$, $m = 1$. Note that, although theoretically the HE_{11} mode exhibits zero cutoff characteristic, the impact of this mode upon the input impedance calculations does not become significant until C/λ_o reaches 0.7. For $C/\lambda_o > 0.7$, the only surface wave mode observed for the conditions associated with Table 4.01 is the HE_{11} mode. Table 4.02 provides the necessary information for the nine occurrences of surface wave excitation which appear for $\epsilon_r = 5.6$, $m = 0$. Under these conditions, the TE_{01} mode is the only mode which may be excited. Cutoff for this mode occurs for $C/\lambda_o < 1.2$. Table 4.03 provides the necessary information for the twenty-one occurrences of surface wave excitation which appear for $\epsilon_r = 5.6$, $m = 1$. Again, note that the impact of the HE_{11} mode becomes significant for $C/\lambda_o = 0.5$. At $C/\lambda_o = 1.8$, the EH_{11} mode begins to propagate and at $C/\lambda_o = 2.0$, the HE_{12} mode begins to propagate. Table 4.04 provides the necessary

information for the five occurrences of surface wave excitation which appear for ϵ_r = 5.6, m = 2. Note that the HE_{21} mode is the only mode which may be excited under these conditions and it exhibits a cutoff at C/λ_o = 1.6. Table 4.05 provides the necessary information for the thirteen occurrences of surface wave excitation which appear for ϵ_r = 9.0, m = 0. The TE_{01} mode begins to propagate at C/λ_o = 0.9 and the TE_{02} mode begins to propagate at C/λ_o = 2.0. Table 4.06 provides the necessary information for the thirty occurrences of surface wave excitation which appear for ϵ_r = 9.0, m = 1. Note that the impact of the HE_{11} mode becomes significant at C/λ_o = 0.4. Cutoff for the EH_{11} and HE_{12} modes is shown to be in the vicinity of C/λ_o = 1.4. The modes HE_{11}, EH_{11}, and HE_{12} are the only modes which may be excited under these conditions. Table 4.07 provides the necessary information for the ten occurrences of surface wave excitation which appear for ϵ_r = 9.0, m = 2. The HE_{21} mode exhibits a cutoff at C/λ_o = 1.9. Finally, Table 4.08 provides the necessary information for the three occurrences of surface wave excitation which appear for ϵ_r = 9.0, m = 3. Under these conditions, the HE_{31} mode is the only mode which can be excited. It exhibits a cutoff at C/λ_o = 1.8. For the input impedance calculations presented in Figures 4.01 to 4.04, one hundred and five occurrences of surface wave excitation were observed. The residue calculations for the surface wave modes provides a significant contribution to the input impedance results.

The current distribution on the loop antenna is of interest in determining the antenna's radiation characteristics. Further, an examination of its Fourier components provides information on the convergence of the current distribution solution,

the input impedance solution, and the dominant radiation mode. To examine the Fourier components of the current distribution, the current on the antenna is defined in a slightly modified form as follows:

$$J_\phi(\phi) = a_o + 2\sum_{n=1}^{\infty} a_n \cos n\phi$$

Figures 4.09 to 4.12 illustrate the magnitudes and phases of the *input modal currents* for the four cases $\epsilon_r = 1.0$, 2.56, 5.6, and 9.0. The input modal currents *IMC*, are simply defined as the values of the co-efficients a_n in the above expression. The antenna excitation is a 1.0 volt rectangular pulse function. Therefore, the input modal currents are directly related to the modal input admittances. For each case of dielectric constant, the *IMC* are presented for two sets of data $\Omega = 10$, and $\Omega = 12$. Since these results are obtained as an intermediate step in the calculation of the input impedance, the discussions associated with the input impedance calculation are relevant here also. The magnitudes of the *IMC* are presented in unit of dBmA, dB with respect to 1.0 mA, and the phases are presented in degrees.

Figure 4.09 illustrates the *IMC* for the case $\epsilon_r = 1.0$. The zero order term is predominant for the small loop sizes. Then the first order term begins to dominant. This is completely consistant with the established behaviour of loop antennas in free space. The phase for the zero order term for small loop sizes is 270 degrees. This again is verified by established loop antenna behaviour in free space. The admittance of a small loop antenna in free space is capacitive in nature. The convergence of the Fourier series solution is evident from this figure. The higher order terms increasingly diminish and their phases are at 90 degrees as expected.

Very little difference is observed between $\Omega = 10$ and $\Omega = 12$ data as expected. A resonance in the first order term is observed at $C/\lambda_o = 1.0$. Again, this is supported by established loop behaviour in free space conditions.

Figure 4.10 illustrates the *IMC* for the case $\epsilon_r = 2.56$. In this situation, the zero, first, and second order terms successively dominate the current distribution. The increase in antenna electrical size is readily apparent from the downward shift in C/λ_o observed for the current peaks. Resonances in the first and second order terms are noted. Figures 4.11 and 4.12 illustrate the *IMC* for the cases $\epsilon_r = 5.6$ and 9.0, respectively. In both situations, solution convergence is observed. However, there appears to be oscillatory behaviour in the zero order magnitude which is also reflected in the phase characteristic.

General conclusions may be drawn from the results presented in this chapter. First, the formulation employed in this research has been verified through a number of comparisons with results which appear elsewhere in the literature. The impact of surface wave excitation on the input impedance of the antenna has been analyzed. And, the convergence of the current distribution solution has been observed.

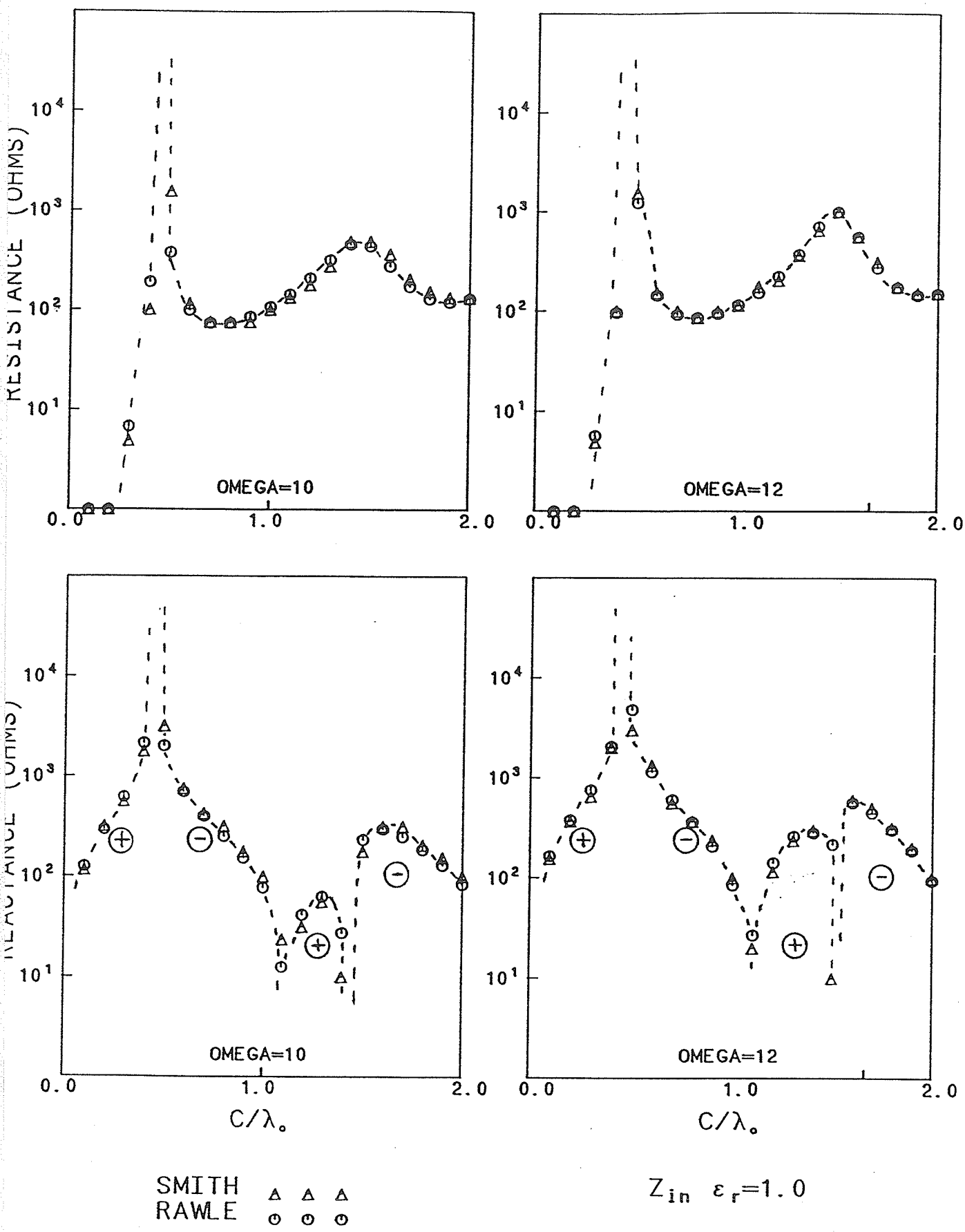

Figure 4.01 Input Impedance $\epsilon_r = 1.0$

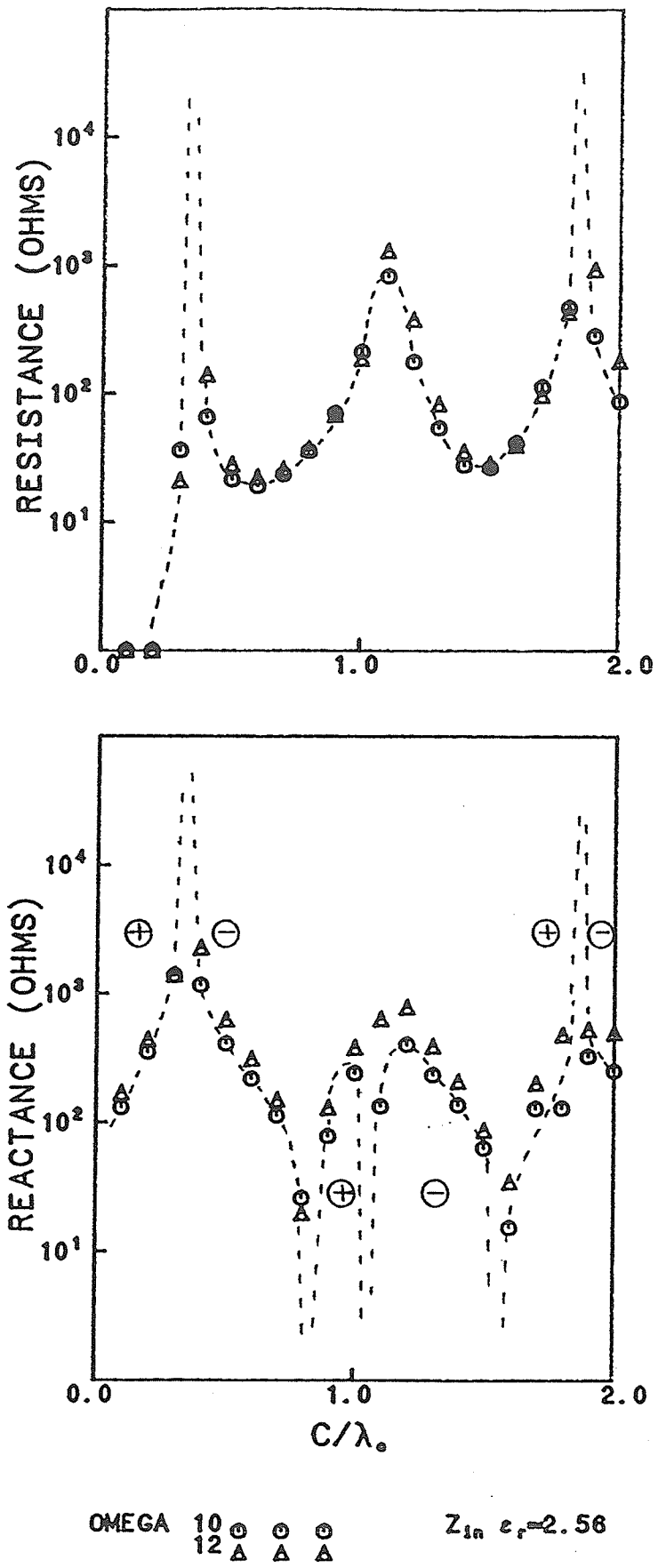

Figure 4.02 Input Impedance $\epsilon_r = 2.56$

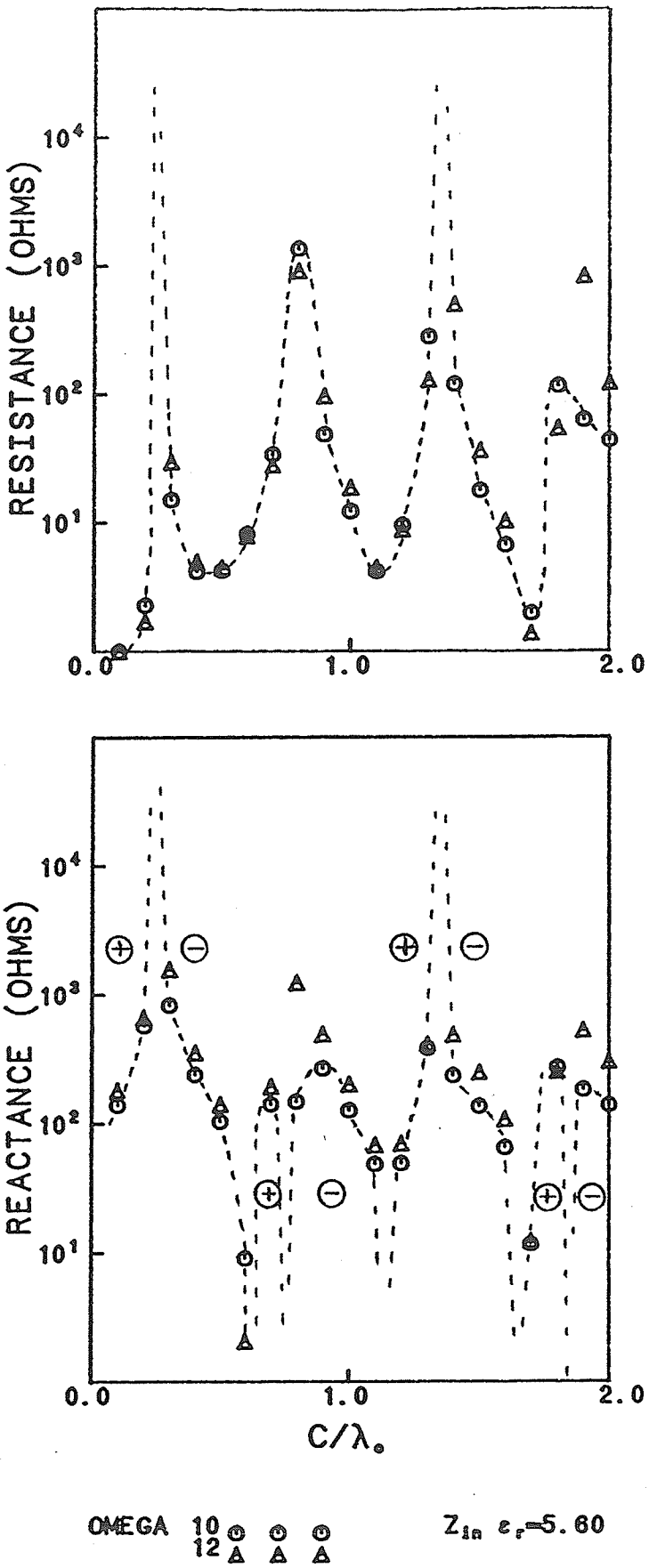

Figure 4.03 Input Impedance $\epsilon_r = 5.6$

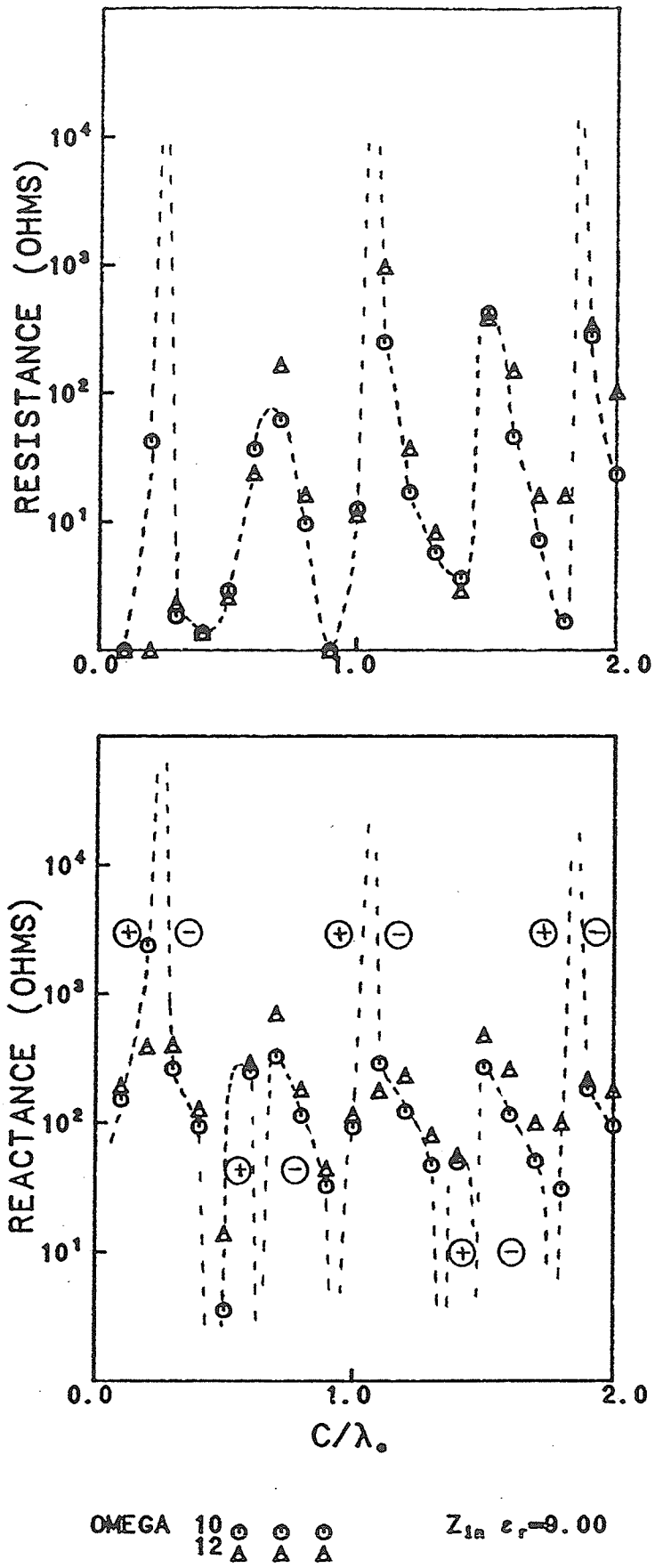

Figure 4.04 Input Impedance $\epsilon_r = 9.0$

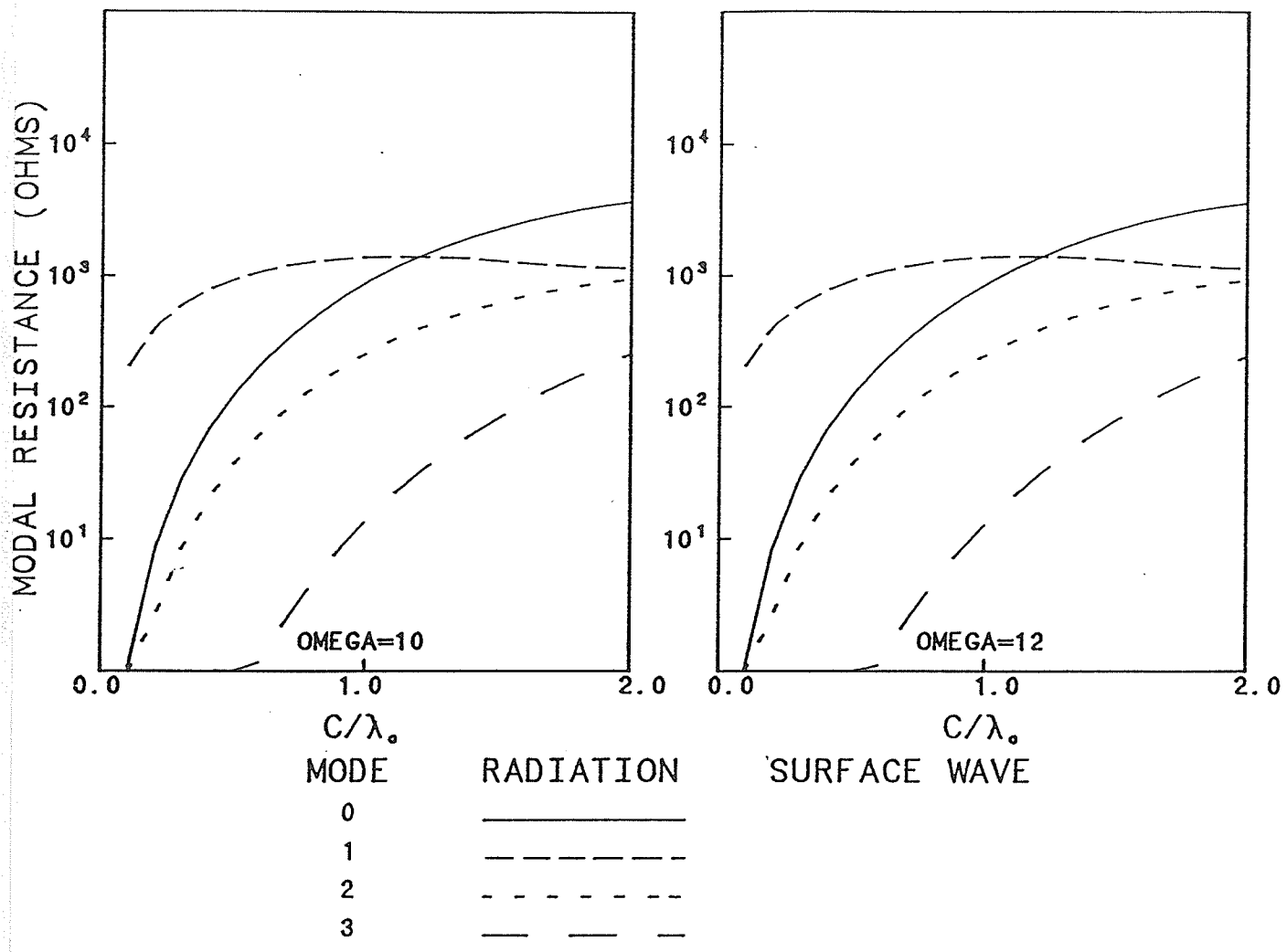

Figure 4.05 Modal Resistance $\epsilon_r = 1.0$

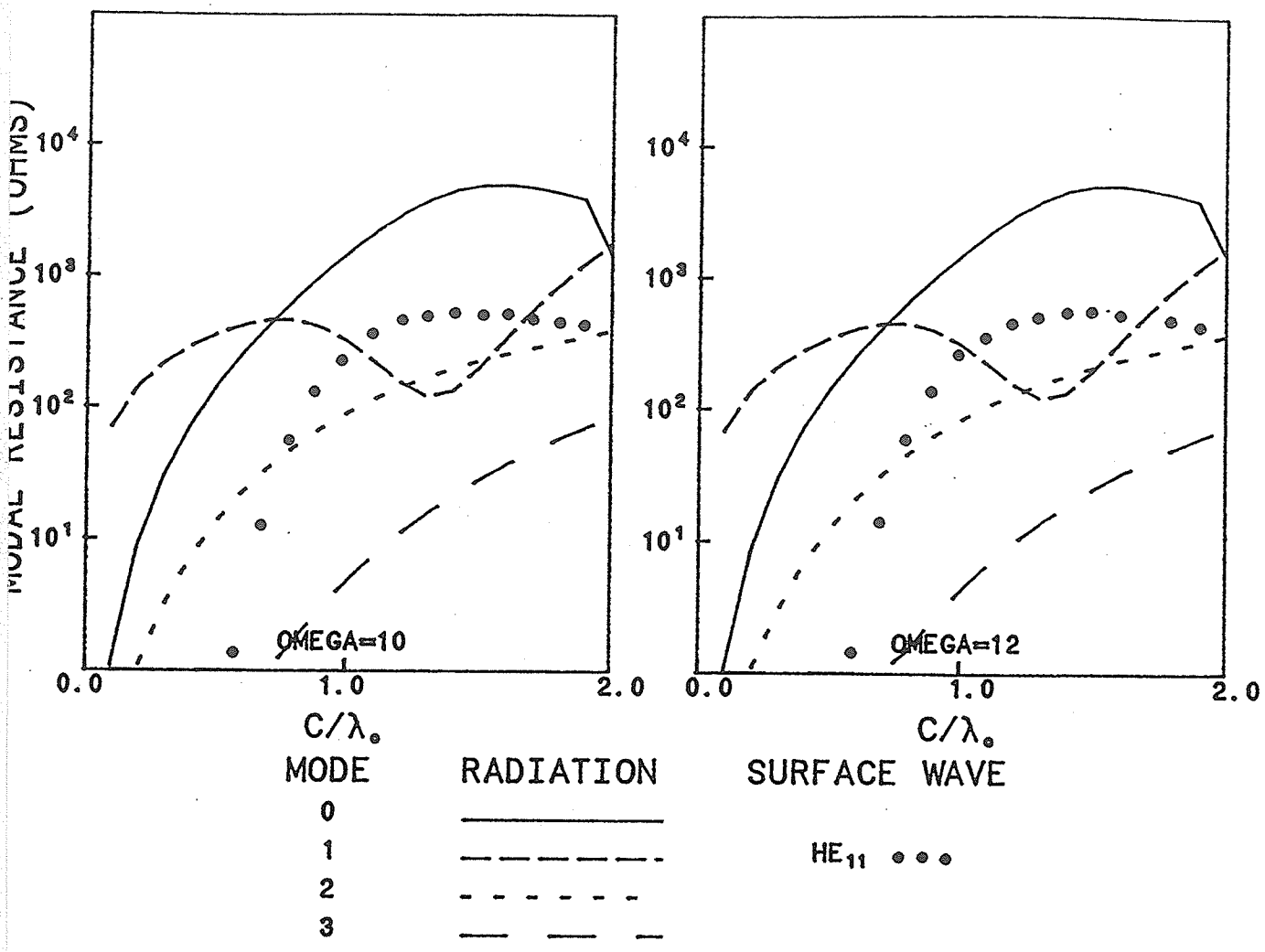

Figure 4.06 Modal Resistance $\epsilon_r = 2.56$

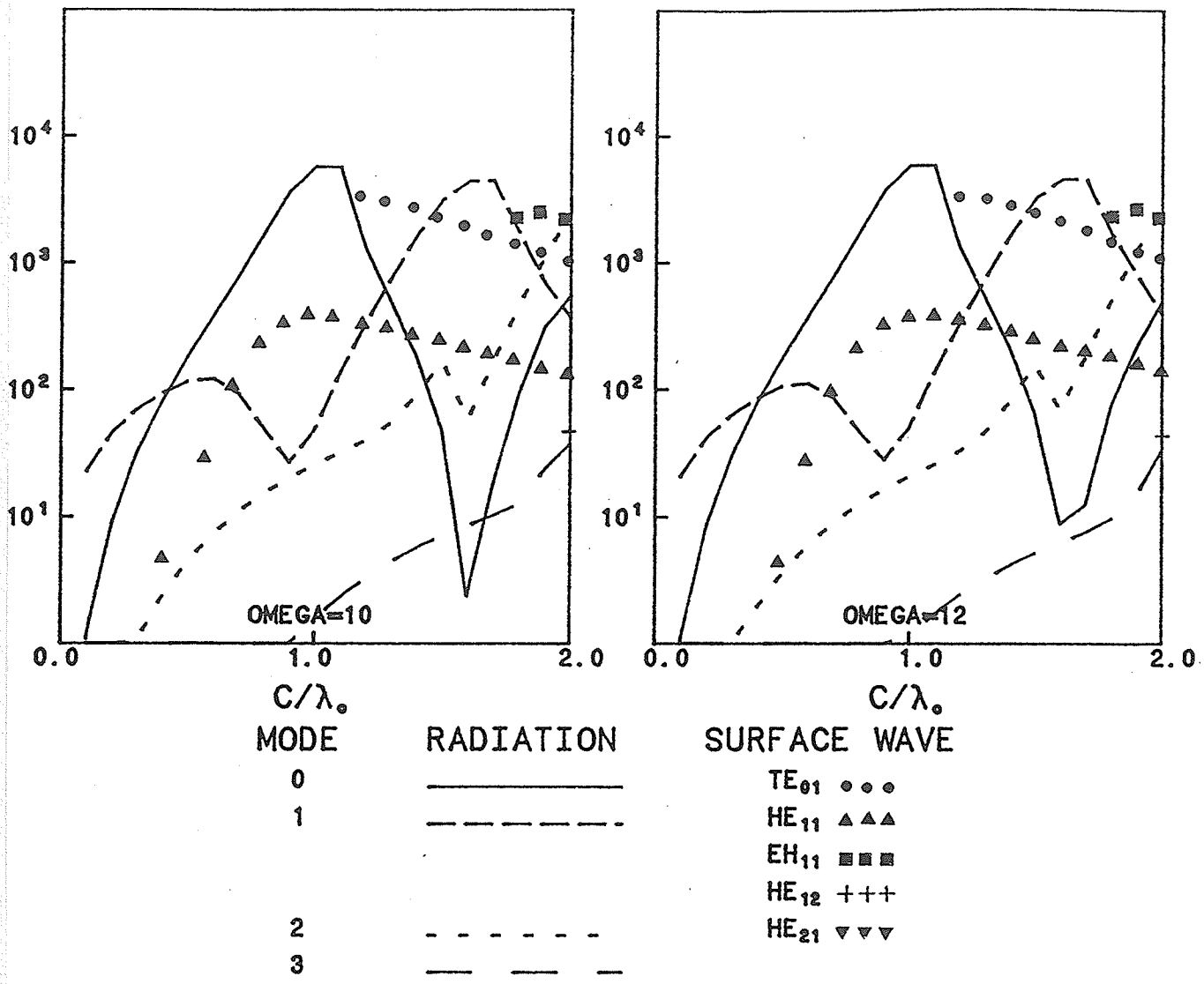

Figure 4.07 Modal Resistance $\epsilon_r = 5.6$

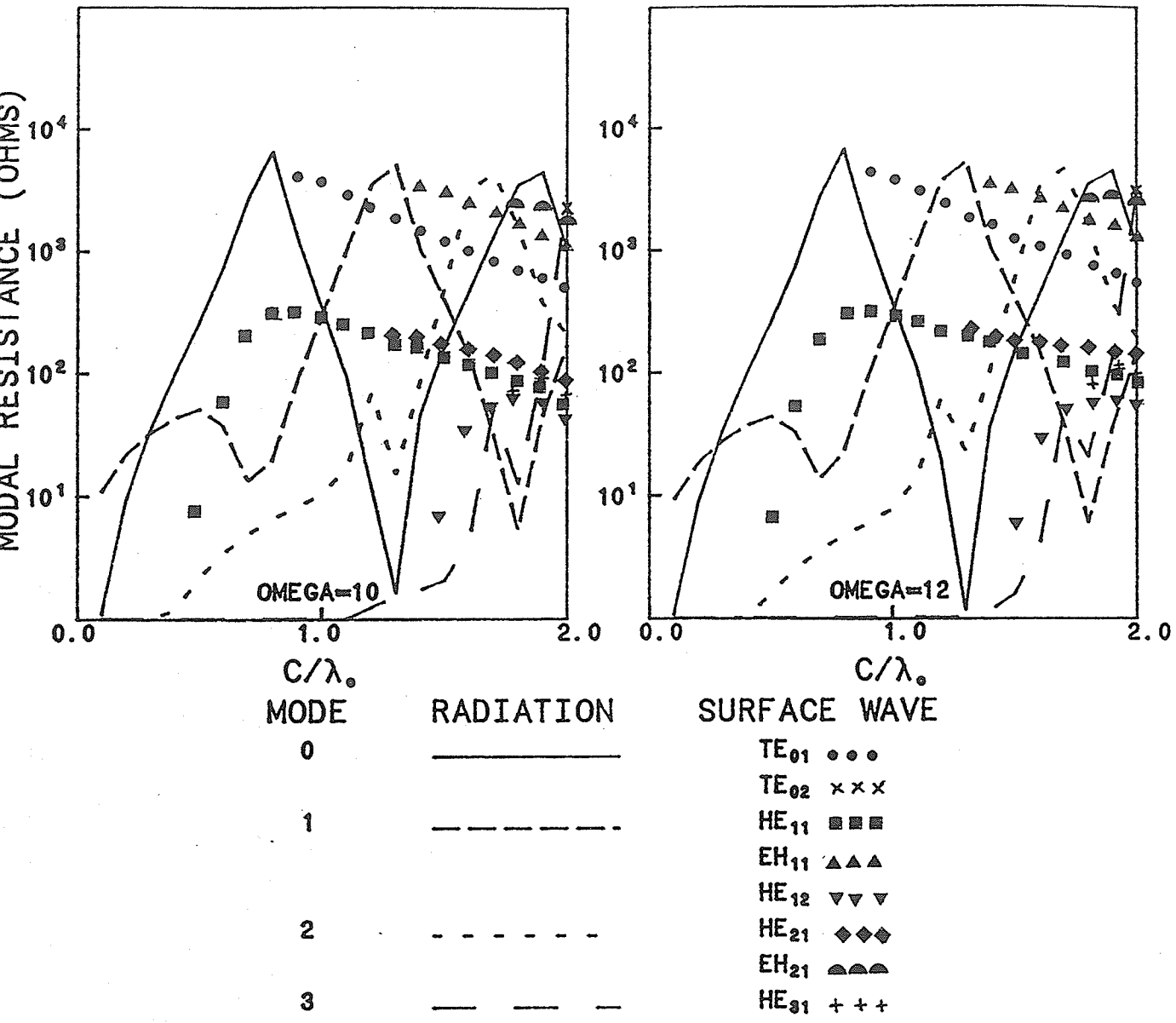

Figure 4.08 Modal Resistance $\epsilon_r = 9.0$

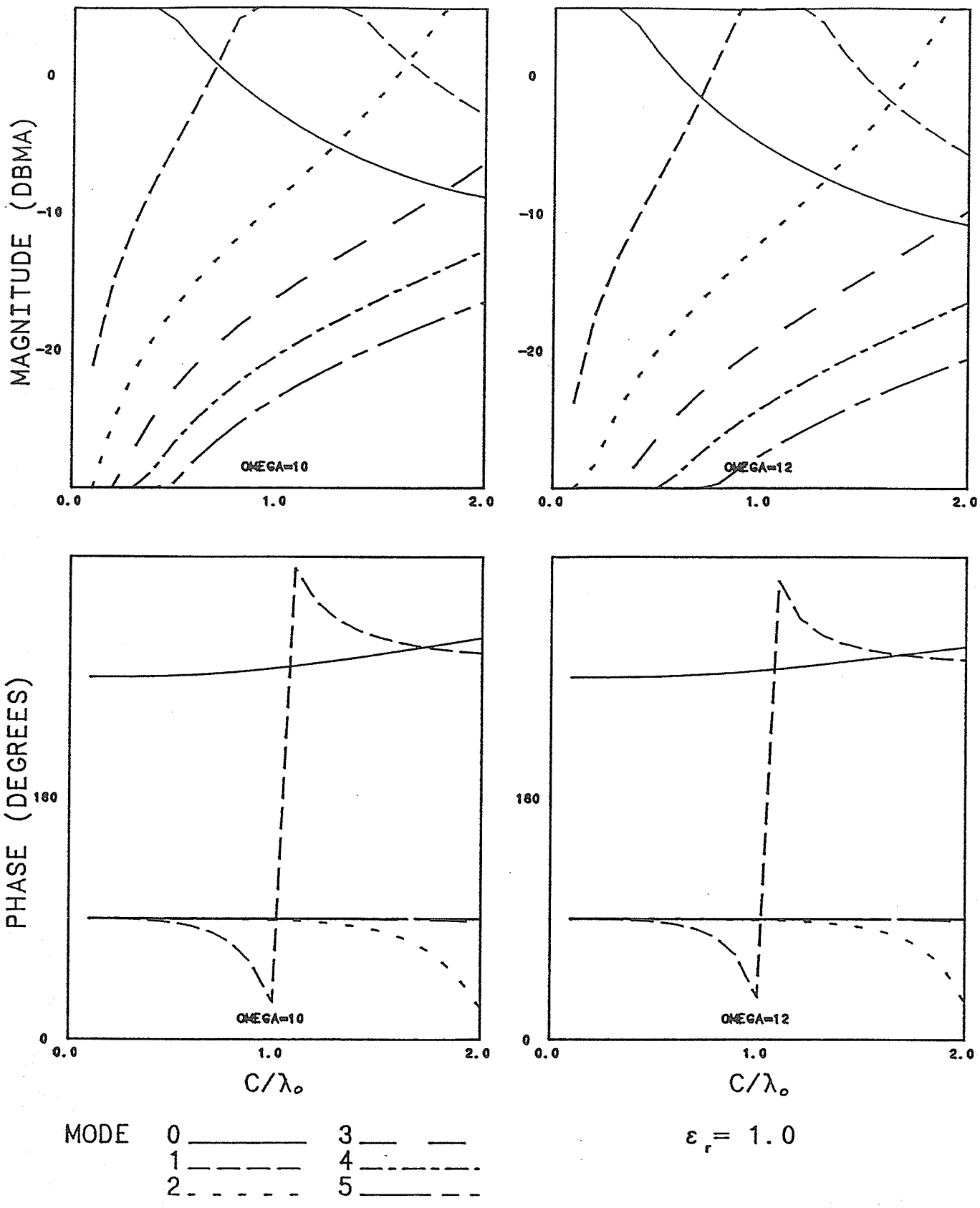

Figure 4.09 Input Modal Current $\epsilon_r = 1.0$

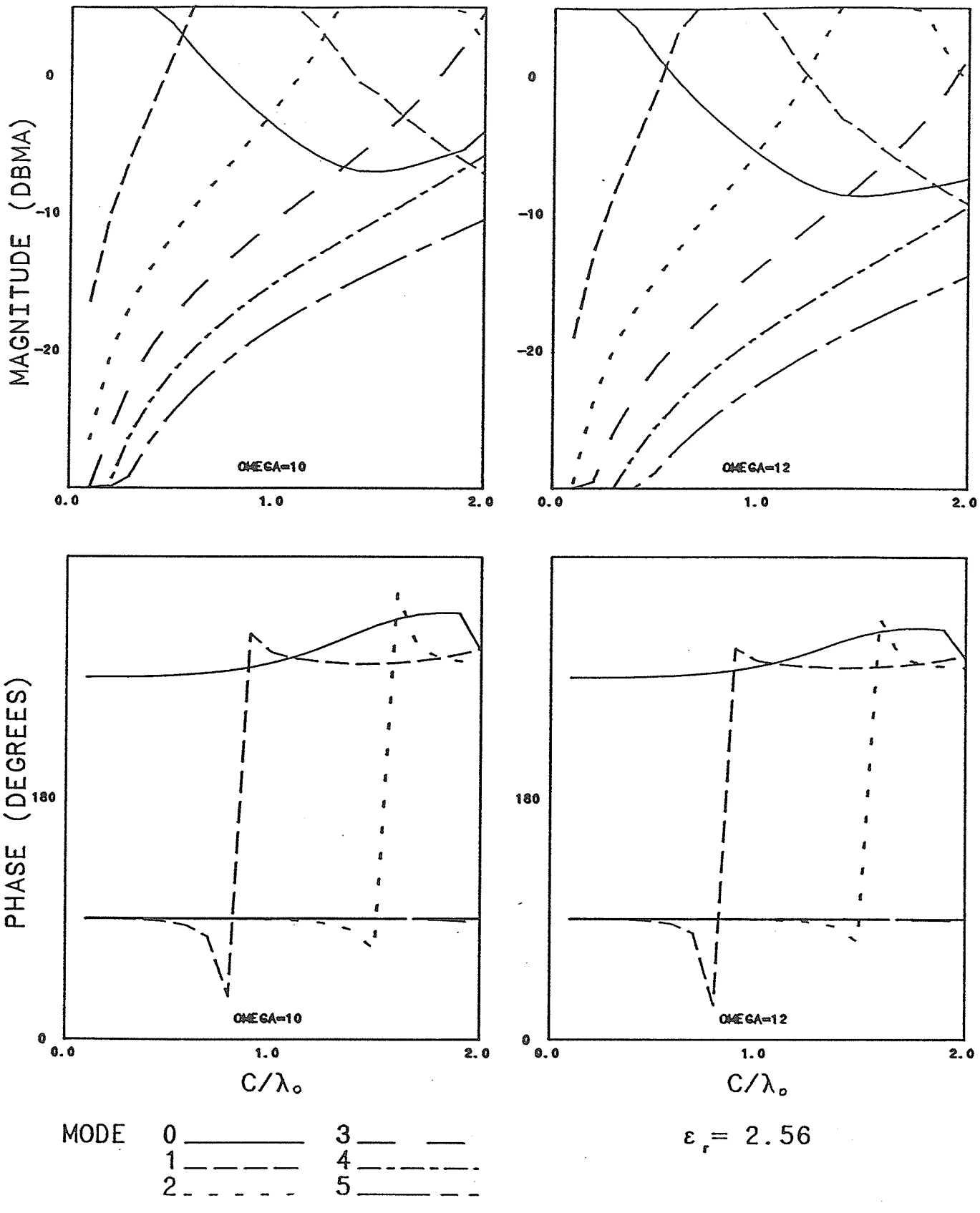

Figure 4.10 Input Modal Current $\epsilon_r = 2.56$

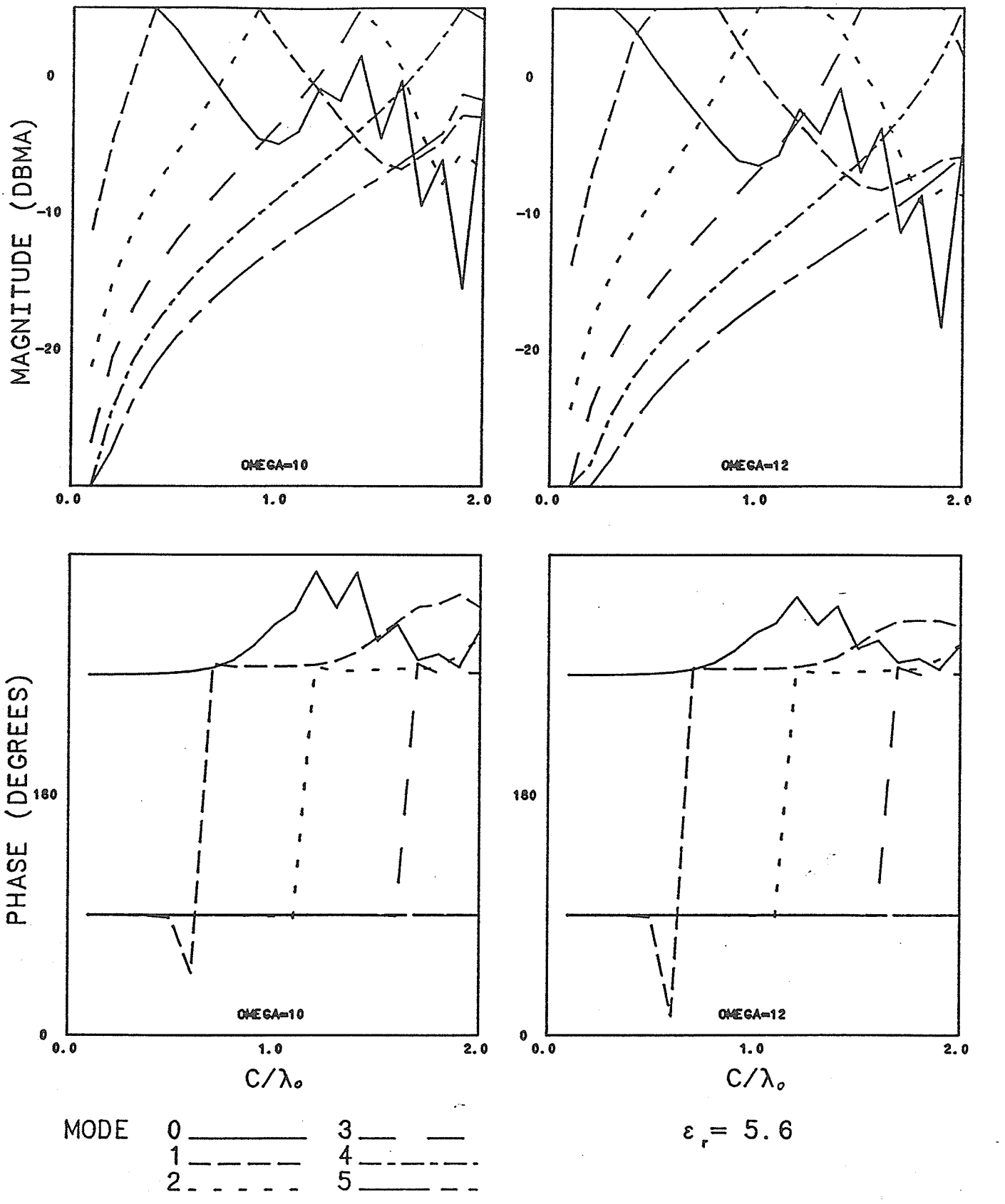

Figure 4.11 Input Modal Current $\epsilon_r = 5.6$

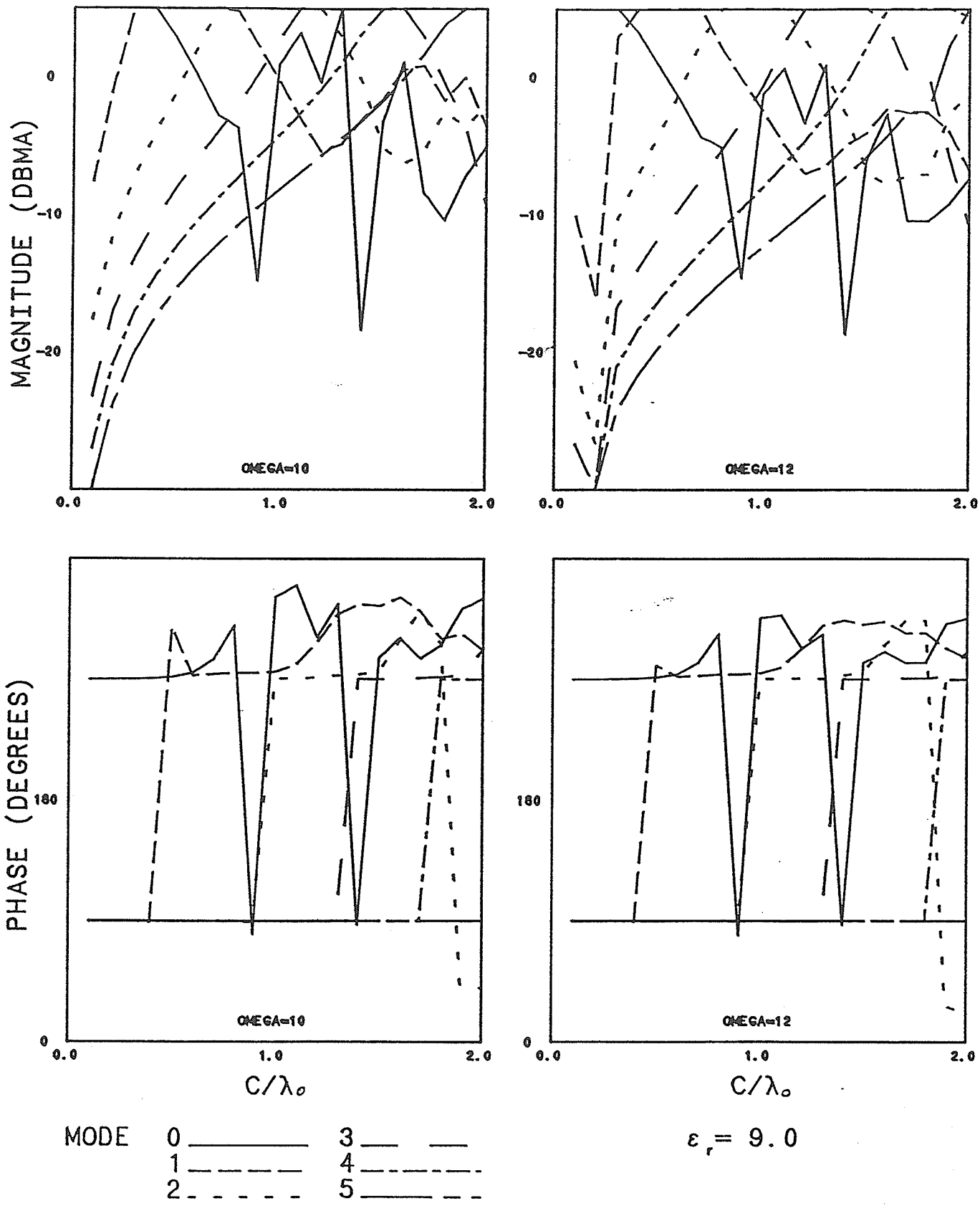

Figure 4.12 Input Modal Current $\epsilon_r = 9.0$

Table 4.01 Surface Wave Data $\epsilon_r = 2.56$ $m = 1$

$\varepsilon_r = 2.56$		$m = 1$
C/λ_o	β/β_o	S/W MODE
0.7	1.000	HE_{11}
0.8	1.002	HE_{11}
0.9	1.007	HE_{11}
1.0	1.019	HE_{11}
1.1	1.037	HE_{11}
1.2	1.062	HE_{11}
1.3	1.091	HE_{11}
1.4	1.124	HE_{11}
1.5	1.158	HE_{11}
1.6	1.191	HE_{11}
1.7	1.222	HE_{11}
1.8	1.251	HE_{11}
1.9	1.278	HE_{11}
2.0	1.302	HE_{11}

Table 4.02 Surface Wave Data $\epsilon_r = 5.6$ $m = 0$

ε_r= 5.60		m= 0
C/λ_o	β/β_o	S/W MODE
1.2	1.091	TE_{01}
1.3	1.227	TE_{01}
1.4	1.351	TE_{01}
1.5	1.459	TE_{01}
1.6	1.551	TE_{01}
1.7	1.631	TE_{01}
1.8	1.700	TE_{01}
1.9	1.759	TE_{01}
2.0	1.811	TE_{01}

Table 4.03 Surface Wave Data $\epsilon_r = 5.6$ $m = 1$

ε_r= 5.60		m= 1
C/λ_o	β/β_o	S/W MODE
0.5	1.000	HE_{11}
0.6	1.004	HE_{11}
0.7	1.026	HE_{11}
0.8	1.094	HE_{11}
0.9	1.229	HE_{11}
1.0	1.395	HE_{11}
1.1	1.547	HE_{11}
1.2	1.671	HE_{11}
1.3	1.771	HE_{11}
1.4	1.850	HE_{11}
1.5	1.915	HE_{11}
1.6	1.968	HE_{11}
1.7	2.012	HE_{11}
1.8	1.014	EH_{11}
1.8	2.049	HE_{11}
1.9	1.000	HE_{12}
1.9	1.123	EH_{11}
1.9	2.080	HE_{11}
2.0	1.007	HE_{12}
2.0	1.229	EH_{11}
2.0	2.107	HE_{11}

Table 4.04 Surface Wave Data $\epsilon_r = 5.6$ $m = 2$

ε_r= 5.60		m= 2
C/λ_o	β/β_o	S/W MODE
1.6	1.109	HE_{21}
1.7	1.270	HE_{21}
1.8	1.408	HE_{21}
1.9	1.520	HE_{21}
2.0	1.613	HE_{21}

Table 4.05 Surface Wave Data $\epsilon_r = 9.0$ $m = 0$

ε_r= 9.00		m= 0
C/λ_o	β/β_o	S/W MODE
0.9	1.125	TE_{01}
1.0	1.409	TE_{01}
1.1	1.645	TE_{01}
1.2	1.834	TE_{01}
1.3	1.987	TE_{01}
1.4	2.111	TE_{01}
1.5	2.213	TE_{01}
1.6	2.298	TE_{01}
1.7	2.370	TE_{01}
1.8	2.431	TE_{01}
1.9	2.484	TE_{01}
2.0	1.069	TE_{02}
2.0	2.529	TE_{01}

Table 4.06 Surface Wave Data $\epsilon_r = 9.0$ $m = 1$

ε_r= 9.00		m= 1
C/λ_o	β/β_o	S/W MODE
0.4	1.000	HE_{11}
0.5	1.002	HE_{11}
0.6	1.034	HE_{11}
0.7	1.230	HE_{11}
0.8	1.615	HE_{11}
0.9	1.927	HE_{11}
1.0	2.144	HE_{11}
1.1	2.299	HE_{11}
1.2	2.413	HE_{11}
1.3	2.501	HE_{11}
1.4	1.105	EH_{11}
1.4	2.570	HE_{11}
1.5	1.001	HE_{12}
1.5	1.335	EH_{11}
1.5	2.625	HE_{11}
1.6	1.016	HE_{12}
1.6	1.532	EH_{11}
1.6	2.670	HE_{11}
1.7	1.069	HE_{12}
1.7	1.697	EH_{11}
1.7	2.707	HE_{11}
1.8	1.186	HE_{12}
1.8	1.835	EH_{11}
1.8	2.738	HE_{11}
1.9	1.358	HE_{12}
1.9	1.951	EH_{11}
1.9	2.764	HE_{11}
2.0	1.538	HE_{12}
2.0	2.051	EH_{11}
2.0	2.786	HE_{11}

Table 4.07 Surface Wave Data $\epsilon_r = 9.0$ $m = 2$

ε_r= 9.00		m= 2
C/λ_o	β/β_o	S/W MODE
1.3	1.320	HE_{21}
1.4	1.640	HE_{21}
1.5	1.862	HE_{21}
1.6	2.027	HE_{21}
1.7	2.155	HE_{21}
1.8	2.257	HE_{21}
1.9	1.187	EH_{21}
1.9	2.340	HE_{21}
2.0	1.378	EH_{21}
2.0	2.409	HE_{21}

Table 4.08 Surface Wave Data $\epsilon_r = 9.0$ $m = 3$

ε_r= 9.00		m= 3
C/λ_o	β/β_c	S/W MODE
1.8	1.310	HE_{31}
1.9	1.573	HE_{31}
2.0	1.764	HE_{31}

Chapter 5

Surface Wave Characteristics

The formulation of surface wave behaviour, as outlined in Chapter 3, was employed to calculate propagation velocities and electromagnetic field structure for a number of surface wave modes. This type of information is particularly useful to engineers involved in fibre-optics, certain areas of bioelectromagnetics, and polyrod antenna design.

Elsasser's eigenvalue equation, which may be obtained by setting $\Delta = 0$ (3.17), was employed to calculate normalized propagation velocities $\bar{\beta} = \beta/\beta_o$, $\beta_o = 2\pi/\lambda_o$, for all hybrid mode surface waves which can be excited on dielectric cylinders of radius up to 2.0 λ_o, $\epsilon_r = 2.56$, 5.6, 9.0, and $n = 1$, 2, 3. The eigenvalues were obtained through a direct search technique. Note that the higher order modes $n \geq 4$ will, in general, exist, as indicated by the cutoff conditions (3.27). However, the first three orders were considered sufficient to illustrate the characteristics of interest. Attention is also drawn to the slight variation in notation between the field expressions and surface wave mode identification. In the field expressions,

(3.13), the azimuthal mode index is denoted by m. In the surface wave designations $HE_{n,m}/EH_{n,m}$, the azimuthal mode index is denoted by n and the successive zeros of the associated cylinder functions are denoted by m. In an attempt to bridge the two notations, (3.36) denotes azimuthal mode index by m and successive zero index by p. Hopefully, (3.36) will resolve any ambiguity which might arise due to modification of notation.

Figure 5.01 illustrates normalized propagation velocities for hybrid mode surface waves which may be excited on a dielectric cylinder $\epsilon_r = 2.56$, radius $a \leq 2\lambda_o$, and $n = 1, 2, 3$. Note that the maximum propagation velocity is 1.6 ($\sqrt{2.56}$). For $n = 1$, the solid line illustrates the normalized propagation velocity for the HE_{11} mode. Note the way in which the line curves as $a \to 0$. This is significant in that, theoretically, the HE_{11} mode has no cut-off. This is verified by the present result. For $n = 1$, $m = 1$,the dotted line illustrates the normalized propagation velocity for the EH_{11} mode and the dashed line illustrates the normalized propagation velocity for the HE_{12} surface wave mode. Similarly, for $n = 1$, $m = 2$, the dotted line illustrates the EH_{12} mode and the dashed line represents the HE_{13} mode. For $n = 1$, $m = 3$, the dotted line represents the EH_{13} mode and the dashed line represents the HE_{14} mode. For $n = 1$, $m = 4$, the dotted line represents the EH_{14} mode and the dashed line represents the HE_{15} mode. As can be seen from the cutoff conditions, for $n = 1$, $EH_{1,m}$ and $HE_{1,m+1}$ surface wave modes exhibit identical cutoff characteristics. This is verified by the present calculation.

Figure 5.01, $n = 2$ results illustrate definite cutoff conditions for all surface waves under consideration here. The solid line represents the HE_{21} mode while

the subsequent dotted and dashed lines illustrate the behaviour of the $EH_{2,m}$ and $HE_{2,m+1}$ modes respectively. Note that for $n = 1$ and $n = 2$, the highest surface wave mode which may be excited is the HE_{15} mode. The $n = 3$ results illustrate the behaviour of the HE_{31}, EH_{31}, HE_{32}, EH_{32}, HE_{33}, EH_{33}, and HE_{34} modes. In this situation, obviously the HE_{34} mode is the highest surface wave mode which may be excited. It is interesting to note that, while for $n = 1$, the $EH_{1,m}$ and $HE_{1,m+1}$ modes exhibit the same cutoff condition, this is not the case for $n > 1$. This behaviour can be predicted by (3.27) and is verified by the present calculation.

Figure 5.02 illustrates normalized propagation velocities for hybrid mode surface waves which may be excited on a dielectric cylinder $\epsilon_r = 5.6$, radius $a \leq 2\lambda_o$, $n =$ 1, 2, and 3. Note that the maximum propagation velocity is 2.37 ($\sqrt{5.6}$). The same convention for identifying the results in Figure 5.01 is used here. For $n = 1$, results are provided for surface wave modes HE_{11} to HE_{19}. Again note the knee at the lower end of the HE_{11} curve, indicating zero cutoff behaviour. For $n = 2$, results are provided for modes HE_{21} to HE_{28} and for $n = 3$, results are provided for modes HE_{31} to HE_{38}.

Figure 5.03 illustrates normalized propagation velocities for hybrid mode surface waves which may be excited on a dielectric cylinder $\epsilon_r = 9.0$, radius $a \leq 2\lambda_o$, and $n =$ 1, 2, and 3. Note that the maximum propagation velocity is 3.0 ($\sqrt{9.0}$). Employing the same convention as used in Figures 5.01 and 5.02, in this figure $n = 1$ illustrates the results for HE_{11} to $HE_{1,11}$. Once again, the zero cut-off behaviour of the HE_{11} mode is noted. For $n = 2$, results are provided for modes HE_{21} to $HE_{2,11}$, and for $n = 3$, results are provided for modes HE_{31} to $HE_{3,10}$.

Surface wave propagation velocities for higher dielectric constant cylinders are presented here in order to illustrate the importance of careful analysis of such phenomena in such applications as fibre-optics systems design. Under certain conditions, a fairly large number of modes may be excited. These modes all transport energy, signals, at different velocities. In digital communications systems, the group delay introduced by multiple mode excitation can lead to severe waveform distortion and intersymbol interference. These conditions simply cannot be tolerated in commercial high speed communications systems. Therefore, careful analysis is required to prevent such problems from occuring.

The analysis and design of dielectric rod antennas has conventionally been based upon viewing this type of antenna as a two element radiator. The first radiating element is the waveguide - dielectric rod interface. The second radiating element is the end of the dielectric rod where the transition from dielectric to free space perturbs the propagating surface wave, resulting in radiation. The phase shift in fields between the two sources is controlled by the length of the rod and the propagation velocity of the surface wave. The radiation from the free end of the rod is often predicted by modelling the end region as an aperture plane transverse to the z axis, where the z axis is the axis of the rod. A knowledge of the electromagnetic field structure at the end of the rod thus establishes the aperture field distribution from which the radiation characteristics may be obtained. A knowledge of the surface wave electromagnetic field structure inside the rod is also useful in designing such items as dielectric waveguide components. In addition, it is interesting to evaluate the magnitudes of the surface wave electromagnetic field components and

compare them to the field components observed in other waveguiding structures, such as a dielectric rod inside a metallic cylindrical waveguide. This last comparison is the method by which Clarricoats [96] established his hybrid mode surface wave identification convention.

The above considerations led to the evaluation of the magnitudes of the surface wave electromagnetic field components in Region I. The magnitudes of E_{ρ_I}, E_{ϕ_I}, E_{z_I}, H_{ρ_I}, H_{ϕ_I}, and H_{z_I} were calculated using (3.36), as a function of ρ, for selected modes under the given geometry $\epsilon_r = 2.56$, $a = 3\lambda/2$ and $n = 1$, 2, and 3. A $\cos n\phi$ current distribution was presumed to exist on the loop. The z dependance of the fields was removed and then calculated results were normalized to the maximum value of the HE_{11} mode seen in each field component.

Figures 5.04 and 5.05 illustrate the magnitude of the surface wave electromagnetic field components, Region I, for $\epsilon_r = 2.56$, $a = 3\lambda/2$, $n = 1$. The fields are plotted as a function of ρ, where $0 < \rho < a$, and normalized with repsect to the maximum value of the HE_{11} field components. In these figures, results are provided for the HE_{11}, EH_{11}, HE_{12}, EH_{12}, HE_{13}, EH_{13}, and HE_{14} modes. An analysis of these results provides information on nulls in the field components, which can be related to the zeros of the cylinder functions which describe the field behaviour.

Additionally, it is interesting to observe the relative magnitude of the various modes. This information may indicate the degree to which a particular mode is excited. A comparison of field magnitudes for HE and EH type modes also indicates the predominance of a transverse magnetic or transverse electric behaviour. Figure 5.06 illustrates the magnitude of the surface wave electromagnetic field components,

Region I, for $\epsilon_r = 2.56$, $a = 3\lambda/2$, and $n = 2$. In this figure, results are provided for the HE_{21}, EH_{21}, HE_{22}, EH_{22} and HE_{23} modes. The comments directed towards Figures 5.04 and 5.05 are also appropriate here. Finally, Figure 5.07, illustrates the magnitudes of the surface wave electromagnetic field components, Region I, for $\epsilon_r = 2.56$, $a = 3\lambda/2$, $n = 3$. In this last figure, results are provided for the HE_{31}, EH_{31}, HE_{32}, EH_{32}, and HE_{33} modes.

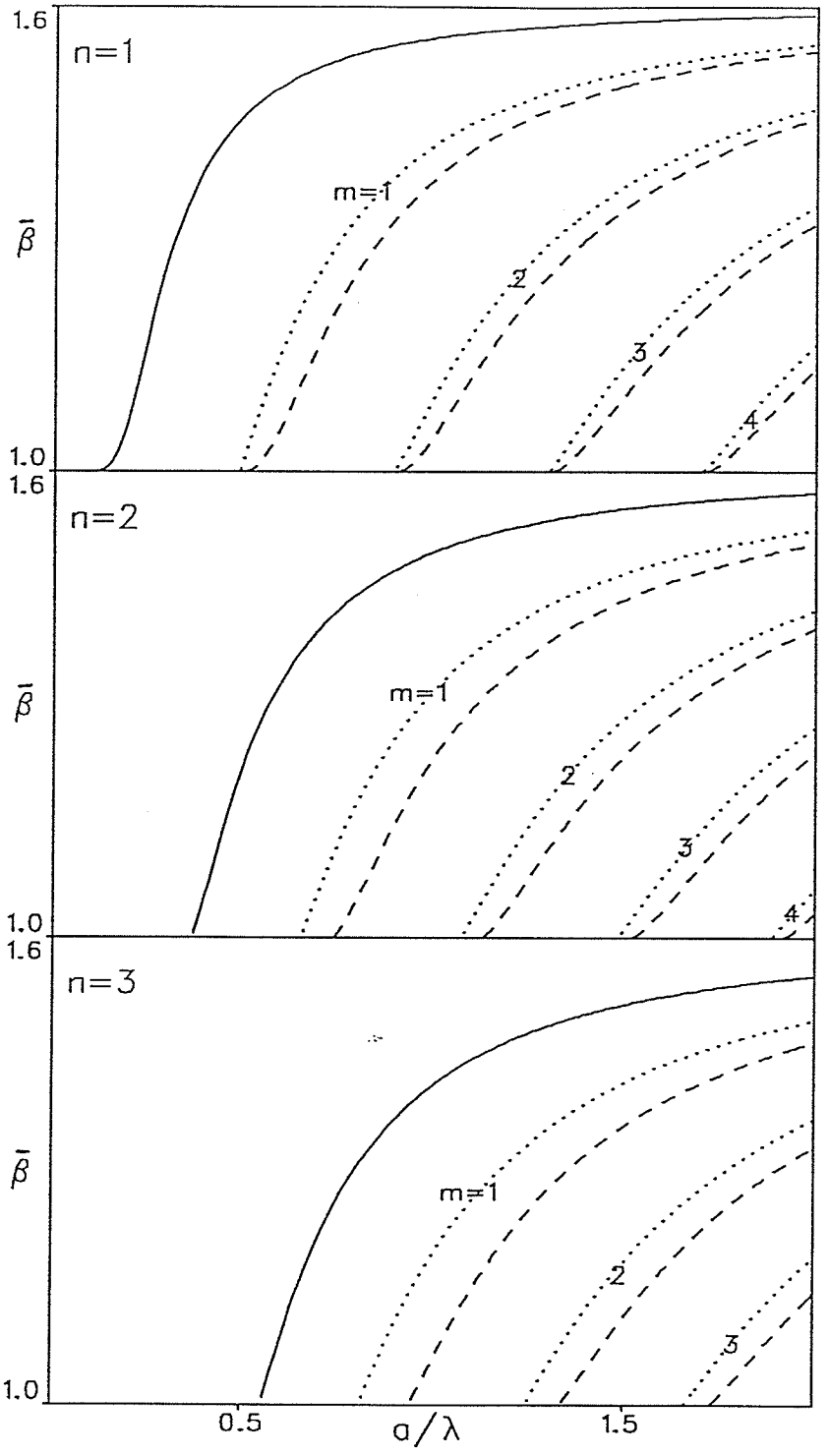

Figure 5.01 Surface Wave Propagation Velocities $\epsilon_r = 2.56$

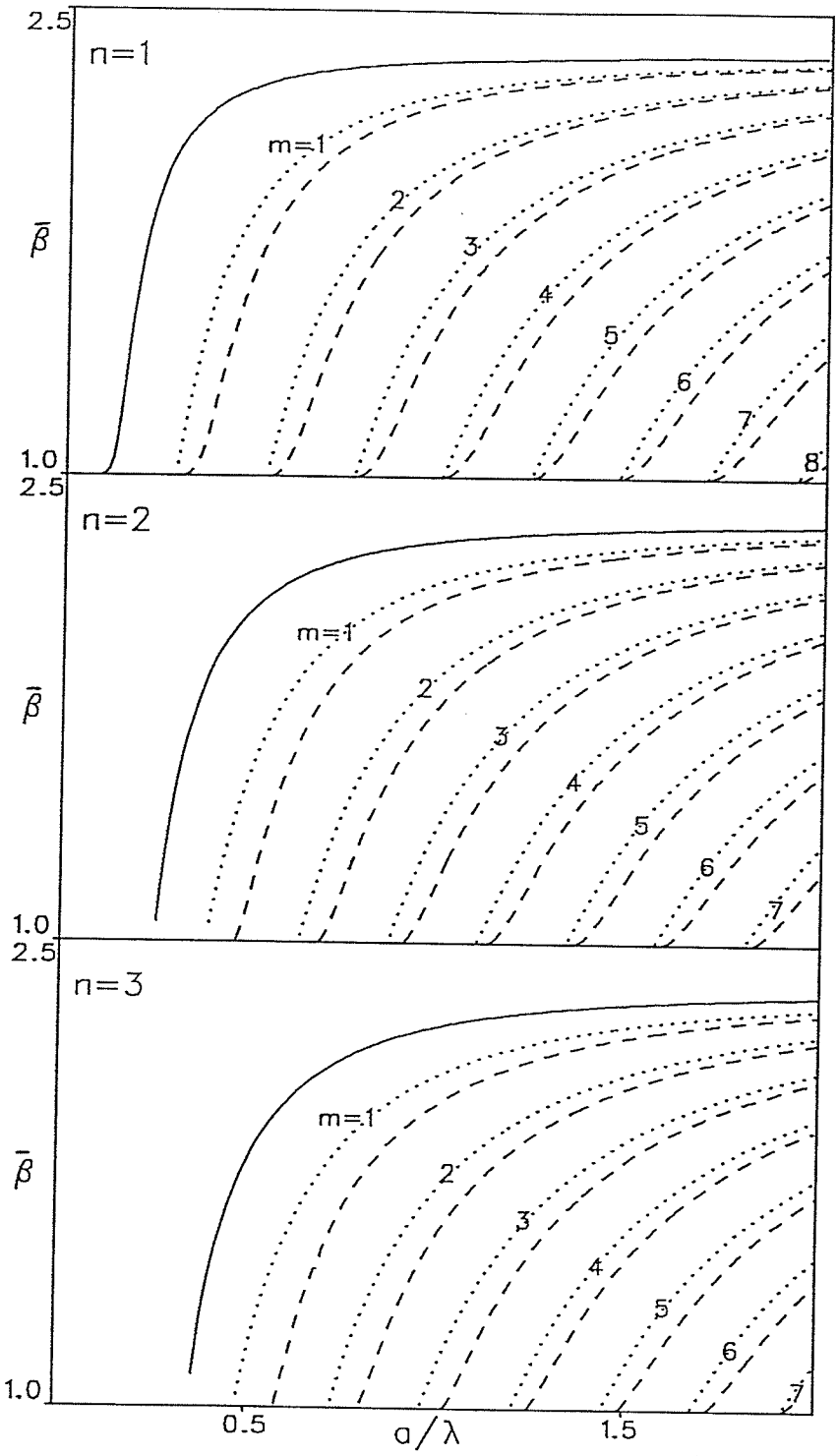

Figure 5.02 Surface Wave Propagation Velocities $\epsilon_r = 5.6$

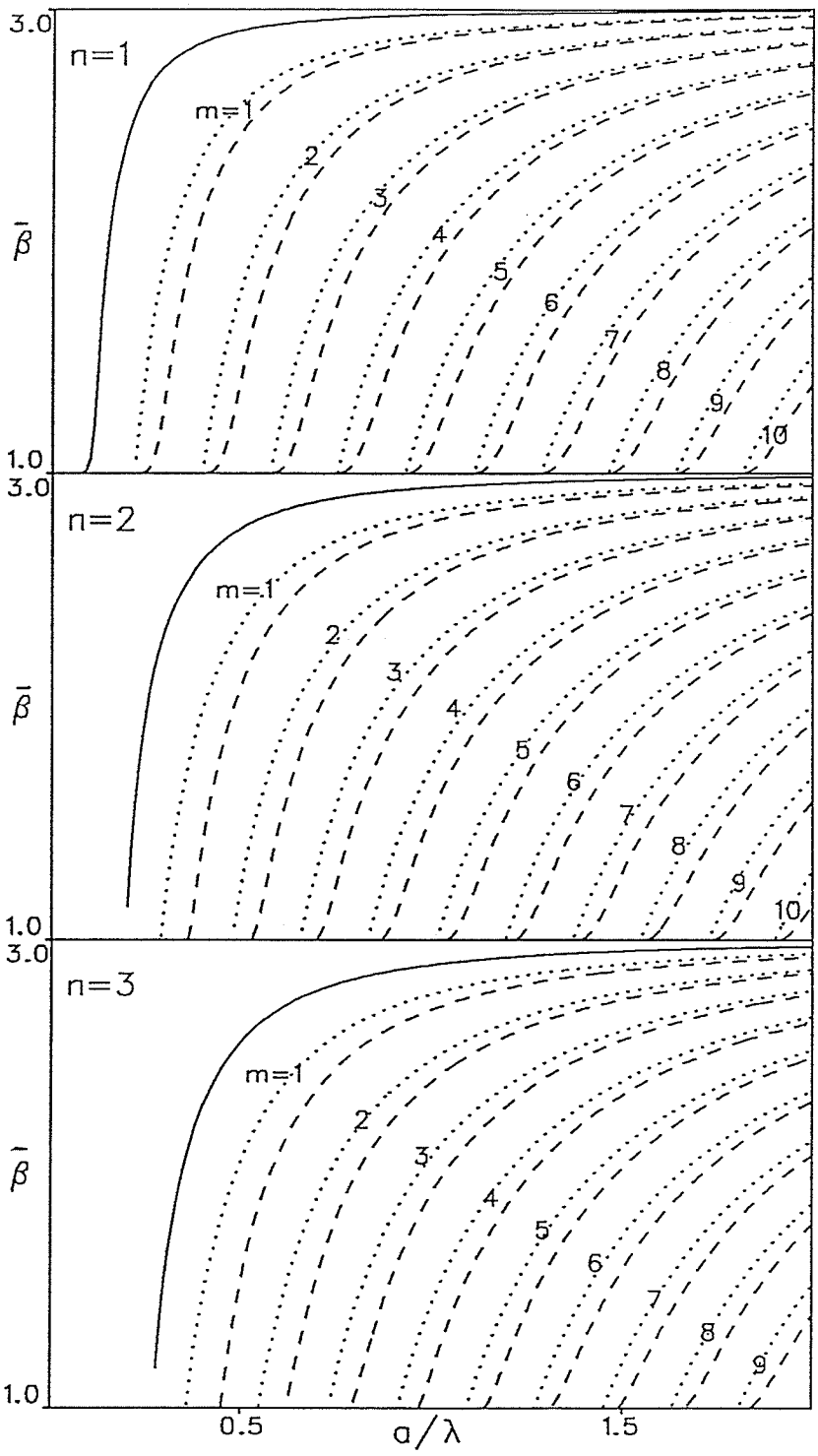

Figure 5.03 Surface Wave Propagation Velocities $\epsilon_r = 9.0$

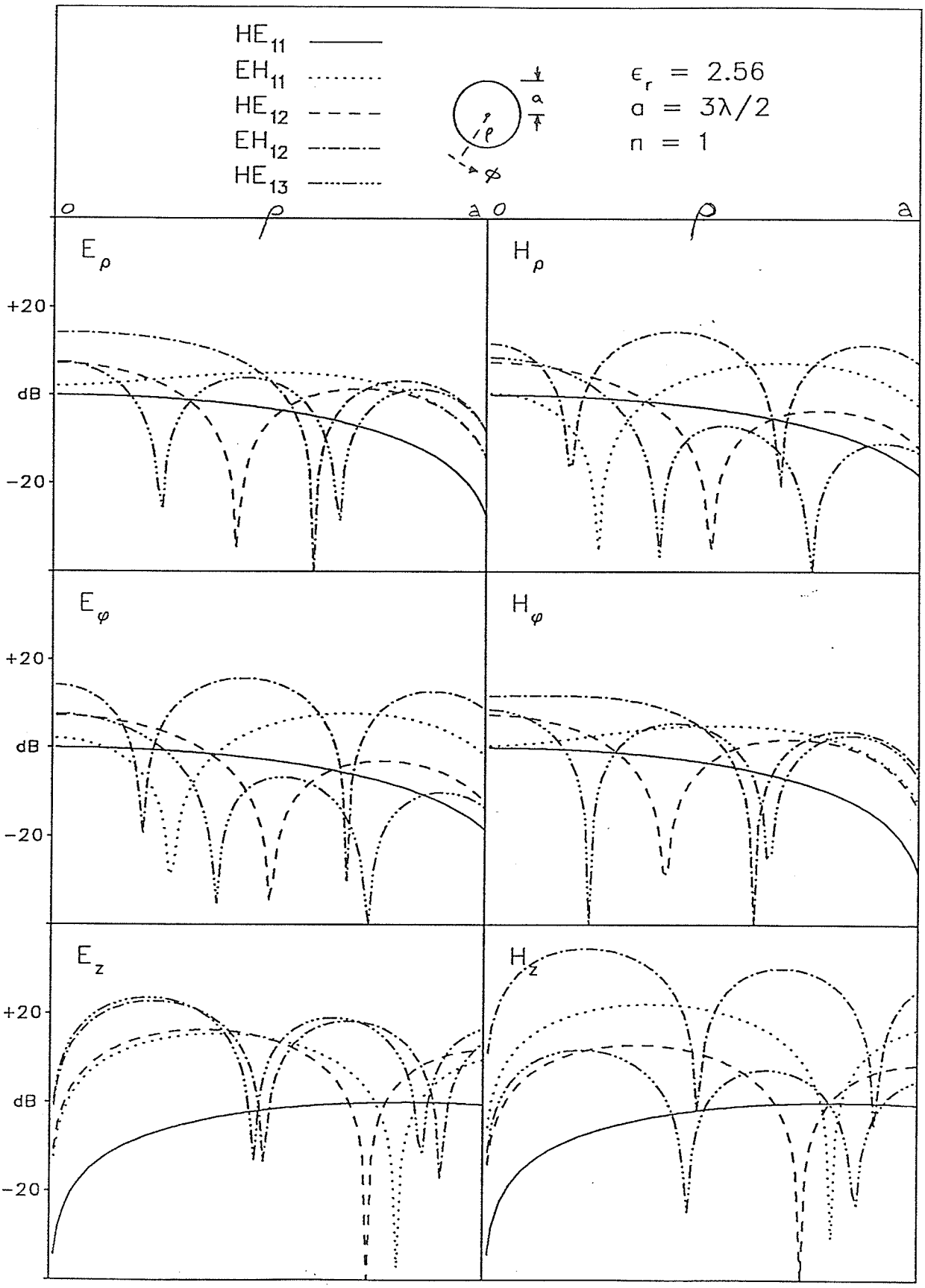

Figure 5.04 Field Amplitude Distribution $HE_{11}EH_{11}HE_{12}EH_{12}HE_{13}$

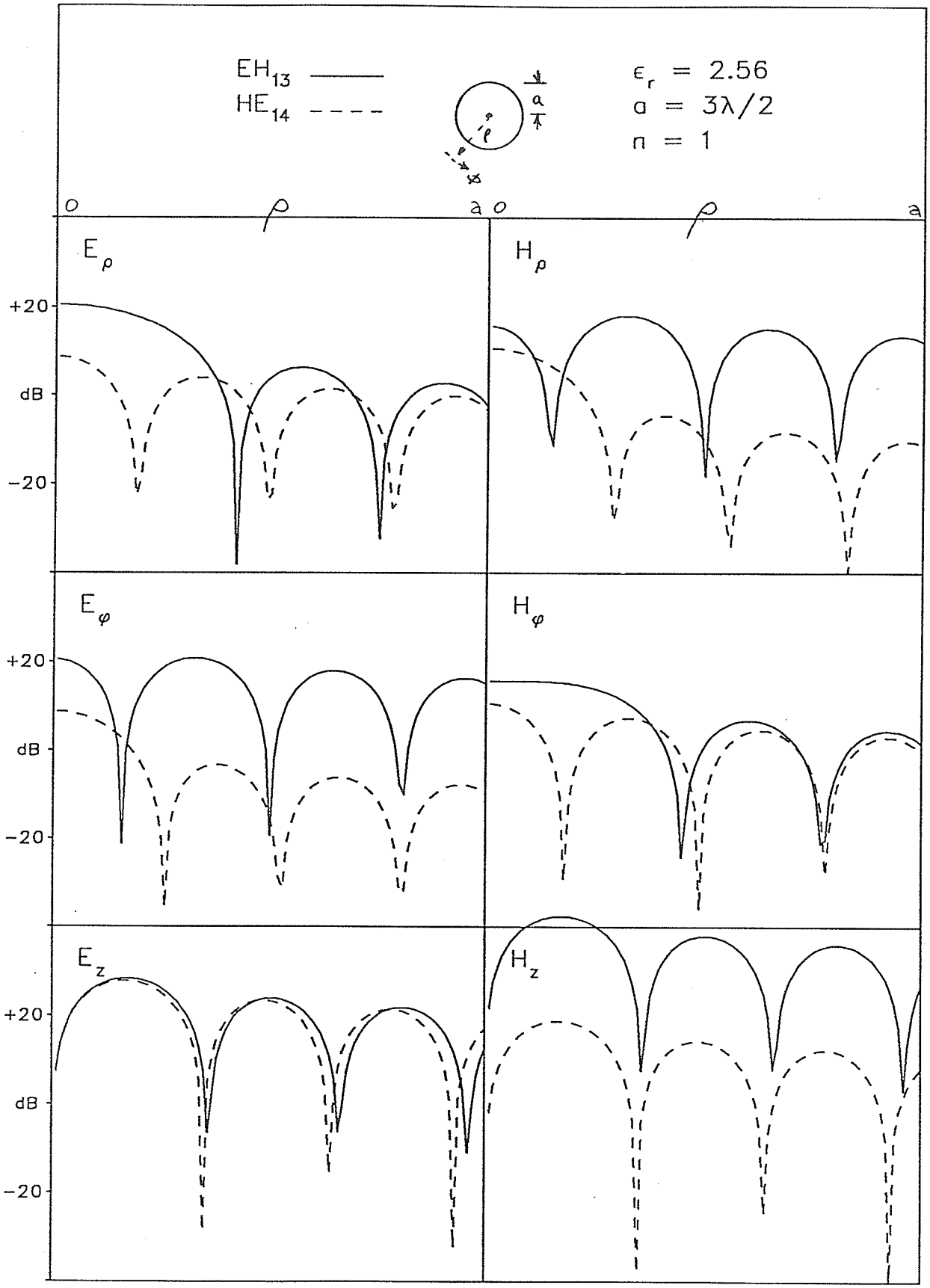

Figure 5.05 Field Amplitude Distribution $EH_{13}HE_{14}$

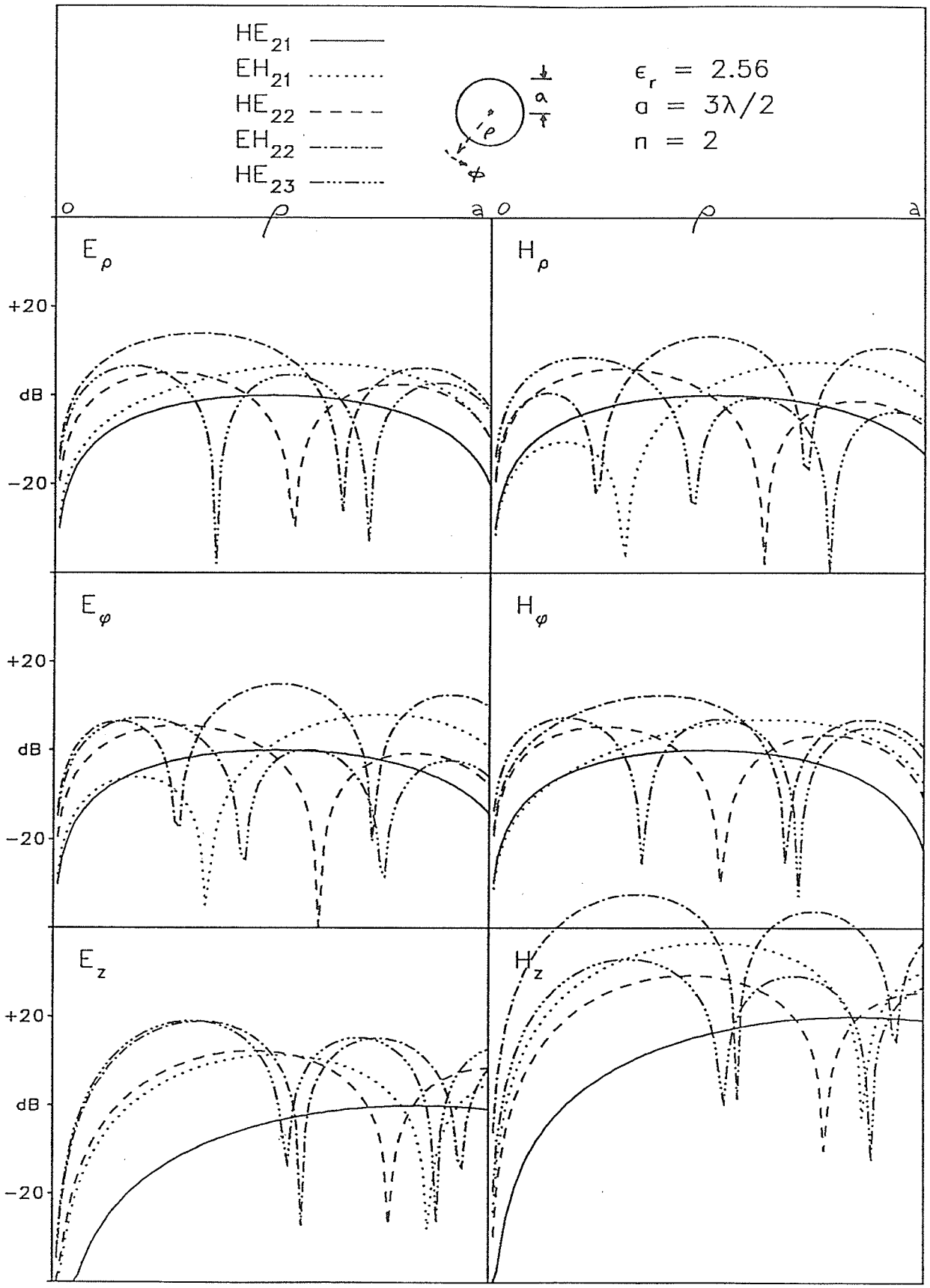

Figure 5.06 Field Amplitude Distribution $HE_{21}EH_{21}HE_{22}EH_{22}HE_{23}$

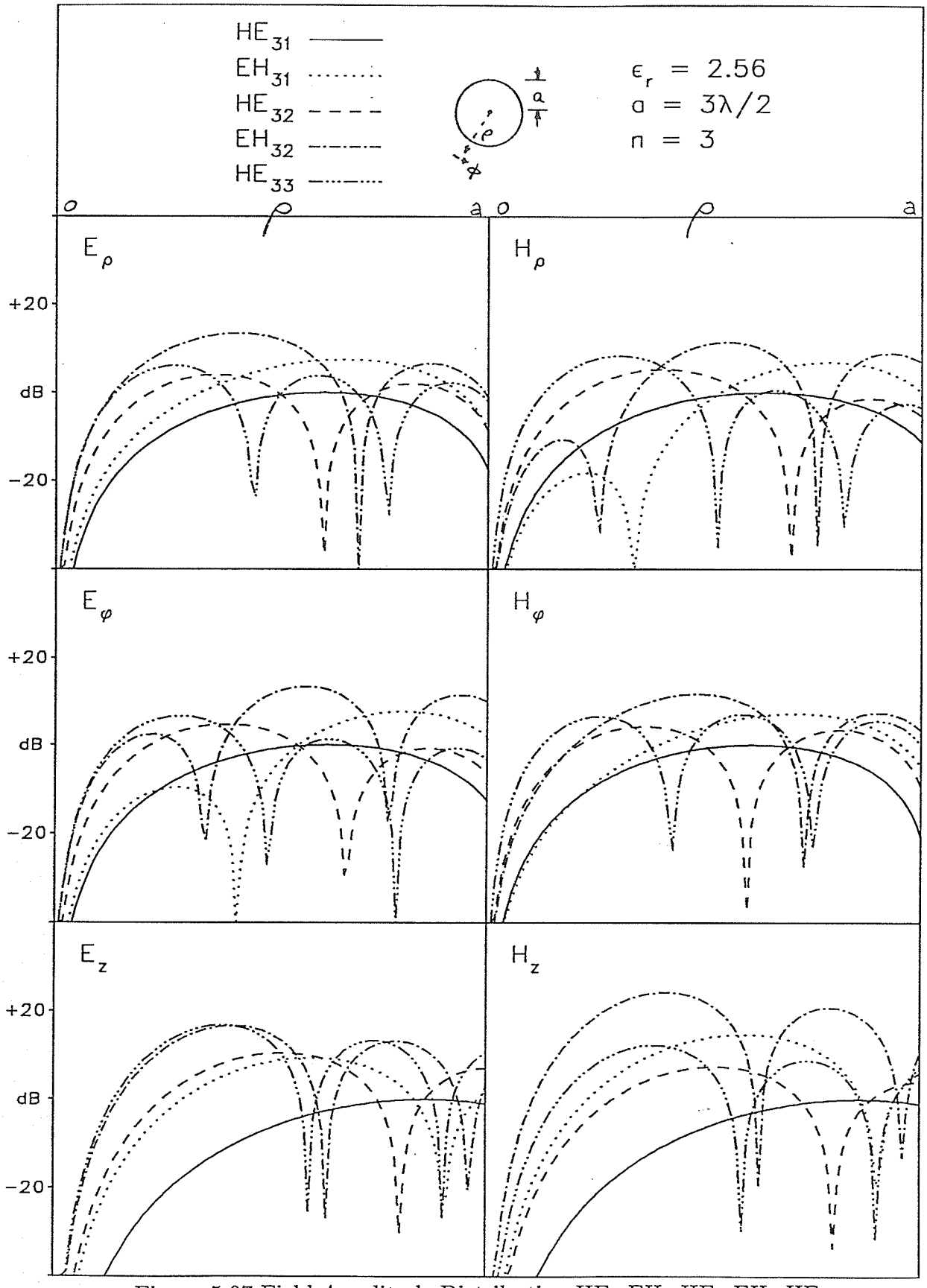

Figure 5.07 Field Amplitude Distribution $HE_{31}EH_{31}HE_{32}EH_{32}HE_{33}$

Chapter 6

Radiation Characteristics

Numerical results have been obtained for the radiation characteristics of loop antennas positioned coaxially on a variety of dielectric cylinders. The current distribution on the antenna is presumed to exhibit a $\cos n\phi$ azimuthal dependance. Under this assumption, only two terms in the Fourier series expansion in ϕ exist, $m = \pm n$. These terms combine to produce the same azimuthal dependance as seen in the surface wave fields. A knowledge of this dependance assists the presentation of the present results in that it defines the principle planes in which the radiation characteristics are calculated. For the present case, E_ϕ exhibits a $\cos n\phi$ dependance and E_θ exhibits a $\sin n\phi$ dependance.

Figures 6.01 to 6.24 present the amplitude of the E_ϕ and E_θ electromagnetic field components in the far field region. In each figure, eight radiation patterns are included which illustrate the effect of increasing the cylinder's dielectric constant. The upper semi-circle of each pattern is graduated in the polar angle θ. Figure 3.01 illustrates the relation of θ to the physical geometry of the structure. The

four semi-circles of decreasing radius indicate the 0, -10, -20, and -30 dB contour lines of the radiation pattern. At the bottom of each pattern, the relative dielectric constant, ϵ_r, of the cylinder is recorded. The maximum value of the field amplitude to which the logarithmic plot is normalized, is also recorded. Both the shape of the radiation pattern and its maximum field amplitude provides information relevant to the analysis of the structure's radiation characteristics.

The top left pattern, $\epsilon_r = 1.001$, is included in each figure to illustrate the loop's radiation characteristics in free space and to emphasize the affect that the dielectric cylinder has upon the loop's radiation pattern. Although computed by solution of a cylindrical boundary value problem, this free space pattern, by way of verification, may also be computed using a radiation integral approach.

Each figure caption contains information regarding the field components observed, the loop radius a, and the azimuthal mode number n. Patterns are presented for the appropriate principle plane as defined above.

By way of brief review, Figure 6.01 to 6.04 illustrate the amplitude of E_ϕ for a $\cos\phi$ 1.0 ampere current distribution. The loop radii considered are $\lambda/8$, $\lambda/4$, , $3\lambda/8$, and $\lambda/2$, respectively. Increases in directivity are observed in the patterns of Figure 6.01 for the cases $\epsilon_r = 1.5,\ 2.0$, and 2.5. The patterns are slightly modified for these cases. These perturbations may be attributed to the influence of the cylinder. The cases of $\epsilon_r = 3.0,\ 3.5,\ 4.0$, and 4.5 show a steady decrease in the maximum field amplitude observed. It is evident that power is being transported away from the loop via surface waves. Obviously, as the dielectric constant increases above 3.0, additional surface waves are excited.

A slightly different behaviour is observed in Figure 6.02. Although the pattern modification is attributable to radiation from the cylinder, the significant observation is the initial rapid reduction in maximum field amplitude. Again, this may be attributed to surface wave action. The further modification of the pattern and gradual increase in maximum field amplitude as the dielectric constant is increased to 4.5 is the result of the cylinder's influence.

In Figure 6.03, again the initial decrease in the maximum field amplitude may be associated with surface wave excitation. The cylinder's influence plays an increasingly significant role up to $\epsilon_r = 3.5$ where a very narrow beamwidth pattern occurs. Narrow beamwidth patterns of this nature are normally seen in travelling or leaky wave wire antennas. The influence of the cylinder appears to be cut off for $\epsilon_r = 4.0$. The further decrease in the maximum field amplitude suggests that higher order surface wave modes are being excited and, as such, transport more power away from the loop in a non-radiative manner.

Similar results are seen in Figure 6.04. Of particular interest is the radiation pattern seen at $\epsilon_r = 2.0$. Similar results to those seen in the $\epsilon_r = 2.0$ case have been observed by Pavlov [59] for a loop antenna situated on a cylinder composed of permeable material.

Figures 6.05 to 6.08 illustrate the amplitude of E_ϕ for a $\cos 2\phi$ 1.0 ampere current distribution. The loop radii considered are $\lambda/8$, $\lambda/4$, $3\lambda/8$ and $\lambda/2$, respectively. Again, the $\epsilon_r = 1.001$ patterns are patterns which would normally be observed from the respective loops radiating in free space.

A very interesting result is observed in Figure 6.05. Through the entire range

of dielectric constants, there is virtually no observable change in the shape of the field pattern. However, the maximum field amplitude decreases exponentially. This clearly illustrates the increasing excitation of a low order surface wave mode with a resultant increase in power transported away from the loop. It is evident that, aside from surface wave action, the cylinder exhibits negligible influence under these conditions.

In Figure 6.06, the increased excitation of the surface wave is again observed. A gradual modification of the pattern illustrates the increasing influence of the cylinder. As the beamwidth of the pattern narrows, a corresponding increase in maximum field amplitude is observed.

The cylinder's influence is very predominant in the patterns of Figure 6.07. The variation of maximum field amplitude with pattern shape is readily apparent for all cases. The introduction of small sidelobes for $\epsilon_r = 4.0$ and 4.5 is also observed.

Behaviour similar to that of Figure 6.03 is again noted in Figure 6.08. Of particular interest is the extremely high directivity condition observed for $\epsilon_r = 3.5$. The shift in cylinder radius observed between Figures 6.03 and 6.08 appears to be connected with the root locations of the first and second order Bessel functions. Once again, the influence of the cylinder appears to be cut off above $\epsilon_r = 4.0$.

Figures 6.09 to 6.12 illustrate the amplitude of E_ϕ for a $\cos 3\phi$ 1.0 ampere current distribution. The loop radii considered are $\lambda/8$, $\lambda/4$, $3\lambda/8$, and $\lambda/2$, respectively. Again, the $\epsilon_r = 1.001$ patterns reflect free space radiation patterns.

The behaviour observed in Figure 6.05 is repeated in both Figure 6.09 and 6.10. In comparing these figures, it is noted that the largest maximum field amplitudes

are observed in Figure 6.10, followed by 6.05, and then 6.09. However, the largest 3 dB beamwidth is observed in the patterns of Figure 6.05, followed by 6.10, and then 6.09. In all cases, an exponential decrease in maximum field amplitude is observed, indicating the increased excitation of electromagnetic surface waves.

In Figure 6.11, the predominant action of surface wave excitation is observed for the cases of $\epsilon_r = 1.5$ and 2.5. Contributions to the pattern from cylinder influence are in evidence for the cases of $\epsilon_r = 3.0$ to 4.5. Although the patterns change significantly over this region, the gradual increase in maximum field amplitude up to the free space value indicates that there will be significant power transport away from the loop via the surface wave.

The radiation patterns presented in Figure 6.12 appear to be similar to those of Figure 6.08. In particular, the $\epsilon_r = 2.0$, 2.5, 3.0, and 3.5 patterns of Figure 6.08 are very close in appearance to the $\epsilon_r = 3.0$, 3.5, 4.0, and 4.5 patterns of Figure 6.12. The various mechanisms involved in the two geometries are presumed to be similar.

Figures 6.13 to 6.16 illustrate the amplitude of E_θ for a $\cos\phi$ 1.0 ampere current distribution. Once again, loop radii $\lambda/8$, $\lambda/4$, $3\lambda/8$, and $\lambda/2$ are considered and the $\epsilon_r = 1.001$ results provide the free space patterns.

Figures 6.17 to 6.20 illustrate the amplitudes of E_θ for a $\cos 2\phi$ 1.0 ampere current distribution and Figures 6.21 to 6.24 illustrate the amplitude of E_θ for a $\cos 3\phi$ 1.0 ampere current distribution. The E_θ characteristics exhibit trends similar to those seen in the E_ϕ patterns. The results of Figures 6.17, 6.21, and 6.22 exhibit trends which are identical to those of Figures 6.05, 6.09, and 6.10.

Radiation characteristics for loop antennas with current distributions calculated

from the present formulation have also been determined. Figures 6.25 to 6.28 display the radiation characteristics of loop antennas, $C/\lambda_o = 0.5$, 1.0, 1.5, and 2.0, which are positioned on a dielectric cylinder, $\epsilon_r = 2.56$. The first five Fourier components of each current distribution are used to calculate these radiation results.

Some general conclusions may be drawn from the results presented in this chapter. First, the influence of the dielectric cylinder is significant in a large number of cases. This influence is presumed to be the phase shift introduced by the cylinder to the radiation emanating from the various point sources which comprise the loop antenna. The antenna may be considered as a circular array of point sources. Each point source exhibits a different amplitude and phase characteristic. The phase characteristic of each point source is further modified by the presence of the cylinder. In a few instances, the dielectric cylinder exhibits no influence on the antenna's radiation pattern. This may occur when the phase shifts introduced by the cylinder are on the order of 2π. In general, there will be a complex relationship with respect to power balance between radiation from the antenna and the excitation of hybrid mode surface waves. It is possible to employ a dielectric support which will not affect the shape of the pattern; the only compromise is a reduction in radiated power. Conversely, it is possible to vary the cylinder geometry and dielectric constant to design a variety of shaped beam antennas. Finally, the implementation of highly directive antennas is also possible under suitably selected parameters.

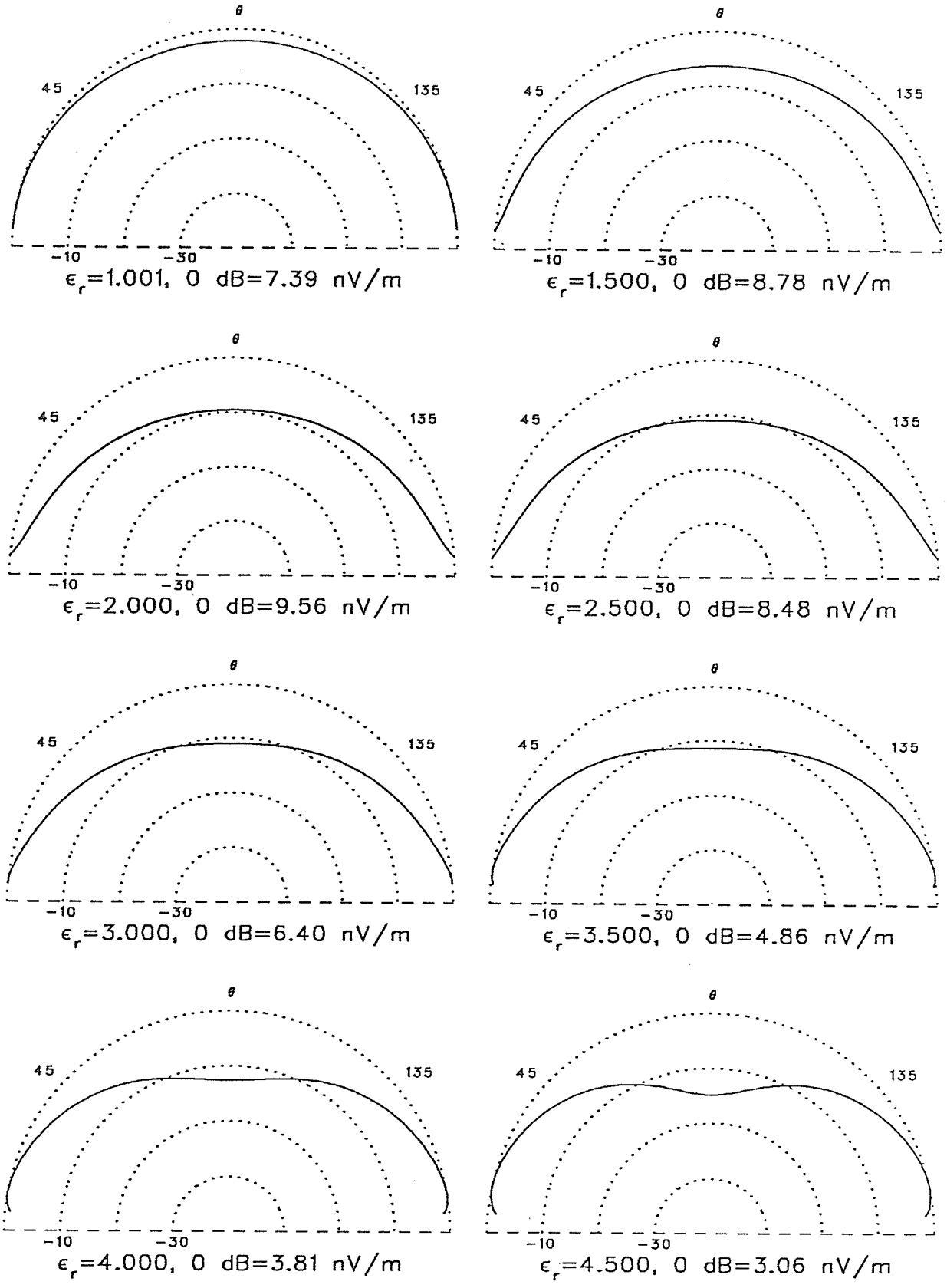

Figure 6.01 E_ϕ $a = \lambda/8$ $n = 1$

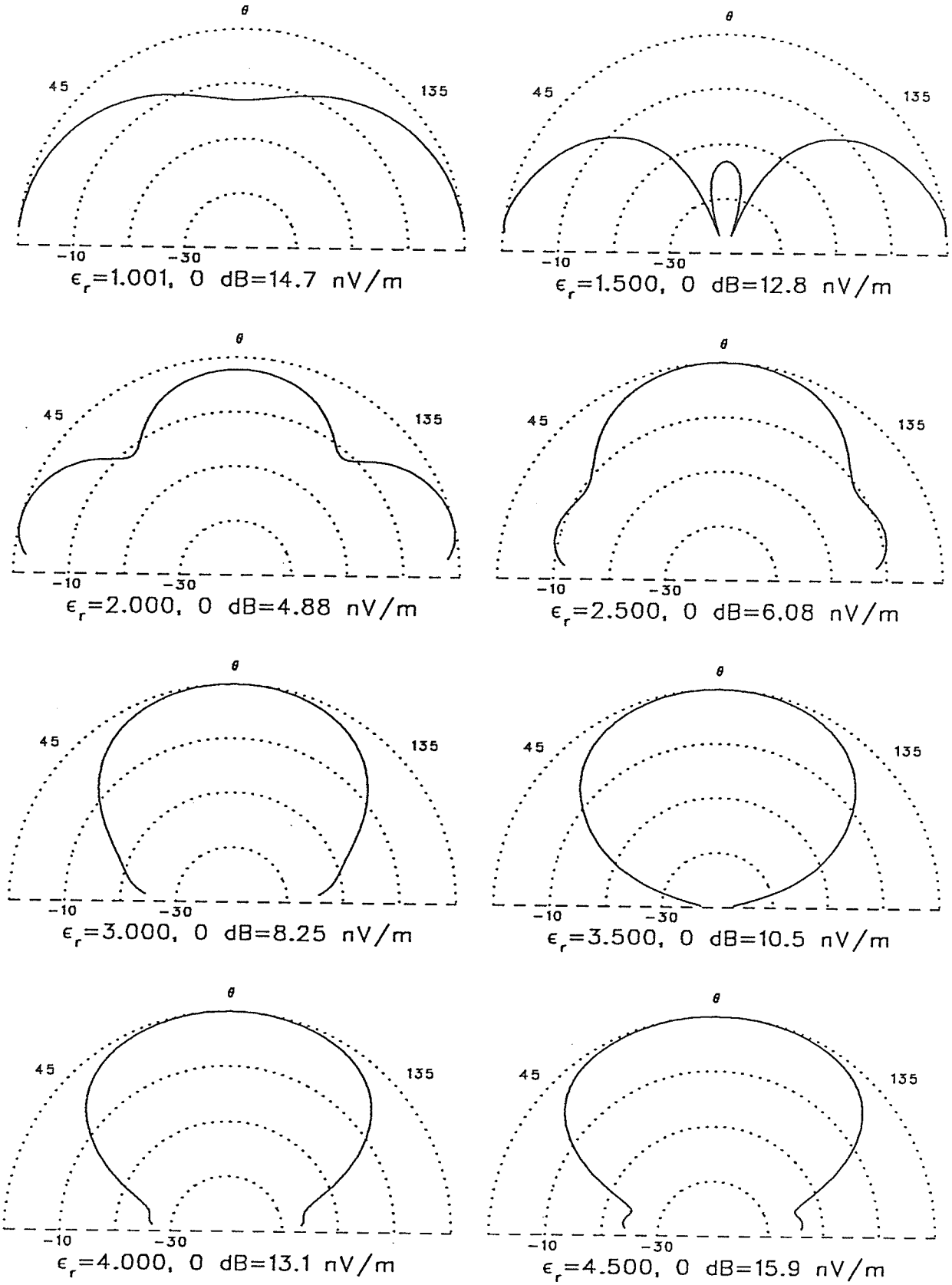

Figure 6.02 E_ϕ $a = \lambda/4$ $n = 1$

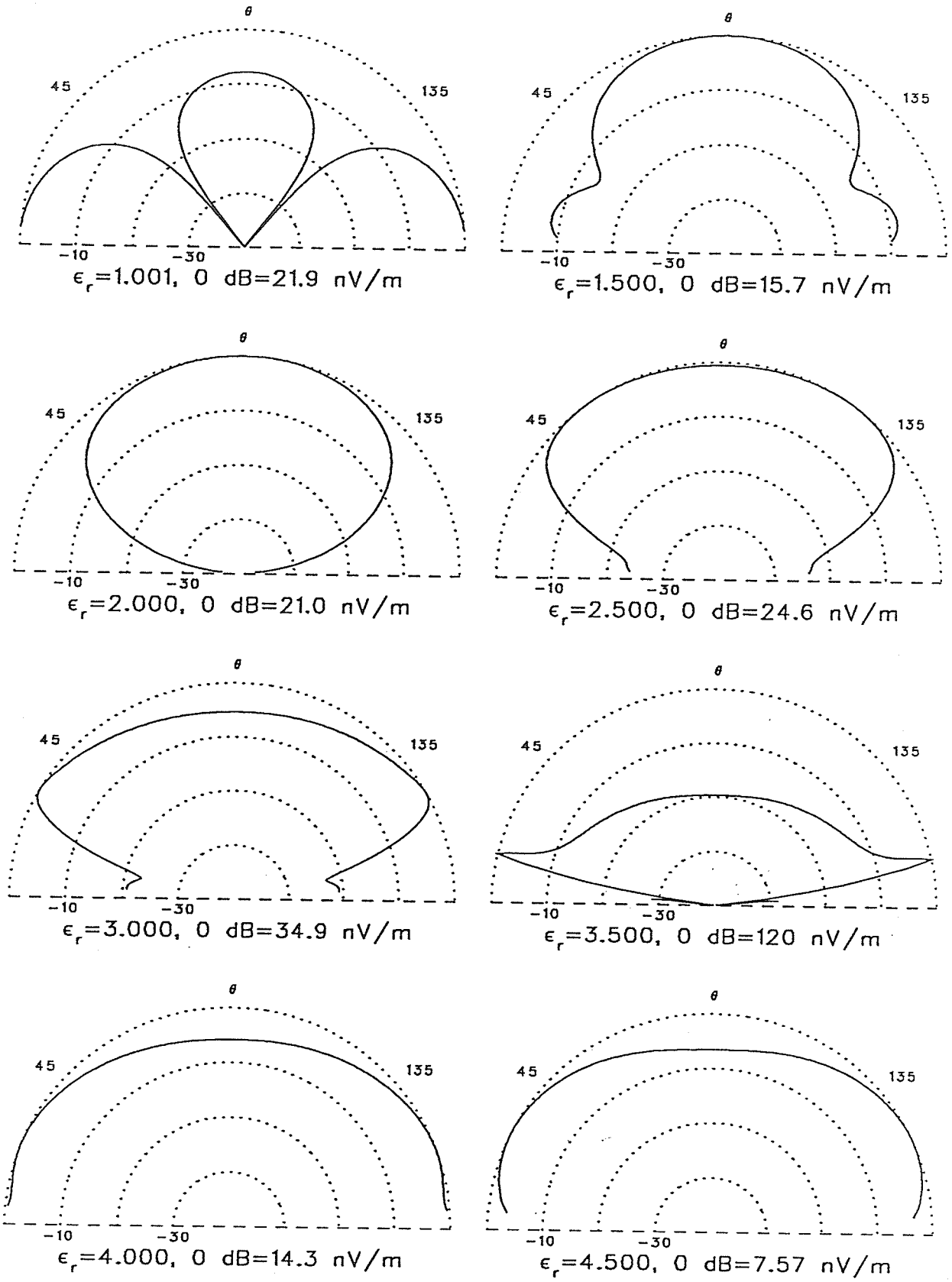

Figure 6.03 E_ϕ $a = 3\lambda/8$ $n = 1$

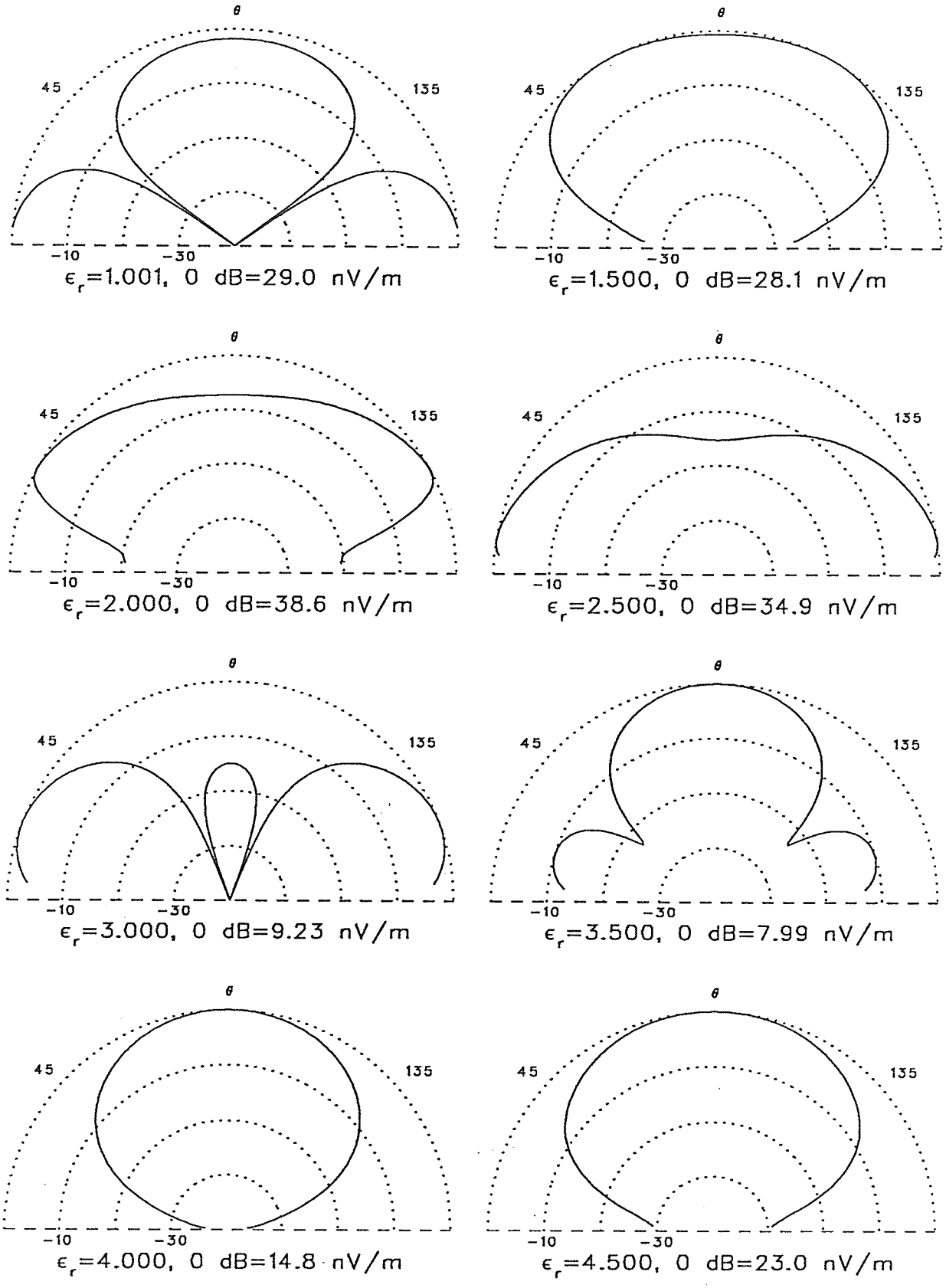

Figure 6.04 E_ϕ $a = \lambda/2$ $n = 1$

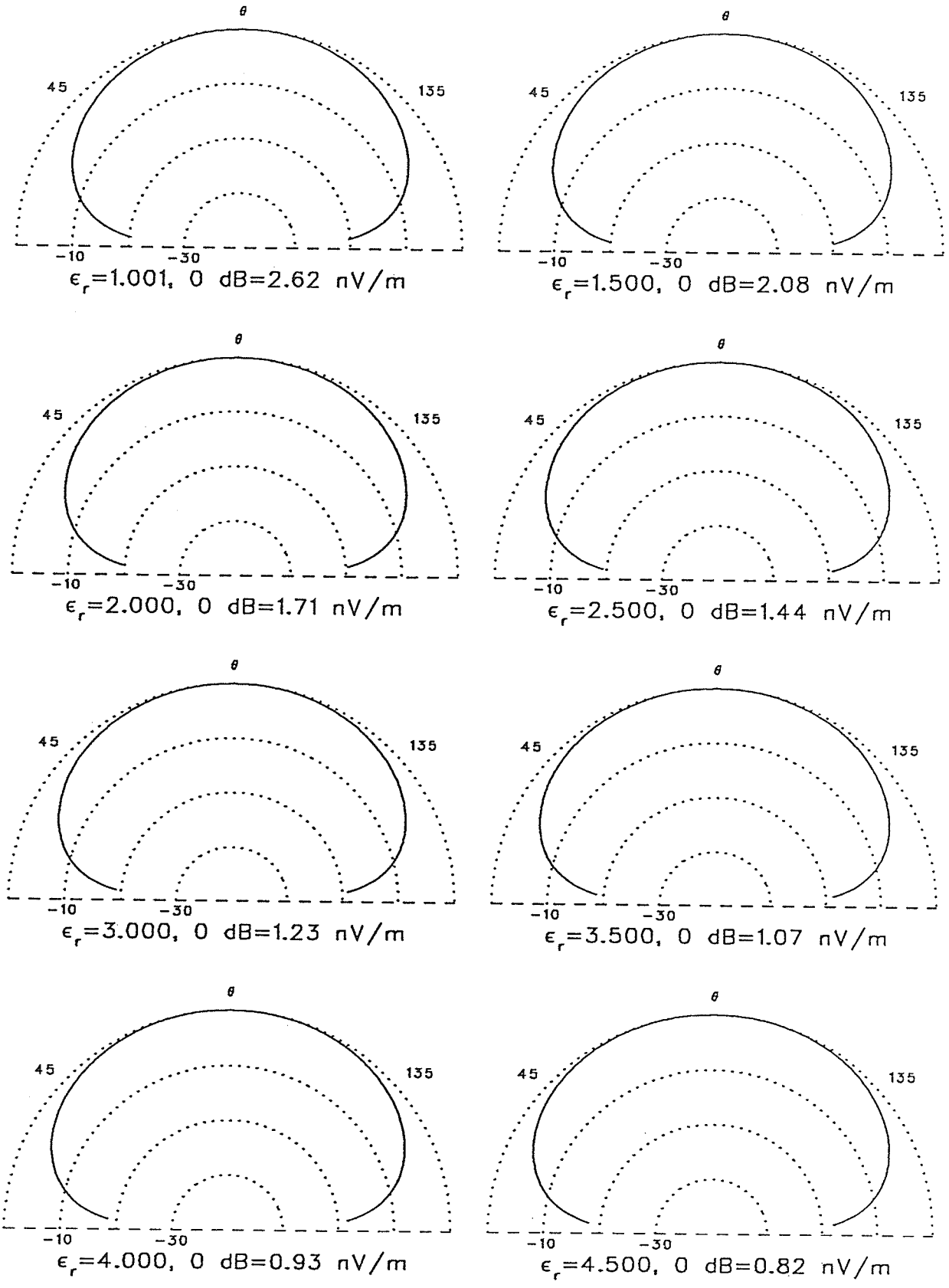

Figure 6.05 E_ϕ $a = \lambda/8$ $n = 2$

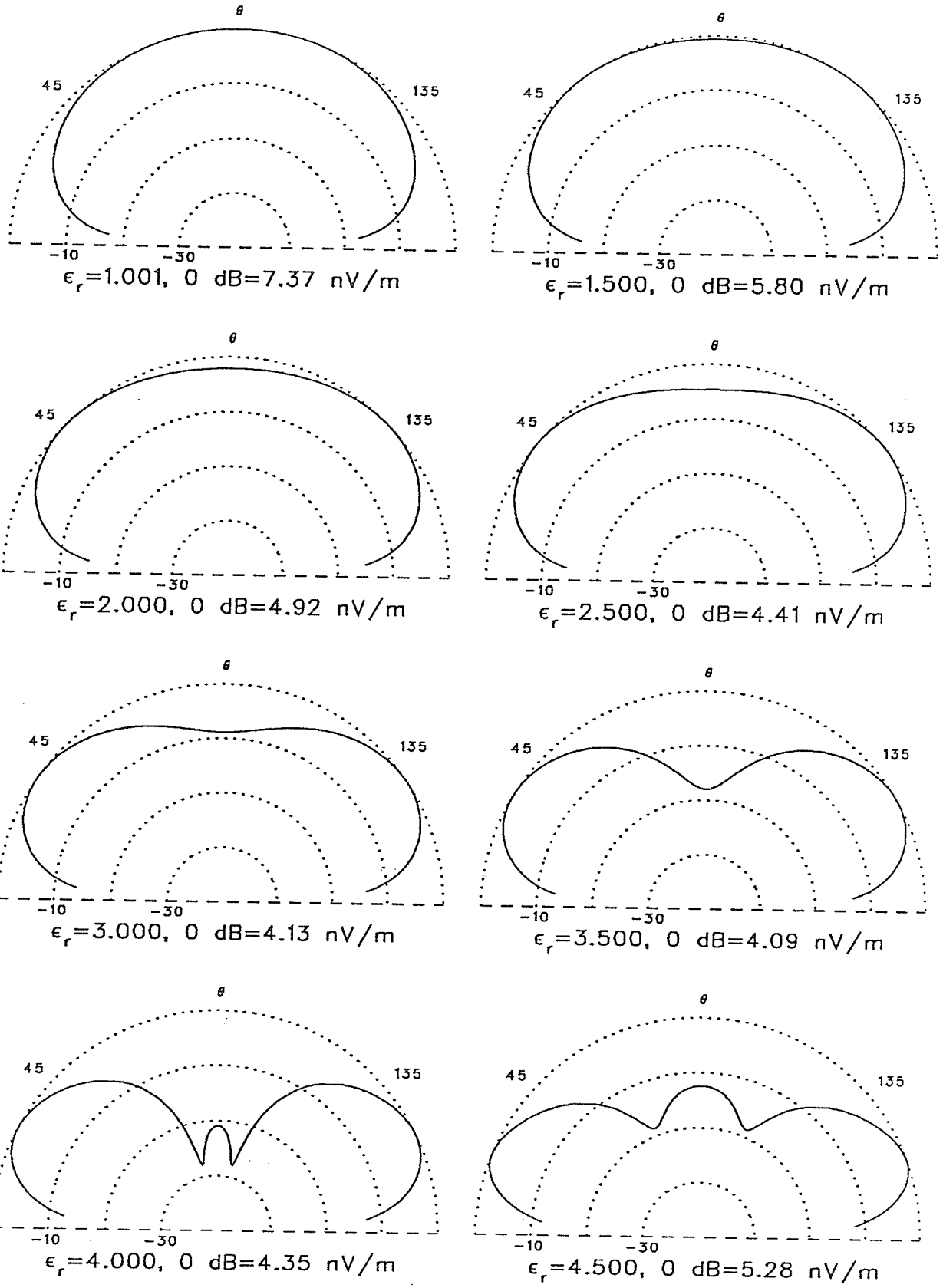

Figure 6.06 E_ϕ $a = \lambda/4$ $n = 2$

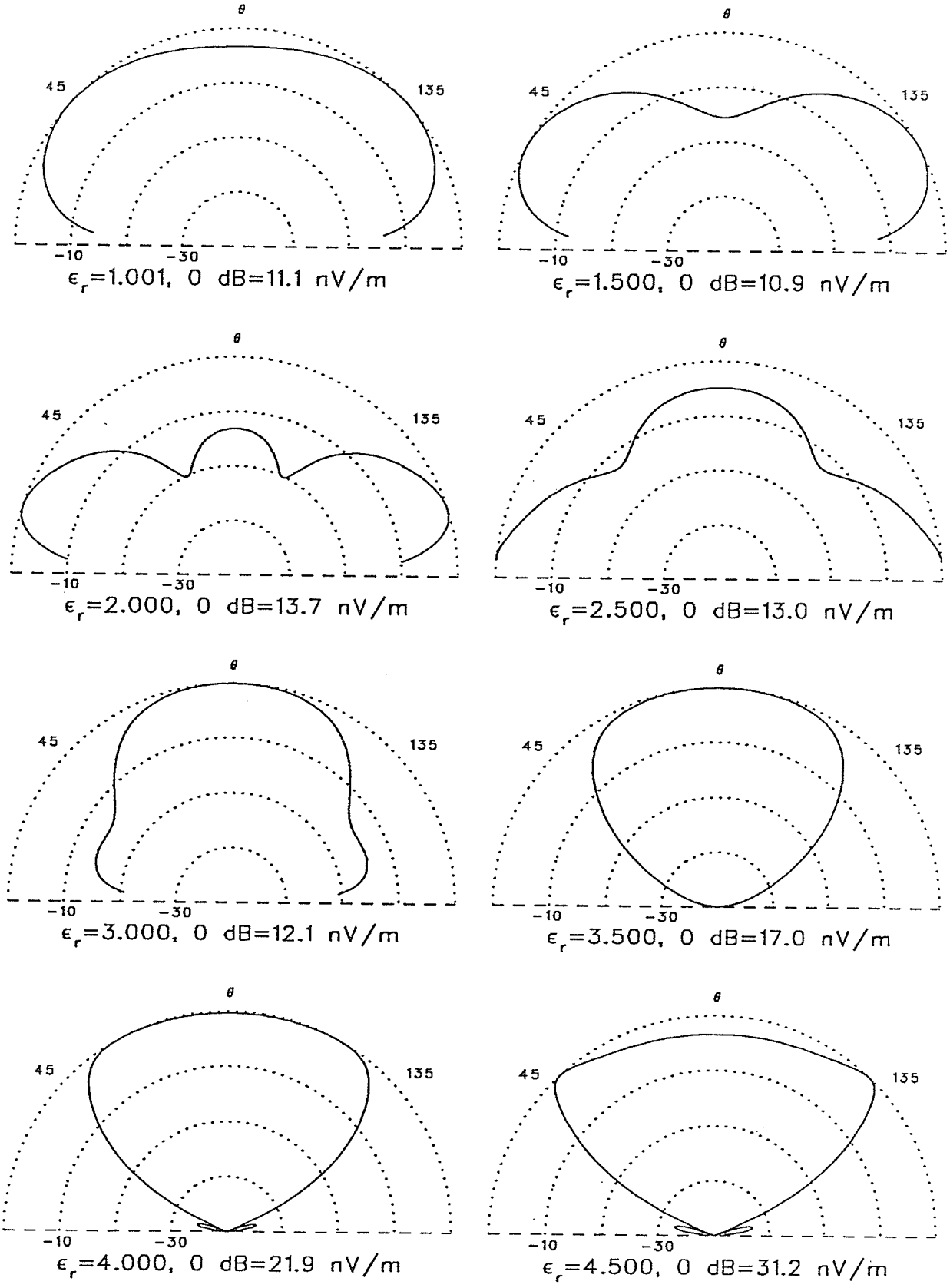

Figure 6.07 E_ϕ $a = 3\lambda/8$ $n = 2$

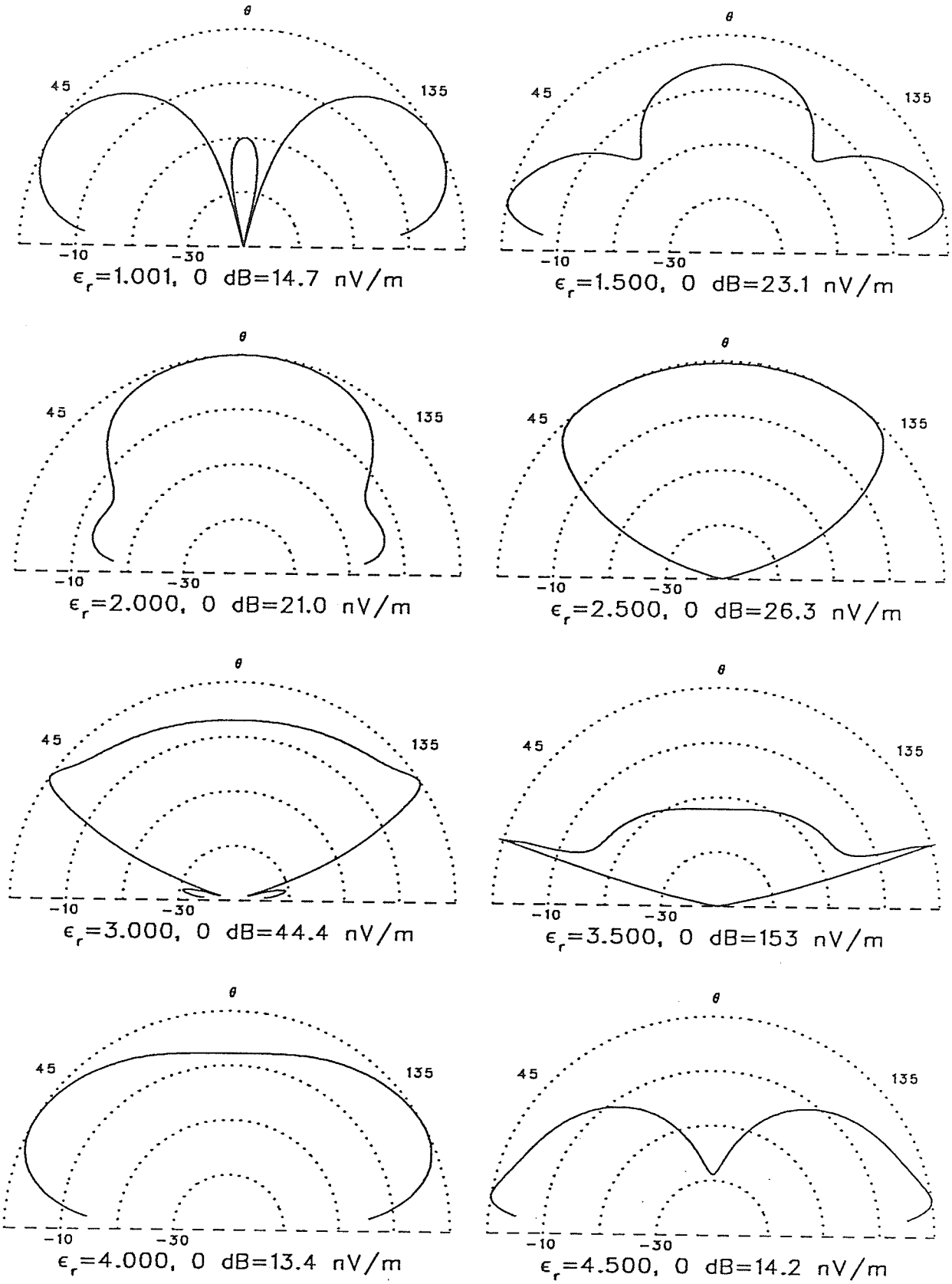

Figure 6.08 E_ϕ $a = \lambda/2$ $n = 2$

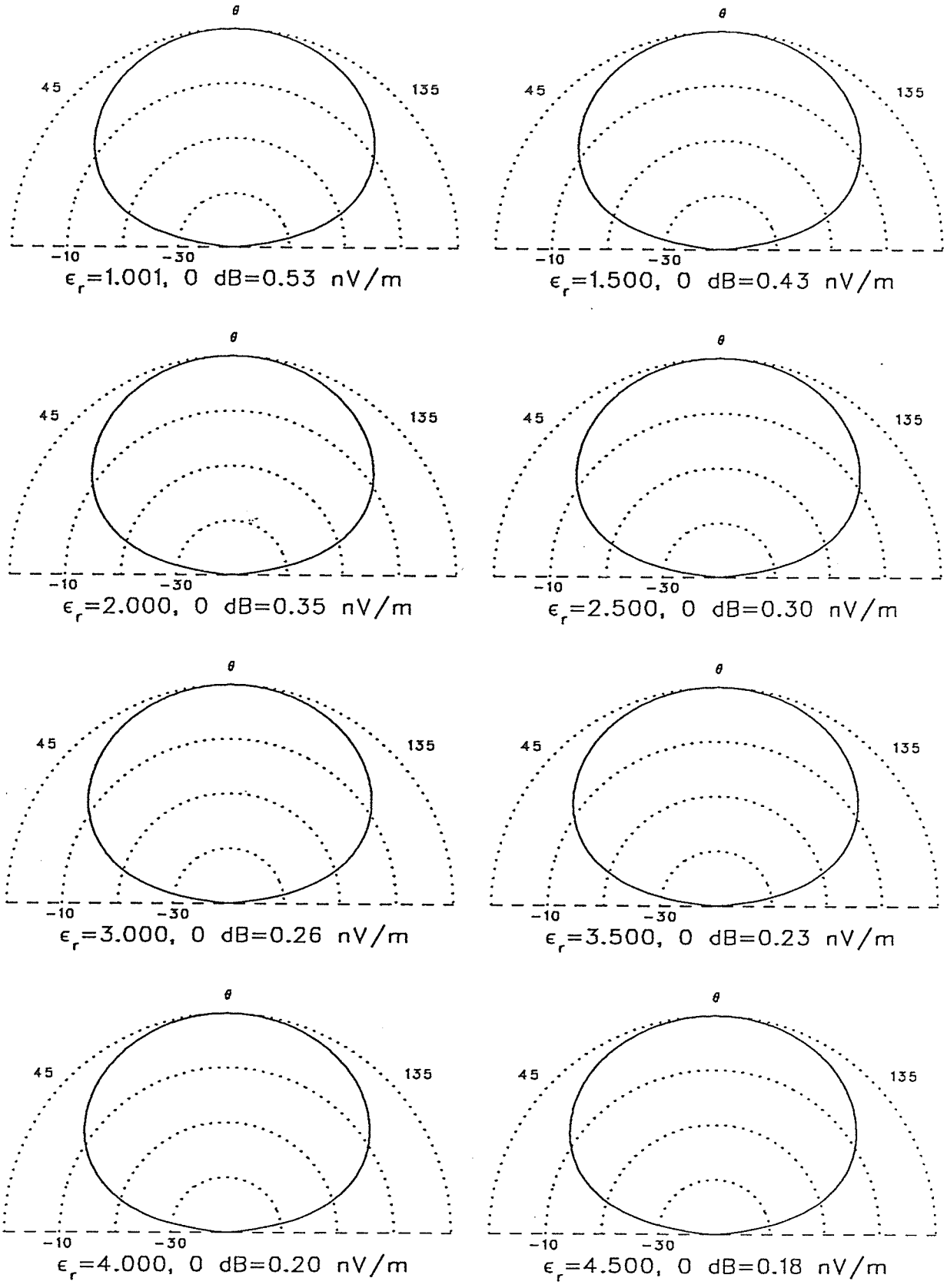

Figure 6.09 E_ϕ $a = \lambda/8$ $n = 3$

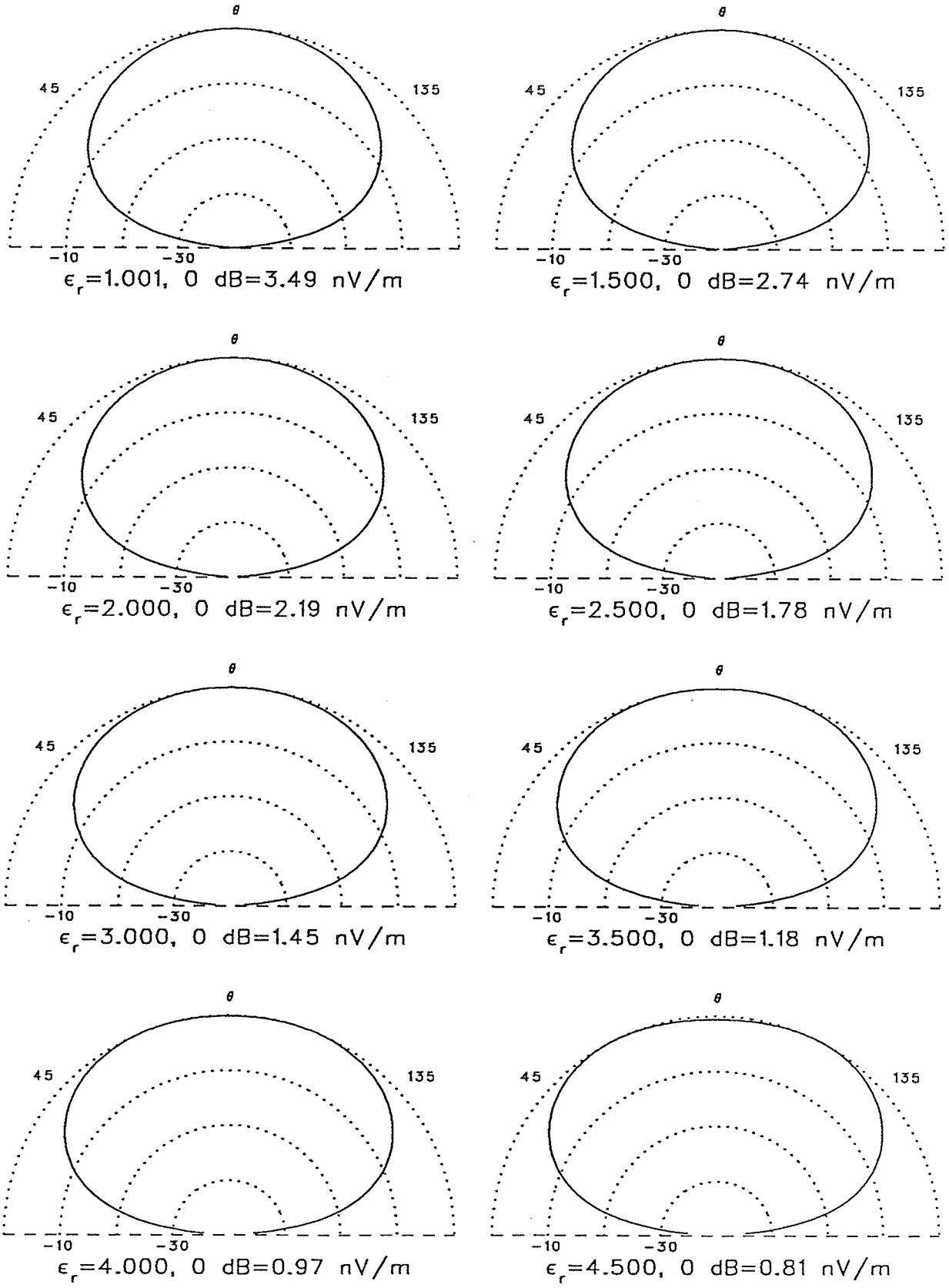

Figure 6.10 E_ϕ $a = \lambda/4$ $n = 3$

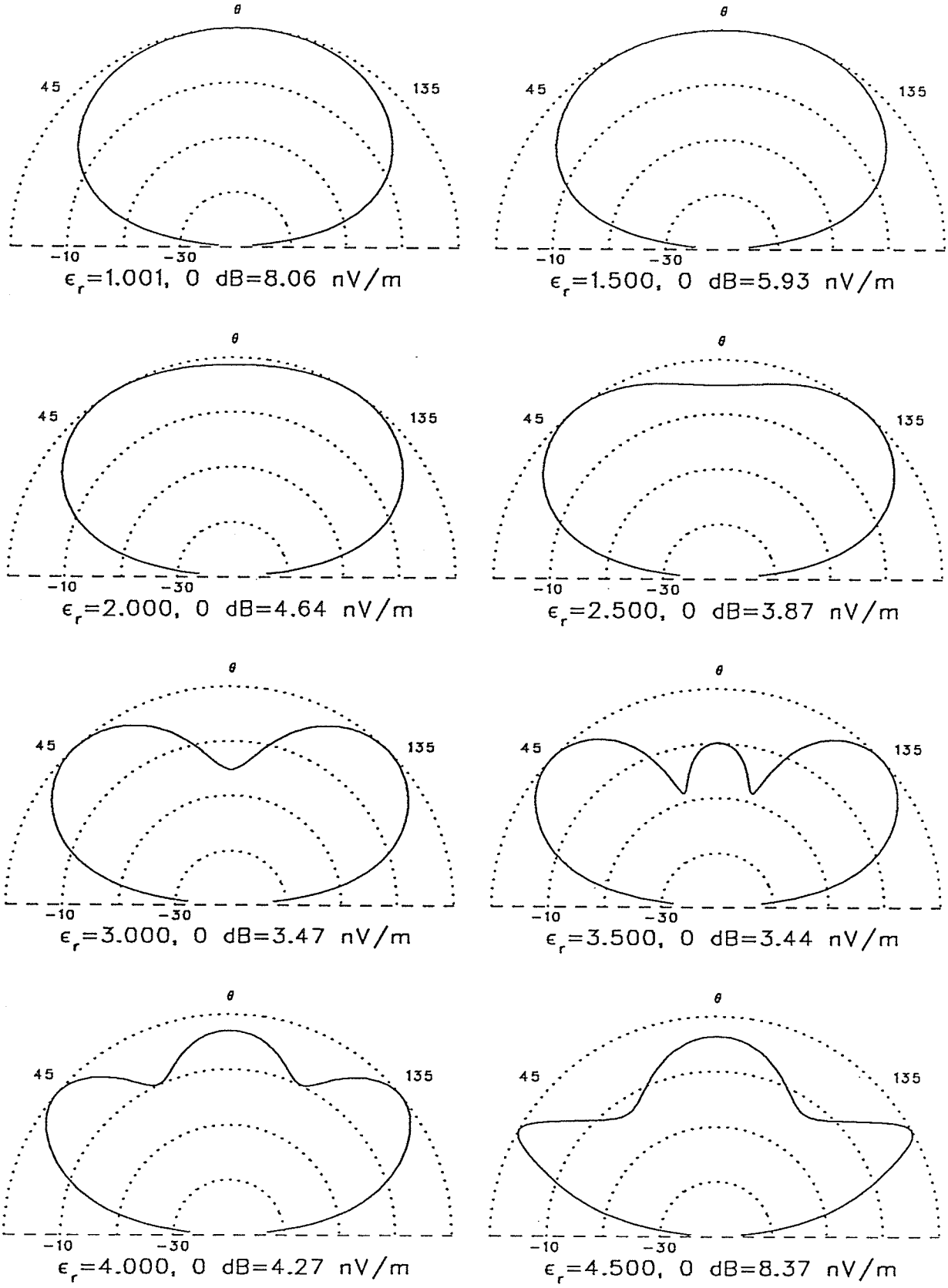

Figure 6.11 E_ϕ $a = 3\lambda/8$ $n = 3$

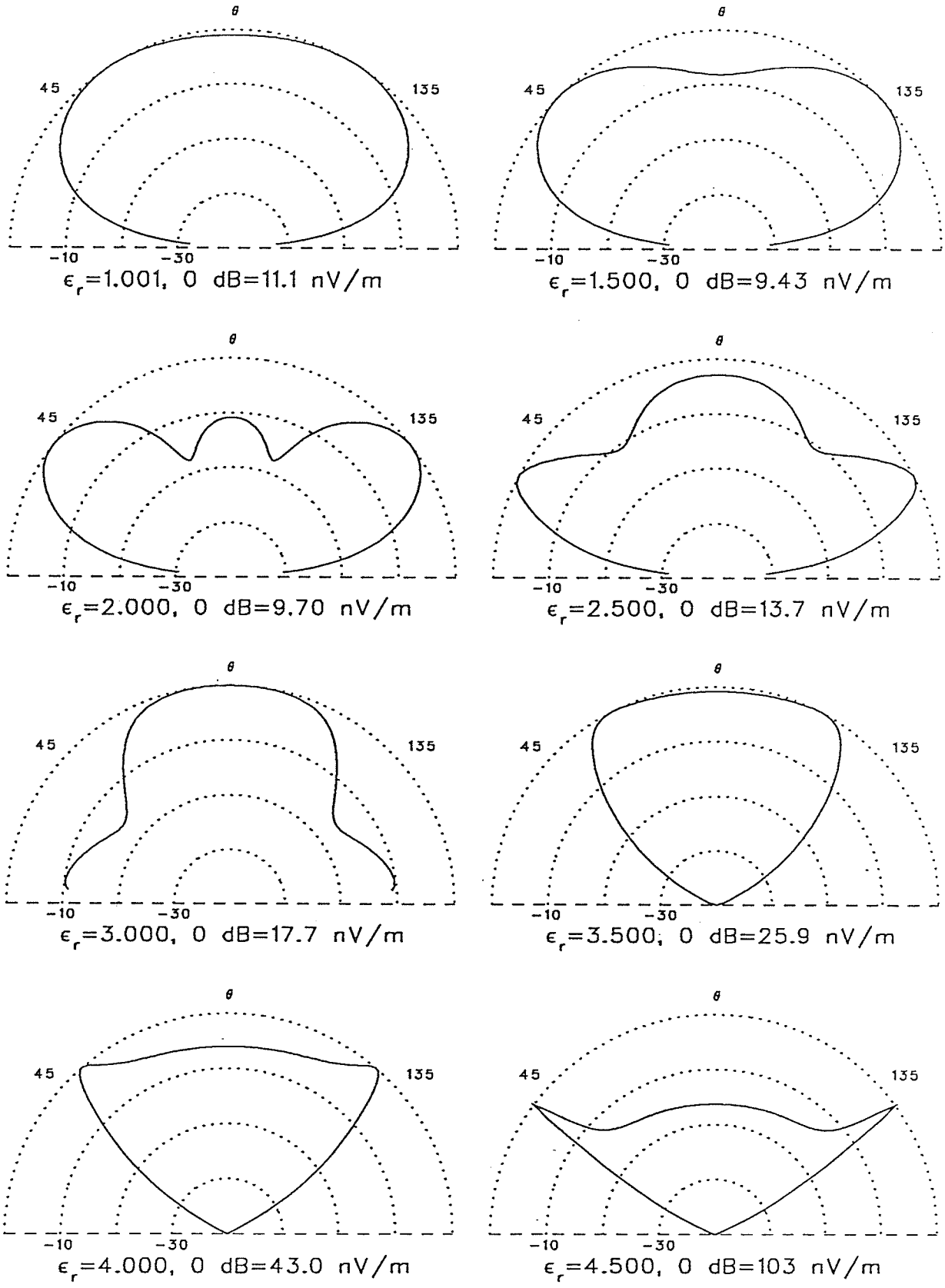

Figure 6.12 E_ϕ $a = \lambda/2$ $n = 3$

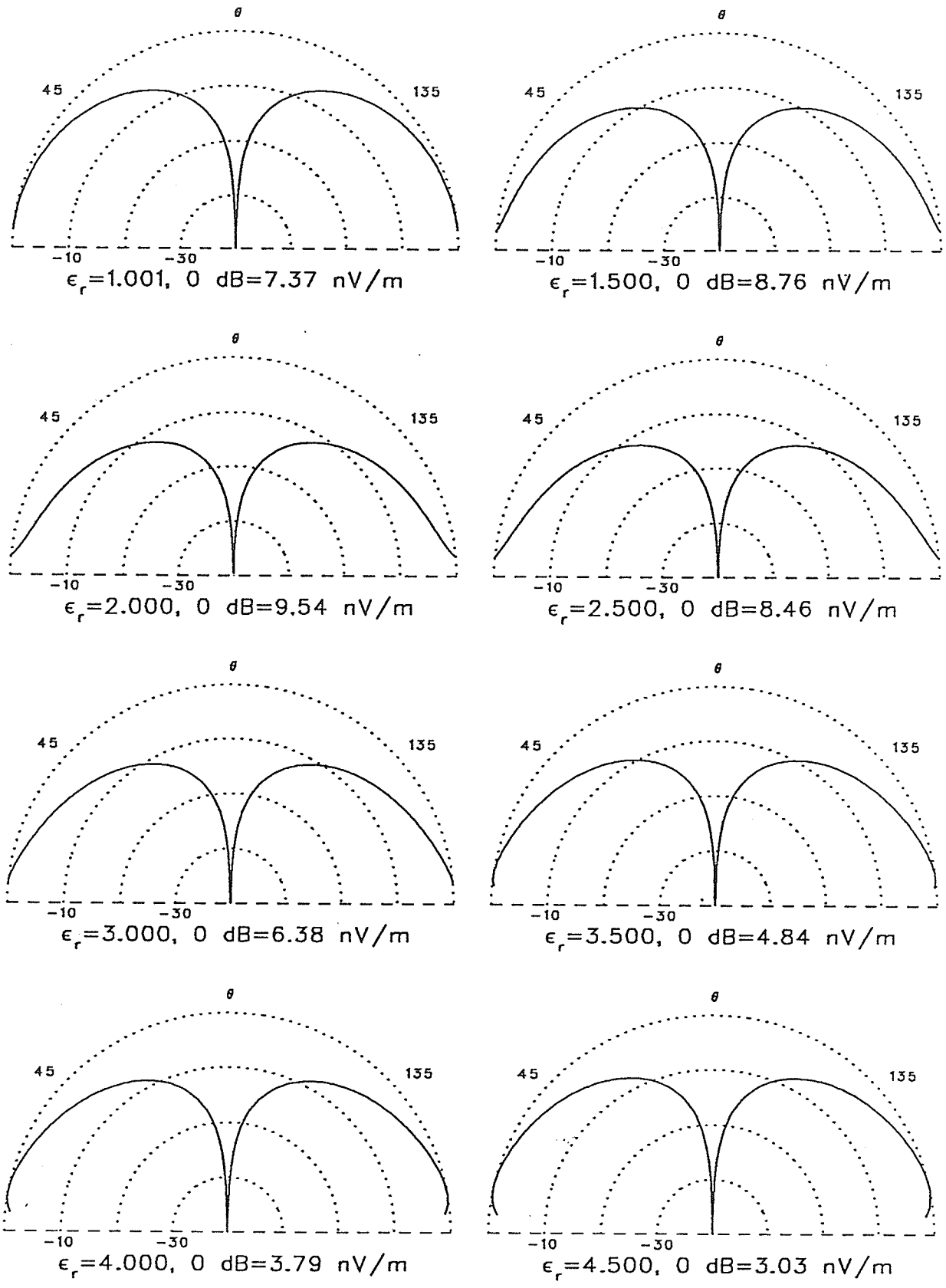

Figure 6.13 E_θ $a = \lambda/8$ $n = 1$

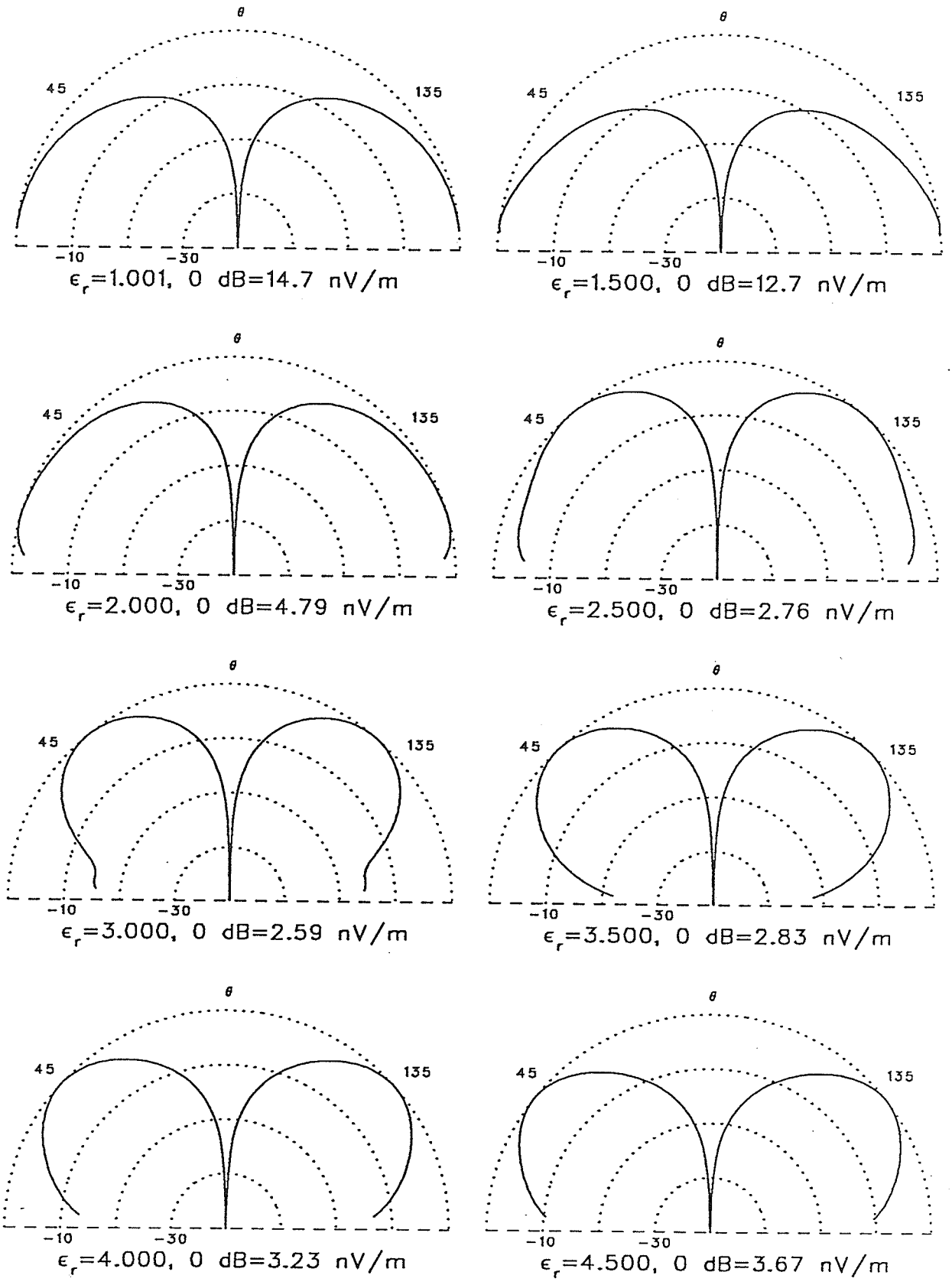

Figure 6.14 E_θ $a = \lambda/4$ $n = 1$

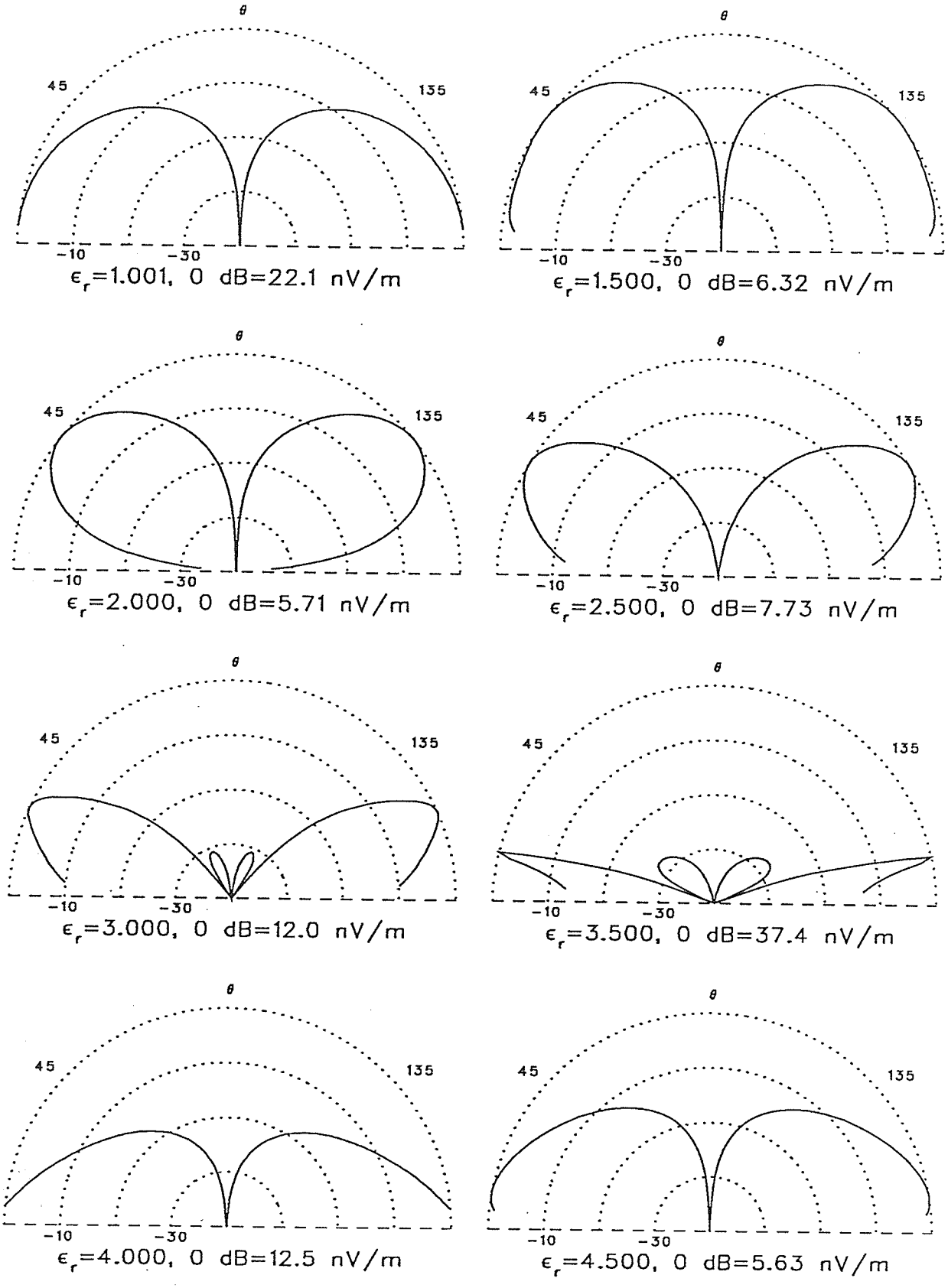

Figure 6.15 E_θ $a = 3\lambda/8$ $n = 1$

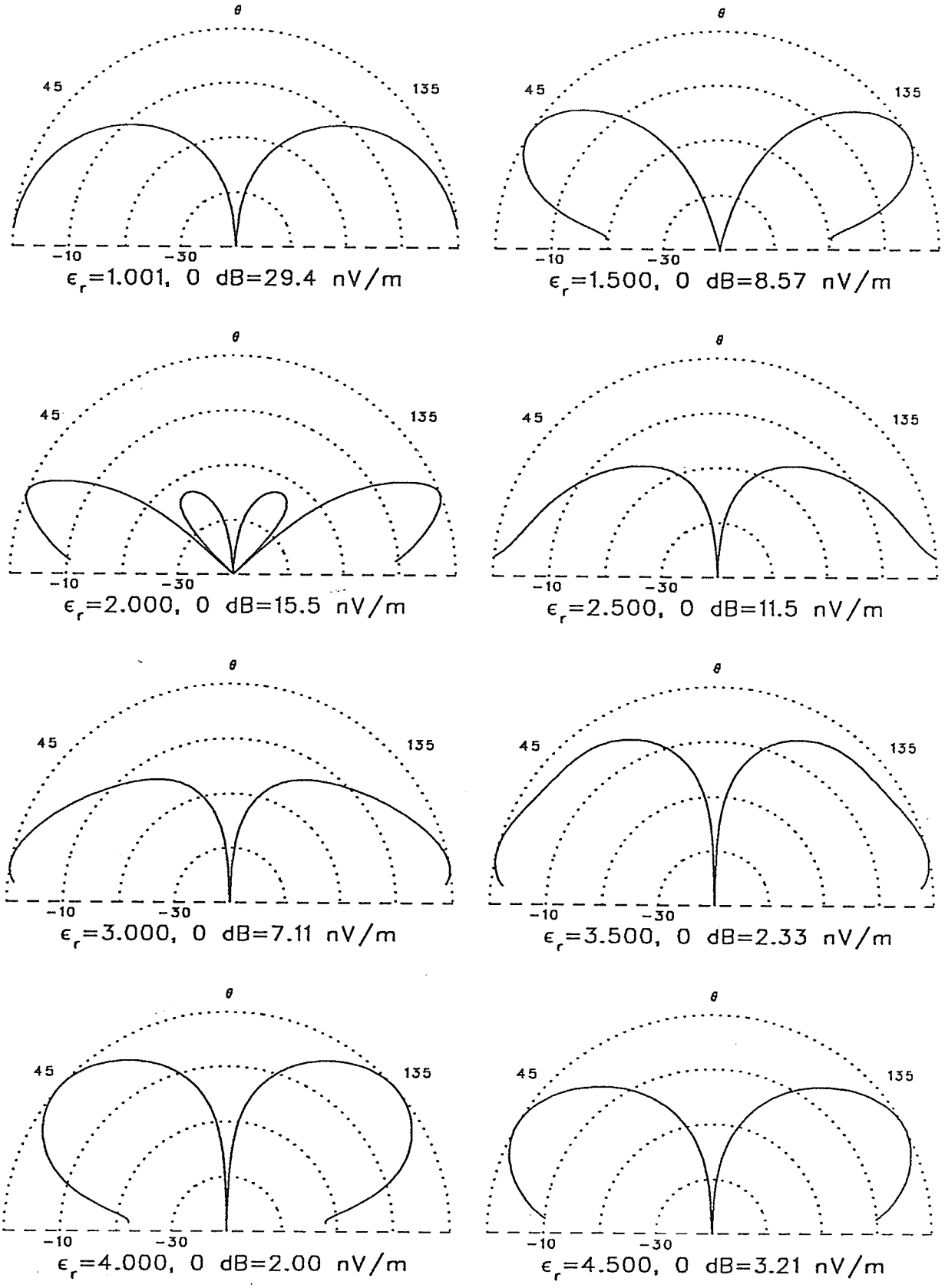

Figure 6.16 E_θ $a = \lambda/2$ $n = 1$

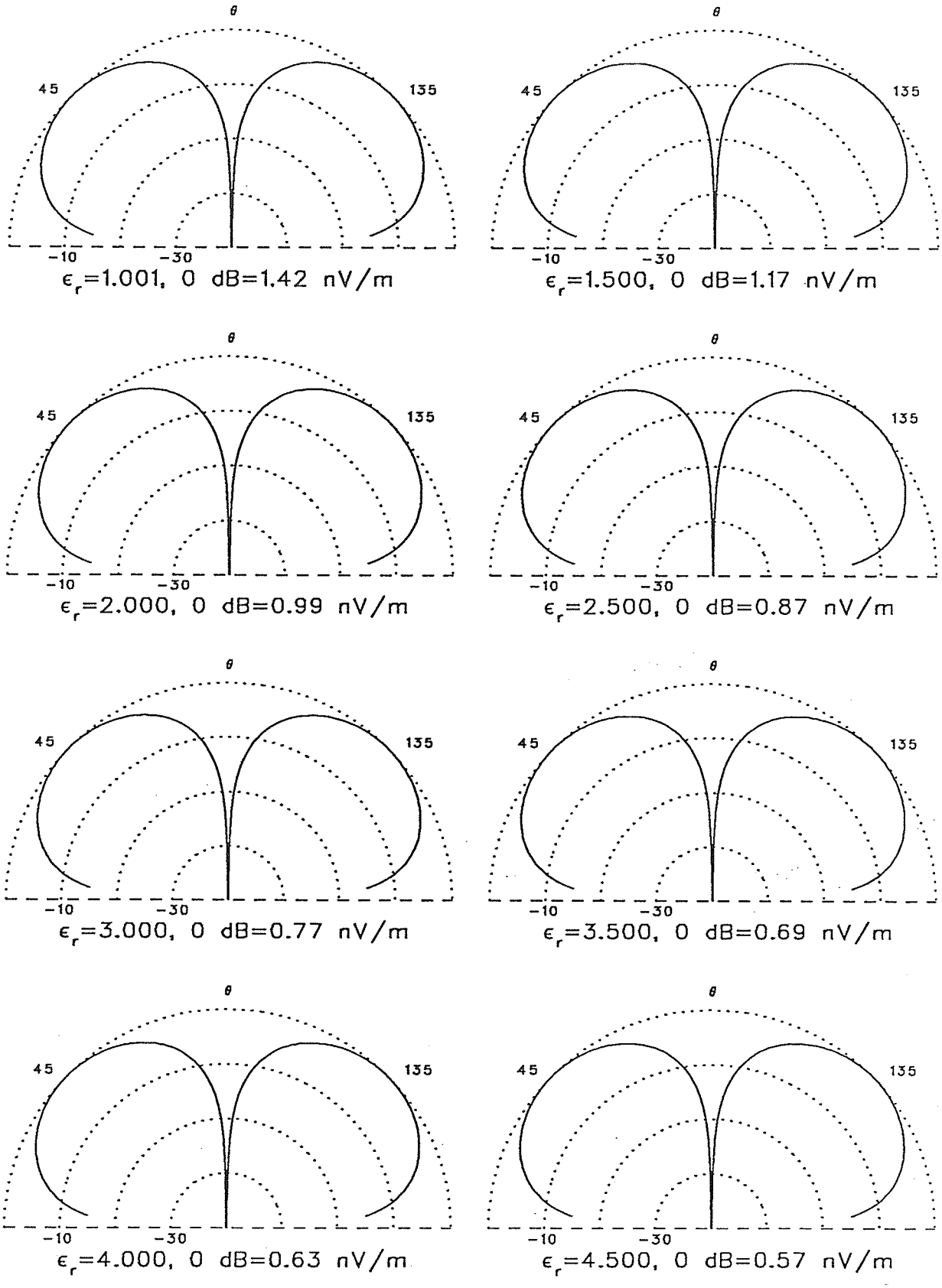

Figure 6.17 E_θ $a = \lambda/8$ $n = 2$

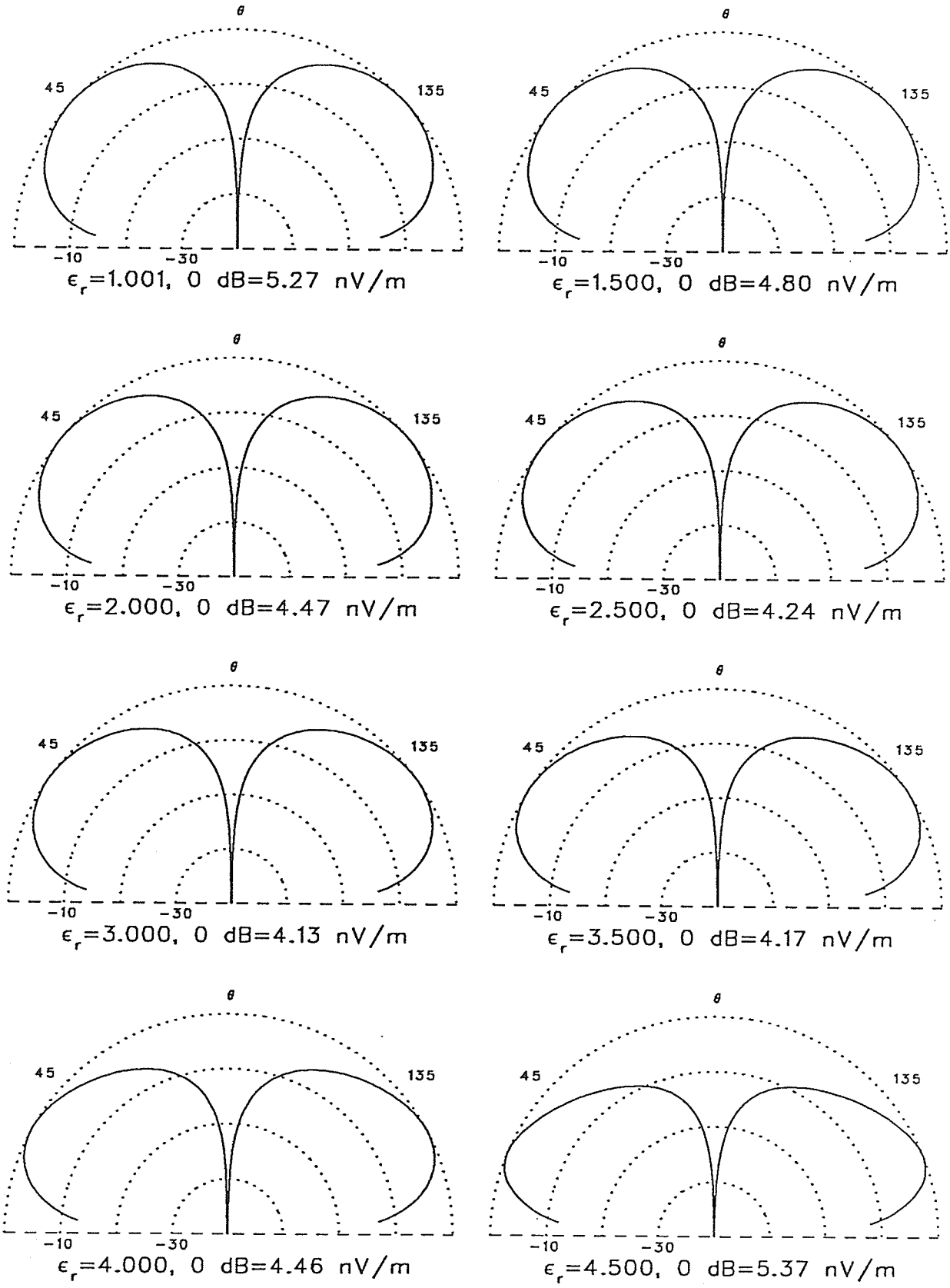

Figure 6.18 E_θ $a = \lambda/4$ $n = 2$

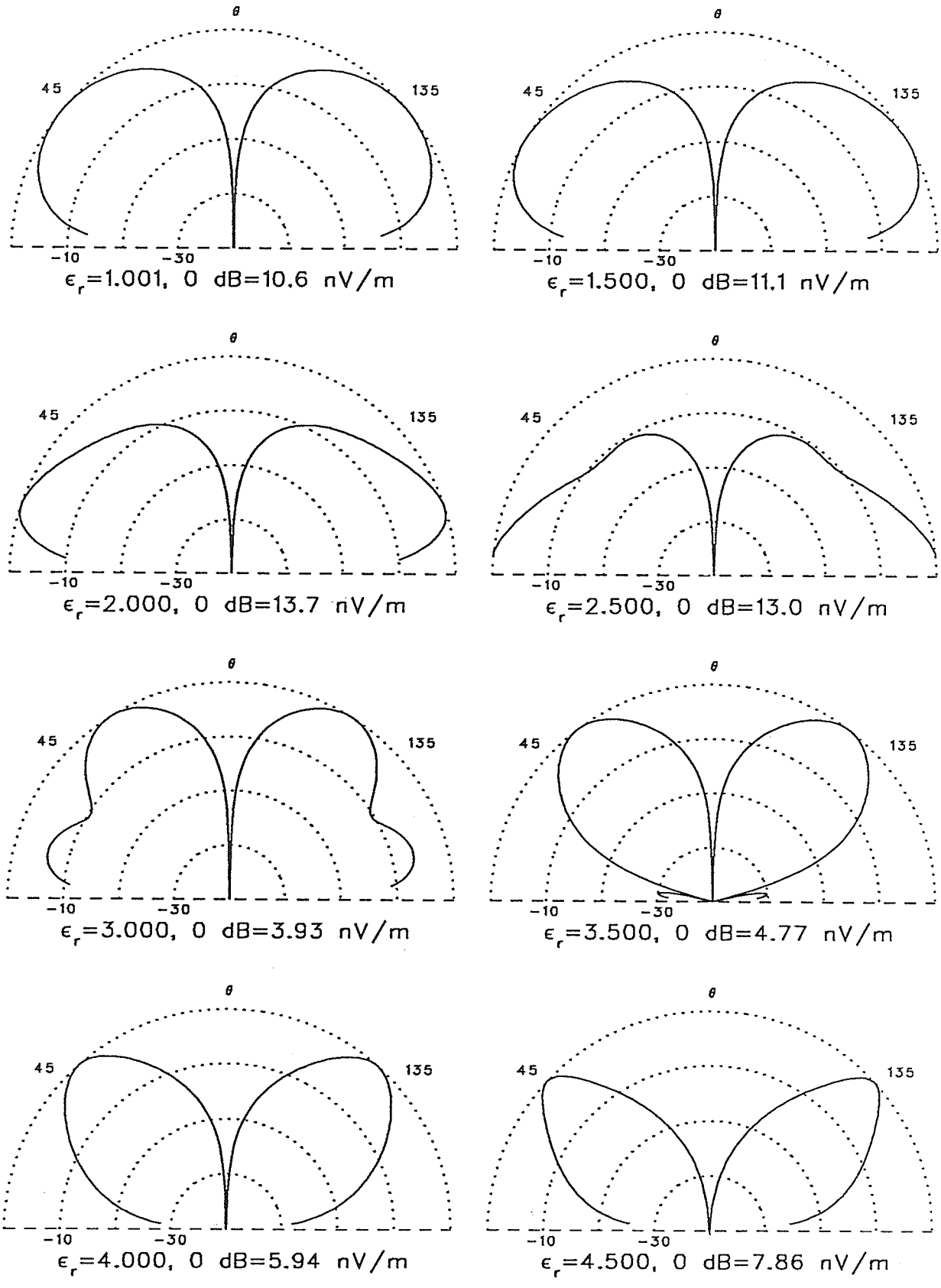

Figure 6.19 E_θ $a = 3\lambda/8$ $n = 2$

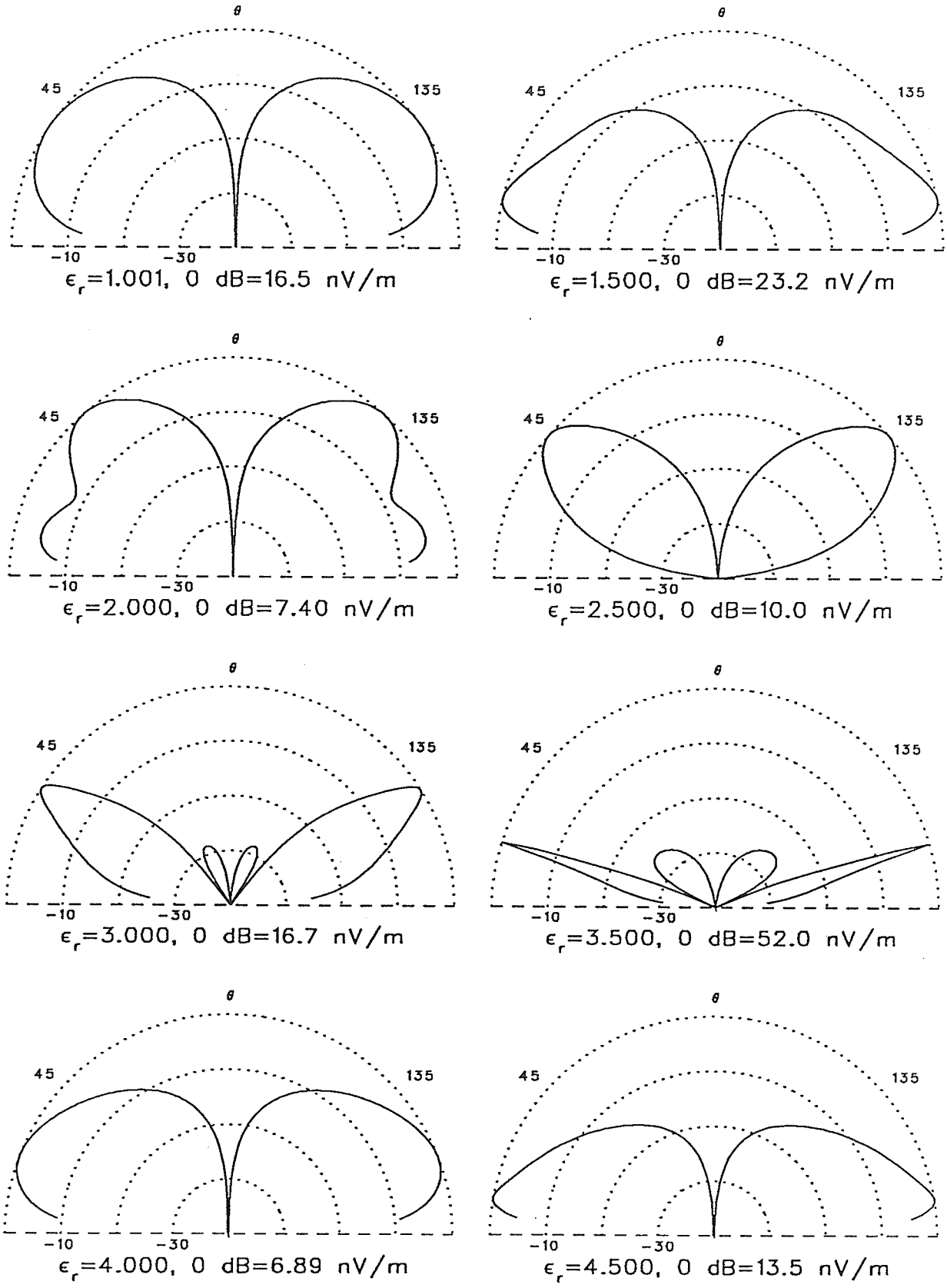

Figure 6.20 E_θ $a = \lambda/2$ $n = 2$

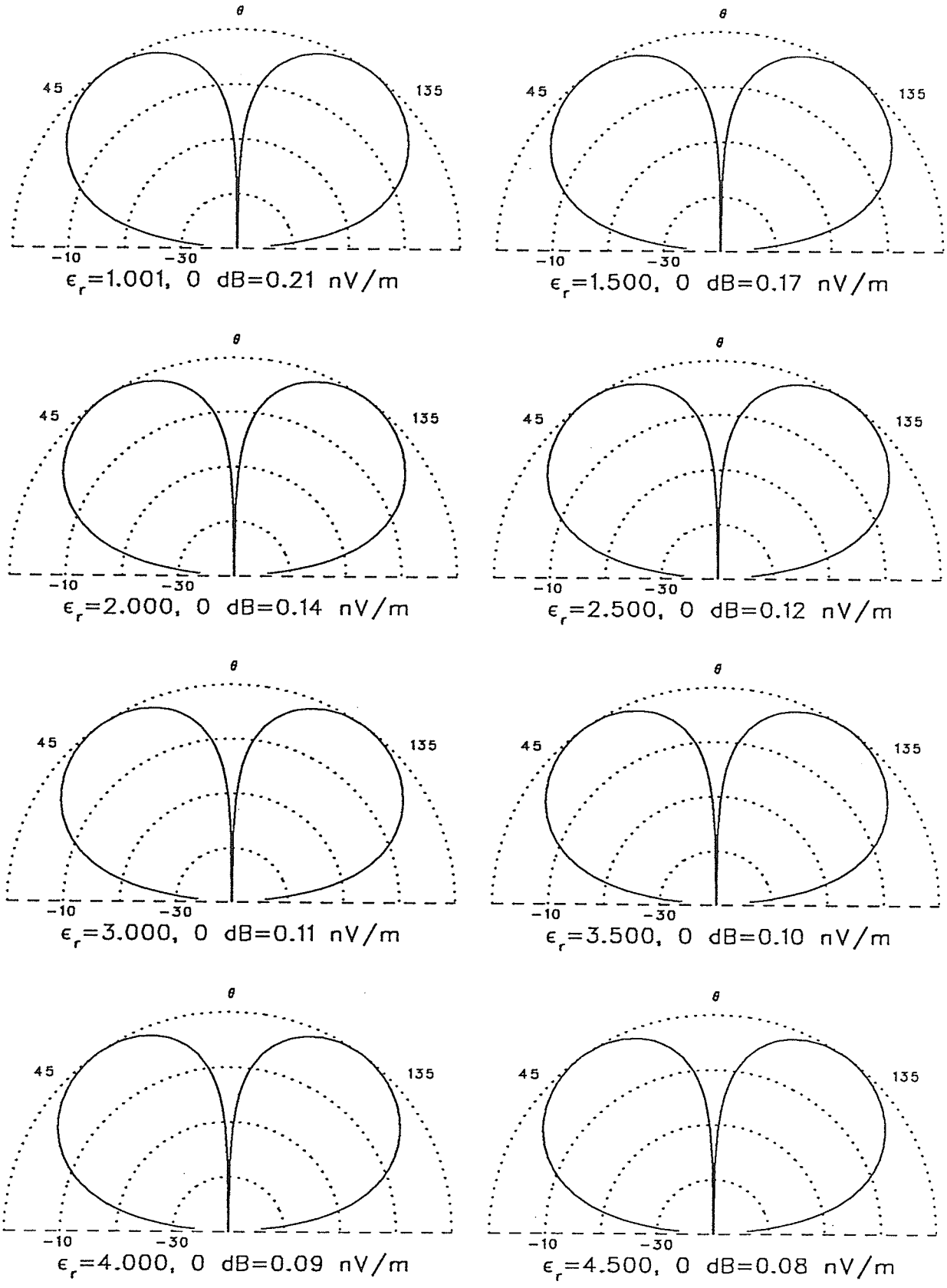

Figure 6.21 E_θ $a = \lambda/8$ $n = 3$

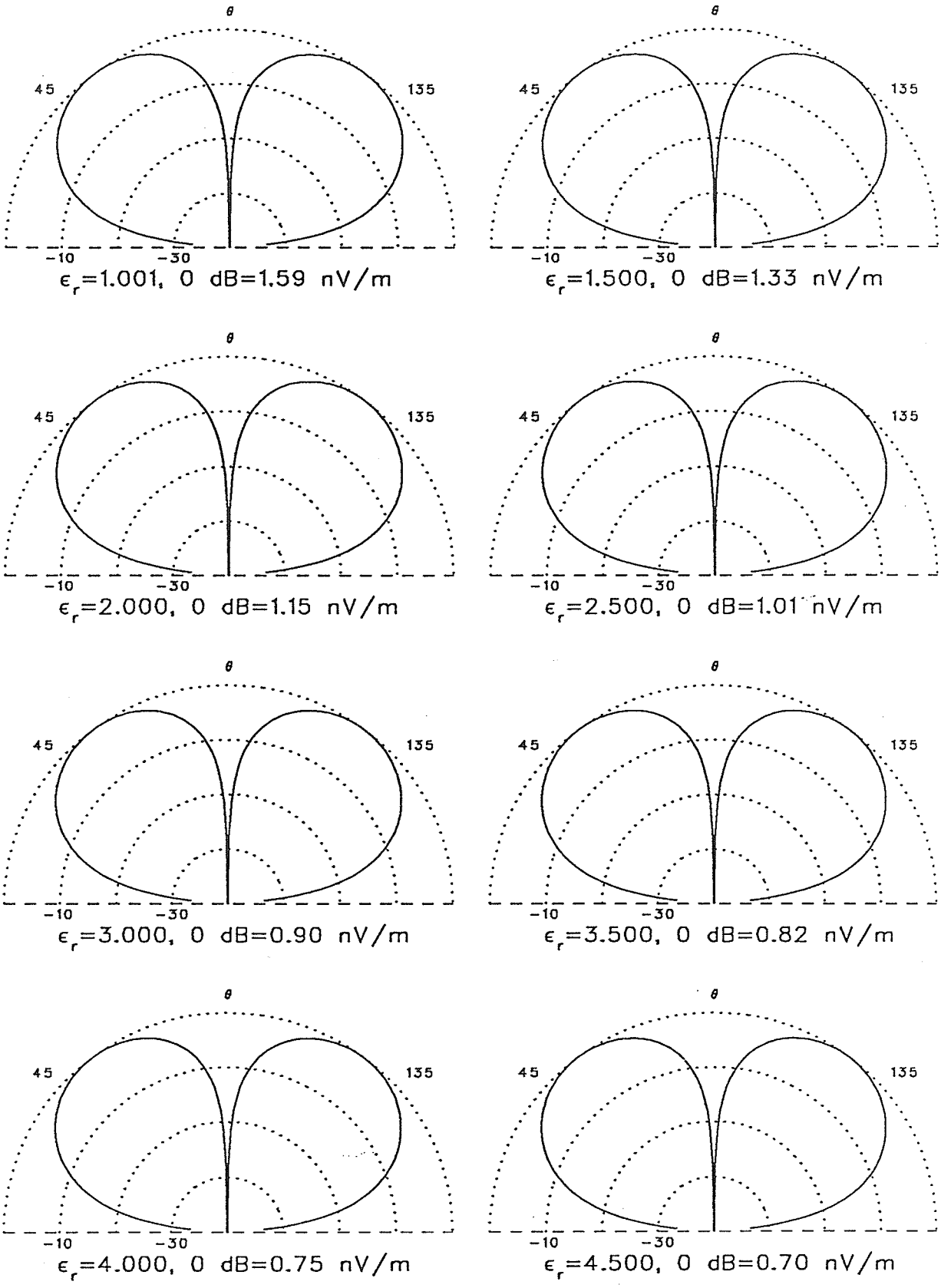

Figure 6.22 E_θ $a = \lambda/4$ $n = 3$

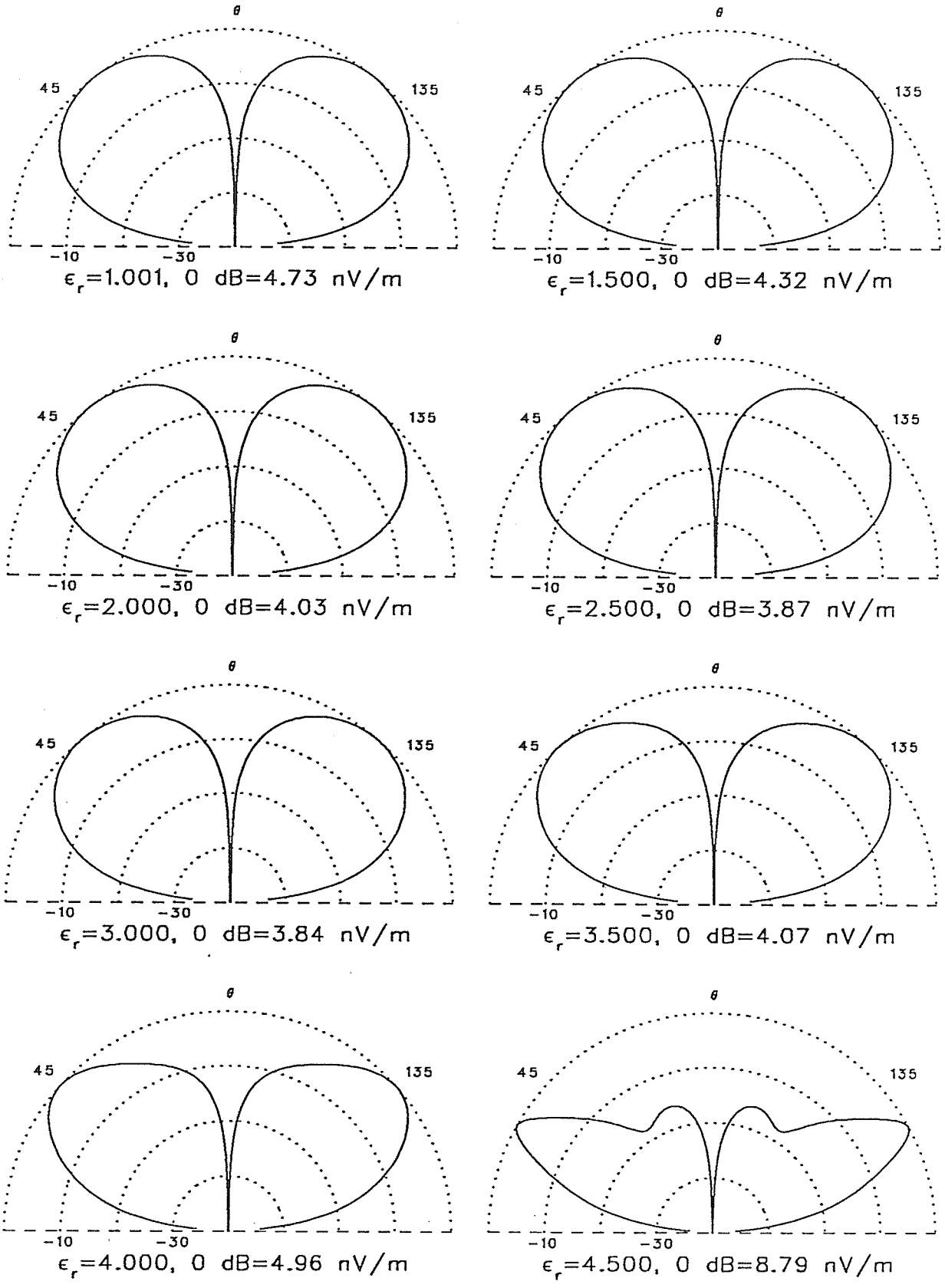

Figure 6.23 E_θ $a = 3\lambda/8$ $n = 3$

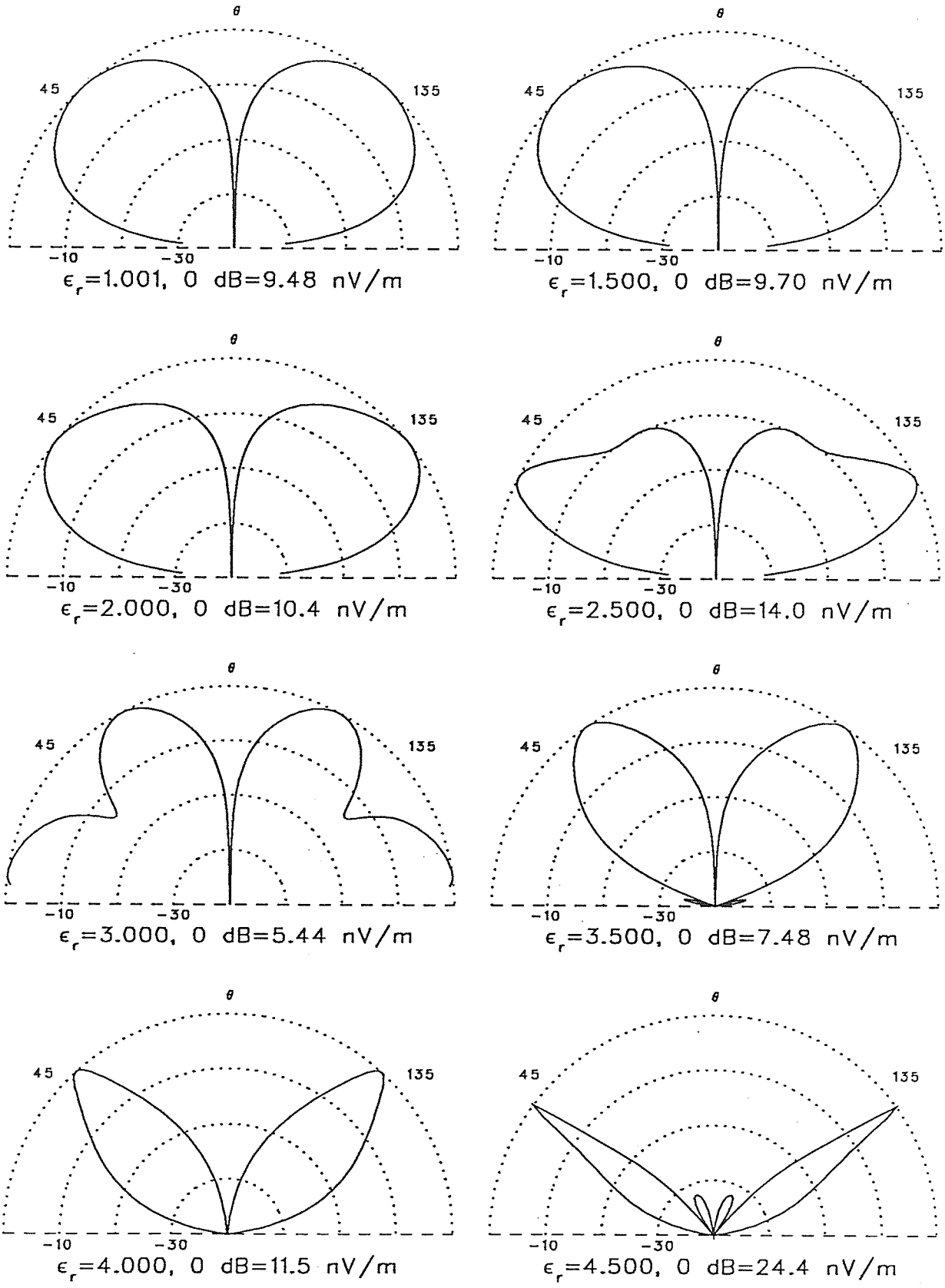

Figure 6.24 E_θ $a = \lambda/2$ $n = 3$

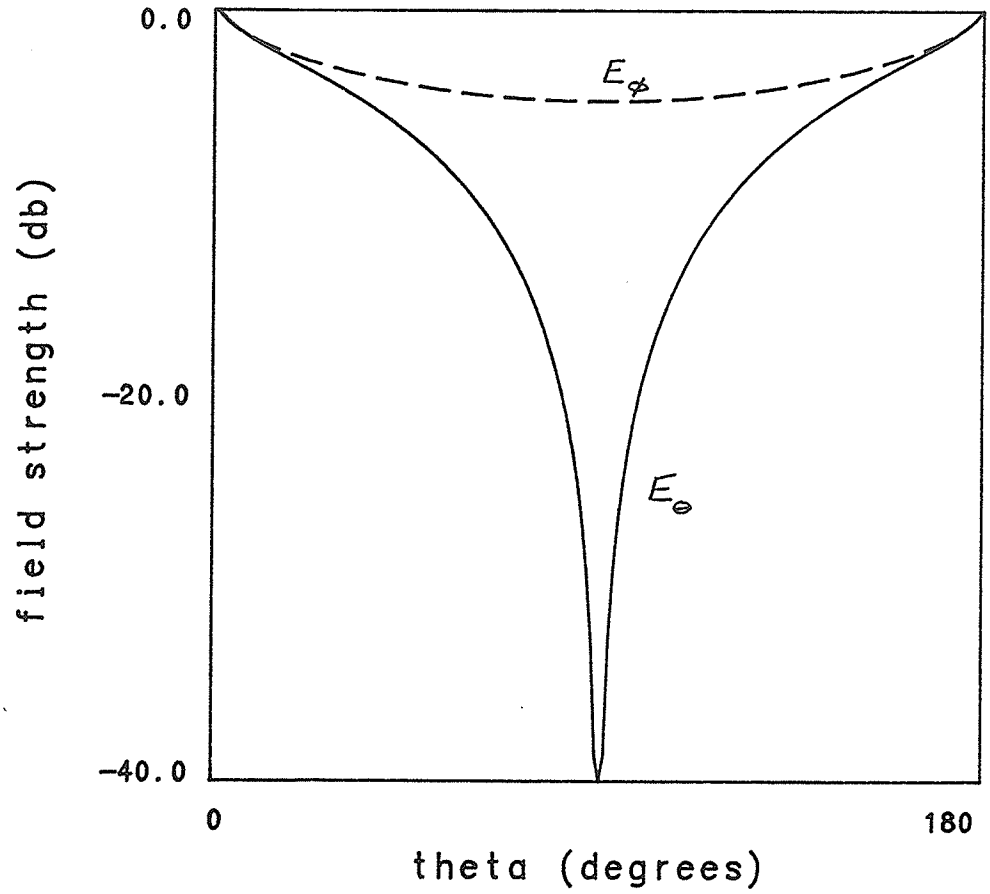

Figure 6.25 Radiation Characteristics $C/\lambda_o = 0.5$ $\epsilon_r = 2.56$

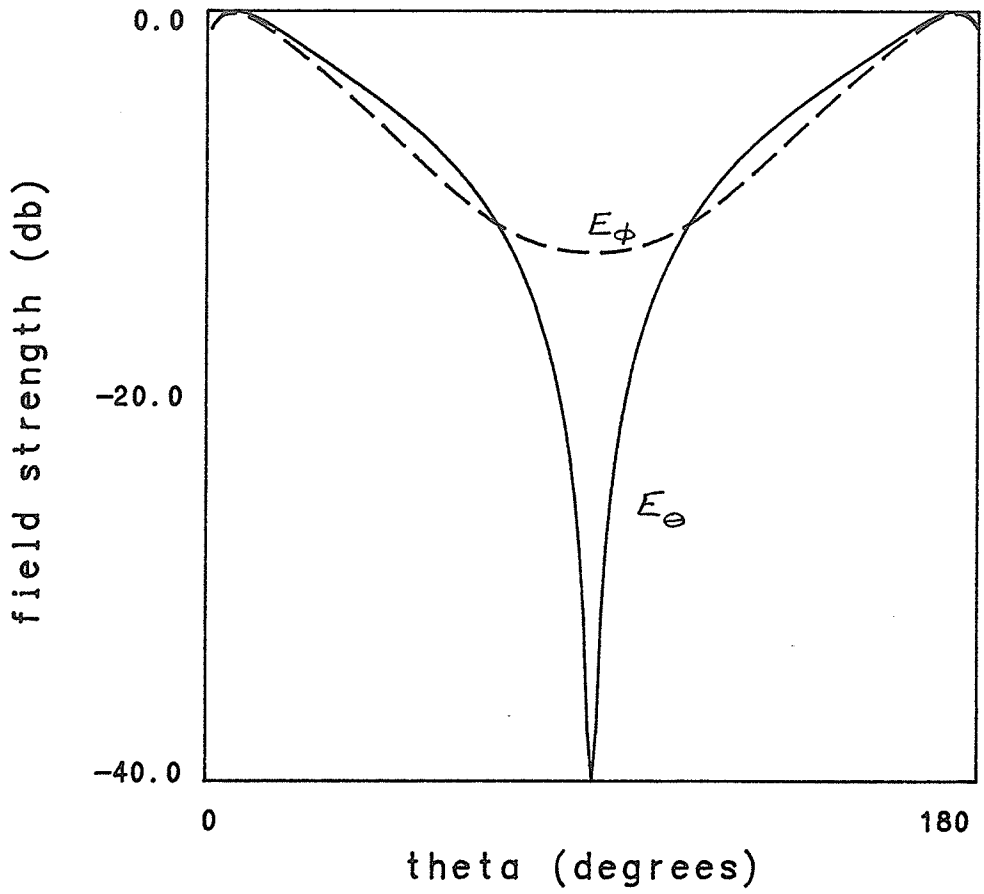

Figure 6.26 Radiation Characteristics $C/\lambda_o = 1.0$ $\epsilon_r = 2.56$

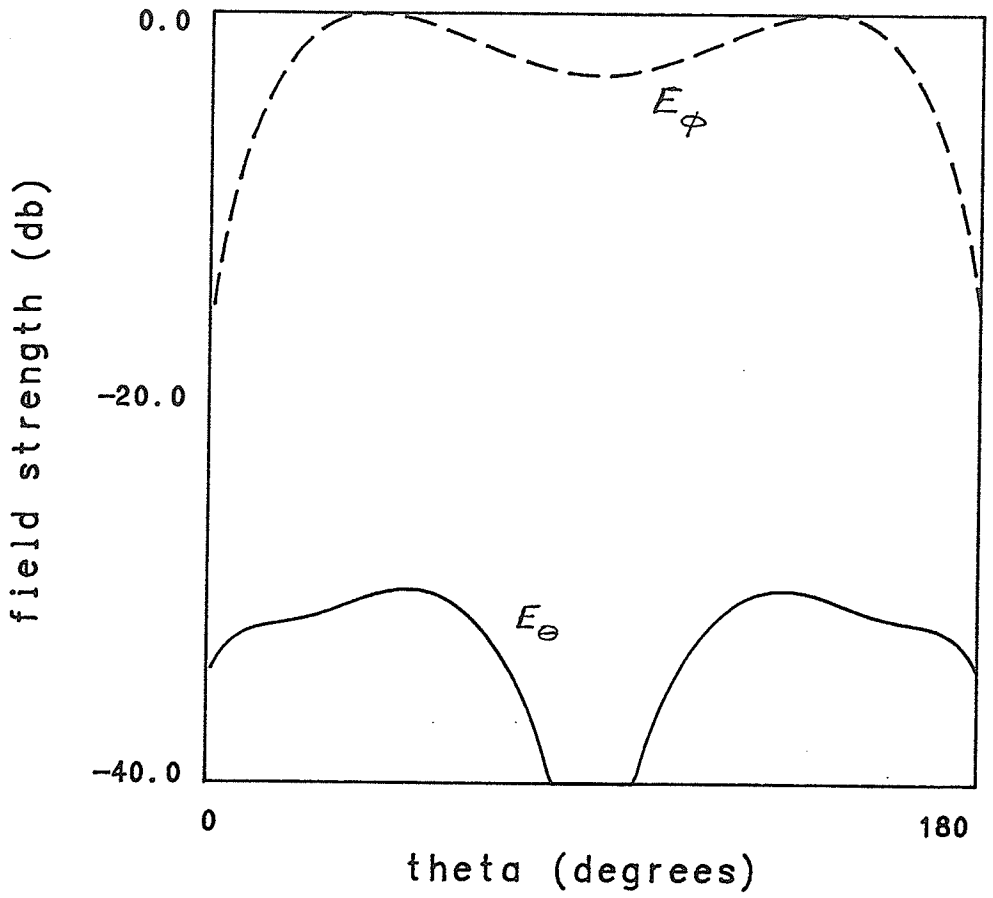

Figure 6.27 Radiation Characteristics $C/\lambda_o = 1.5$ $\epsilon_r = 2.56$

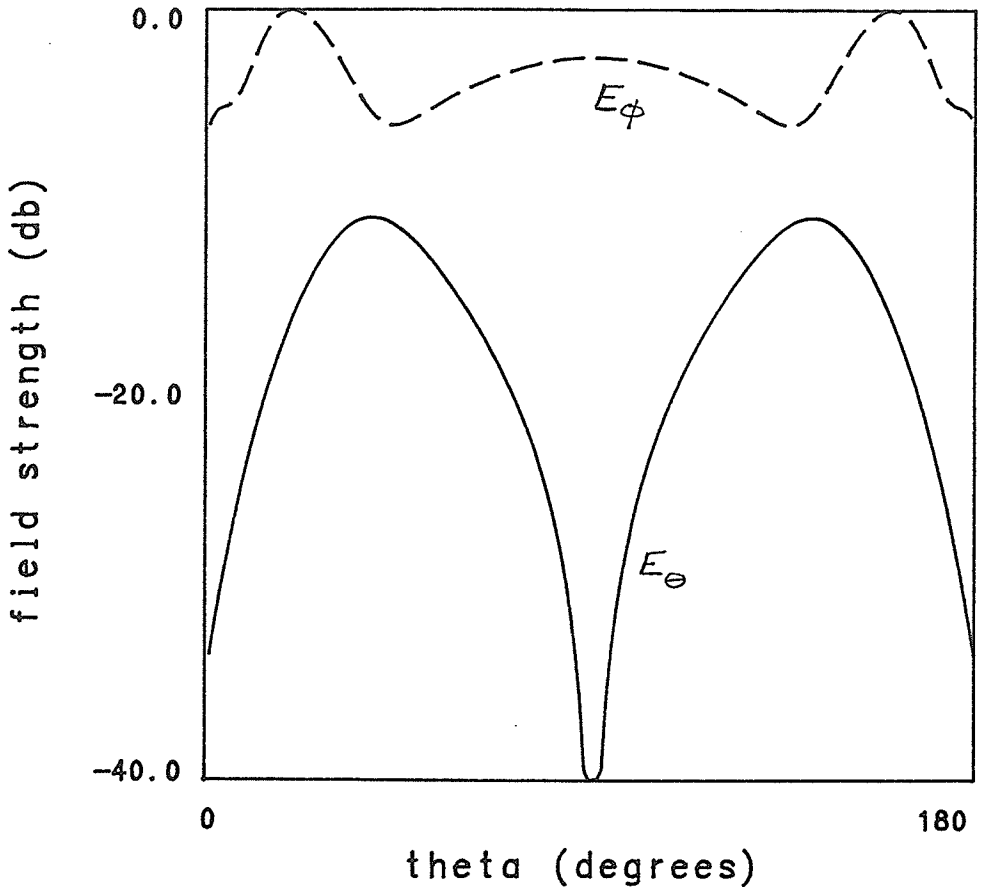

Figure 6.28 Radiation Characteristics $C/\lambda_o = 2.0$ $\epsilon_r = 2.56$

Chapter 7

Conclusions and Recommendations for Future Work

This thesis has presented an analysis of the electromagnetic characteristics of a loop antenna which is positioned on an infinitely long dielectric circular cylinder. The problem has been formulated as a cylindrical boundary value problem in which the wave equation for the Debye potential functions is solved. Extensions to the basic formulation are performed in order to evaluate input impedance and current distribution, surface wave behaviour, and radiation characteristics for the antenna. A comparison of results from the present formulation with results presented elsewhere in the literature verify the present results most satisfactorily.

A number of conclusions may be drawn from the numerical results obtained in this work for various antenna characteristics. With respect to input impedance,

the dielectric cylinder does exert considerable influence on the input impedance of the antenna. This influence is exerted in two ways. First, the excitation of surface waves on the cylinder adds to the resistive component of the input impedance. Second, the higher dielectric constant of the cylinder increases the electrical size of the antenna, which in turn influences both the resistive and reactive components of the input impedance. In comparing the contributions to the resistive part of the input impedance by radiation and surface wave excitation, the surface wave contribution appears to have a stabilizing influence on the resistance while the radiation contribution has a perturbing influence. Specifically, as C/λ_o increases, the surface wave contribution stabilizes after an initial transition while the radiation contribution varies widely. The significance of the surface wave excitation upon the general input impedance characteristics is shown by the large number of surface wave modes which can be excited under the geometries studied. The loop antenna wire radius exerts an influence upon the input impedance also. This influence appears to be consistant for all values of dielectric constant and is verified by results published elsewhere in the literature.

The calculations associated with surface wave behaviour, in large part, confirm and extend results which are already available. To date, an emphasis on the first and second order terms appears to dominate the literature. Therefore, the information presented here for the higher order modes in particular, is of interest. Certainly, the results of Chapter 5 emphasize the significance of surface wave analysis in engineering applications.

The information presented in Chapter 6 illustrates the impact of the cylinder

upon the radiation characteristics of the antenna. Such information is useful in various antenna design activities. In certain situations, the physical dimensions of a loop antenna and its support structure cannot be altered but the support structure's material can be altered. The change in dielectric constant then permits a certain degree of pattern control for the radiating system. Loop antennas with high directivity may be designed in a straightforward manner.

Numerous extensions to the present work would prove useful. As noted in Chapters 5 and 6, arbitrary current distributions on the antenna were presumed for the calculation of surface wave and radiation behaviour. The next step is to take the results of Chapter 4 and actually determine the surface wave and radiation characteristics for the current distribution calculated. An array of loop antennas on a dielectric cylinder would be the next obvious major step in this work. It would be particularly interesting to separate the mutual coupling into that part which is created by the near field structure and that part which is created by surface wave activity. The radiation characteristics of the loop antenna array would be of interest. In particular, the possibility of backward wave action should be explored. The whole area of surface wave and leaky wave antenna design requires an analysis of the loop antenna on a lossy dielectric cylinder. The complexities associated with analyzing leaky wave structures would establish this project as a major undertaking. Finally, of personal interest to the author, is the possibility of obtaining series solutions for the field expressions presented in this work. The evaluation of these expressions by numerical quadrature is a lengthy process which could possibly be alleviated if a suitable technique were employed to find all leaky wave poles in the

domain of the integration variable λ.

Additional numerical results which arise from this work have been presented in the literature. Radiation characteristics for certain geometries have been published in [117]. The characteristics of certain hybrid mode surface waves appear in [118]. Although not reported in this thesis but of interest to the author is the near field electromagnetic field structure in the vicinity of the loop antenna for presumed current distributions. An evaluation of such a field structure permits the definition of the well known Fresnel and Fraunhoffer zones around the antenna. Numerical results for such a field structure appear in [119]. The calculation of input impedance and current distribution are considered by the author to be the most significant aspect of this work. To that end, a number of publications have appeared [120], [121], [122],. A detailed discussion of the intermediate results obtained during the input impedance calculations appears in [123].

REFERENCES

[1] J.E. Storer, 'Impedance of Thin Wire Loop Antennas', *AIEE Trans. Comm. Electron.,* No. 27, pp 606-619, Nov. 1956.

[2] T.T. Wu, 'Theory of Thin Circular Loop Antennas', *J. Math. Phys.,* Vol. 3, No. 6, pp 1301-1304, 1962.

[3] S. Balaram Rao, 'Terminated Circular Loop Aerial', *Electron. Radio Engineer,* Vol. 34, No. 9, pp 347-350, Sept. 1957.

[4] E.J. Martins, Jr., 'Radiation Fields of Circular Loop Antennas by a Direct Integration Process', *IRE Trans. Antennas Propagat.,* Vol. AP-8, No. 1, pp 105-107, Jan. 1960.

[5] E.J. Martins, Jr., 'Exact Expressions for the Vector Potential Produced by Circular Loop Antennas', *Proc. IEEE,* Vol. 51, No. 7, pp 1042-1043, July 1963.

[6] J.E. Lindsay, Jr., 'A Circular Loop Antenna with a Non-Uniform Current Distribution', *IRE Trans. Antennas Propagat.,* Vol. AP-8, No. 4, pp 439-441, July 1960.

[7] K.S. Imrie, 'A Note on the Radiation Resistance and Field Strength of Large Loop Antennas', *Proc. IRE,* Vol. 50, No. 4(I), pp 477, April 1962.

[8] R. Redlich, 'Radiation from Filamentary Circular Loops', *Proc. IEEE,* Vol. 52, No. 9, pp 1060-1061, Sept. 1964.

[9] T.G. Shockley, Jr., 'Radiation Fields of Loop Antennas', *Proc. IEEE,* Vol. 52, No. 8, pp 970-971, Aug. 1964.

[10] K.K. Mei, 'On the Integral Equations of Thin Wire Antennas', *IEEE Trans. Antennas Propagat.,* Vol. AP-13, No. 3, pp 374-378, May 1965.

[11] A. Baghdasarian, D.J. Angelakos, 'Scattering from Conducting Loops and Solution of Circular Loop Antennas by Numerical Methods', *Proc. IEEE,* Vol. 53, No. 9, pp 818-822, Aug. 1965.

[12] T.G. Shockley, Jr., D.G. Glekas, H. Mott, 'Current Distribution on an L Band Loop Antenna', *Proc. IEEE,* Vol. 53, No. 9, pp 1248, Sept. 1965.

[13] B.R. Rao, 'Far Field Patterns for Large Circular Loop Antennas - Theoretical and Experimental Results', *IEEE Trans. Antennas Propagat.,* Vol. AP-16, No. 2, pp 269-276, March 1968.

[14] S.M. Prasad, B.N. Das, 'A Circular Loop Antenna with Travelling Wave Current Distribution', *IEEE Trans. Antennas Propagat.,* Vol. AP-18, No. 2, pp 278-280, March 1970.

[15] K. Iizuka, 'The Circular Loop Antenna Multi-Loaded with Positive and Negative Resistors', *IEEE Trans. Antennas Propagat.,* Vol. AP-13, No. 1, pp 7-20, Jan. 1965.

[16] K. Iizuka, F. La Russa, C. Dunne, 'Table of Field Patterns of a Loaded Resonant Circular Loop', *IEEE Trans. Antennas Propagat.,* Vol. AP-18, No. 3, pp 416-418, May 1970.

[17] R.W.P. King, 'The Shunt Driven Circular Loop Antenna', *IEEE Trans. Antennas Propagat.,* Vol. AP-19, No. 5, pp 692-694, Sept. 1971.

[18] J.L. Lin, 'The Imperfectly Conducting Circular Loop Antenna', *Radio Sci.,* Vol. 8, No. 3, pp 251-257, March 1973.

[19] G. Gonzalez, M.A. Huerta, 'Fresnel Field Regions produced by Circular Loops and Annular Slot Antennas', *J. Appl. Phys.,* Vol. 44, No. 8, pp 3500-3504, Aug. 1973.

[20] T. Tsukiji, 'Analysis of Center Line Driven Circular Loop Antennas', *Proc. Inst. Elect. Eng.,* Vol. 121, No. 11, pp 1355-1359, Nov. 1974.

[21] A. Richtscheid, 'Calculation of the Radiation Resistance of Loop Antennas with Sinusoidal Current Distributions', *IEEE Trans. Antennas Propagat.,* Vol. AP-24, No.6, pp 889-891, Nov. 1976.

[22] H.T. Chang, 'A Mode Expansion Theory for the EM Fields from a Circular Loop Antenna', *Radio Sci.,* Vol. 11, No. 8-9, pp 653-659, Aug.-Sept. 1976.

[23] S. Adachi, 'Comments on 'Calculation of the Radiation Resistance of Loop Antennas with Sinusoidal Current Distribution', *IEEE Trans. Antennas Propagat.,* Vol. AP-25, No.6, pp 900-901, Nov. 1977.

[24] S.A. Adekola, 'On the Excitation of a Circular Loop Antenna by Travelling and Standing Wave Current Distributions', *Int. J. Electron.,* Vol. 54, No. 6, pp 705-732, June 1982.

[25] K.H. Awadella, A.A. Sharshar, "A Simple Method to Determine the Input Impedance of a Loop Antenna', *IEEE Trans. Antennas Propagat.,* Vol. AP-32, No. 11, pp 1248-1251, Nov. 1984.

[26] K.J. Langenburg, 'Transient Fields of Small Loop Antennas', *IEEE Trans. Antennas Propagat.,* Vol. AP-24, No. 2, pp 236-239, March 1976.

[27] R.F. Blackburn, D.F. Wilton, 'Analysis and Synthesis of an Impedance Loaded Loop Antenna using the Singularity Expansion Method', *IEEE Trans. Antennas Propagat.,* Vol. AP-26, No. 1, pp 136-140, Jan. 1978.

[28] G.W. Streable, W. Pearson, 'A Numerical Study on Realizable Broadband and Equivalent Admittances for Dipole and Loop Antennas', *IEEE Trans. Antennas Propagat.,* Vol. AP-29, No. 5, pp 707-717, Sept. 1981.

[29] R.W.P. King, H.J. Schmidt, 'The Transient Response of Linear Antennas and Loops', *IEEE Trans. Antennas Propagat.* Vol. AP-10, No. 3, pp 222-228, May 1962.

[30] J.E. Clark, J.L. Tauritz, 'Cross Section Control of a Thin Wire Loop By Impedance Loading Techniques', *IEEE Trans. Antennas Propagat.,* Vol. AP-17, No. 1, pp 106-107, Jan. 1969.

[31] A.M. Abo-Zena, R.E. Beam, 'Transient Radiation Field of a Circular Loop Antenna', *IEEE Trans. Antennas Propagat.,* Vol. AP-20, No. 3, pp 380-383, May 1972.

[32] G.A. Thiele, 'Radar Cross Section of Open Circular Loops', *IEEE Trans. Antennas Propagat.,* Vol. AP-16, No. 3, pp 373-375, May 1968.

[33] J.A. Landt, E.K. Miller, 'Short Pulse Response of a Circular Loop', *IEEE Trans. Antennas Propagat.,* Vol. AP-22, No.1, pp 114-116, Jan. 1974.

[34] K.A. Michalski, L.W. Pearson, 'Equivalent Circuit Synthesis for a Circular Loop Antenna based upon the Singularity Expansion Method', *IEEE Trans. Antennas Propagat.,* Vol. AP-32, No. 5, pp 433-441, May, 1984.

[35] H. Whiteside, R.W.P. King, 'The Loop Antenna as a Probe', *IEEE Trans. Antennas Propagat.,* Vol. AP-12, No. 3, pp 291-297, May 1964.

[36] G.S. Smith, 'A Comparison of Field Patterns for Bare and Insulated Circular Loop Antennas', *Radio Sci.,* Vol. 11, No. 4, pp 351-356, April 1976.

[37] R.W.P. King, C.W. Harrison, D.G. Tingley, 'The Admittance of Bare Circular Loop Antennas in a Dissipative Medium', *IEEE Trans. Antennas Propagat.,* Vol. AP-12, No. 4, pp 434-438, July, 1964.

[38] R.W.P. King, C.W. Harrison, D.G. Tingley, 'The Current in Bare Circular Loop Antennas in a Dissipative Medium', *IEEE Trans. Antennas Propagat.,* Vol. AP-13, No. 4, pp 529-531, July, 1965.

[39] K. Iizuka, 'The Circular Loop Antenna Immersed in a Dissipative Medium', *IEEE Trans. Antennas Propagat.,* Vol. AP-13, No. 1, pp 43-47, Jan. 1965.

[40] J. Galejs, 'Admittance of Insulated Loop Antennas in a Dissipative Medium', *IEEE Trans. Antennas Propagat.,* Vol. AP-13, No. 2, pp 229-235, March 1965.

[41] C.L. Chen, R.W.P. King, 'The Small Bare Loop Antenna Immersed in a Dissipative Medium', *IEEE Trans. Antennas Propagat.,* Vol. AP-11, No. 3, pp 266-269, May, 1963.

[42] C.J. Benning, 'Impedance of a Loop Antenna in a Conducting Medium', *IEEE Trans. Antennas Propagat.,* Vol. AP-14, No. 2, pp 242-243, Mar. 1966.

[43] K.M. Lee, G.S. Smith, 'Measured Properties of Bare and Insulated Antennas in Sand', *IEEE Trans. Antennas Propagat.,* Vol. AP-23, No. 5, pp 664-670, Sept. 1965.

[44] G.S. Smith, 'On the Electrically Small Bare Loop Antenna in a Dissipative Medium', *IEEE Trans. Antennas Propagat.,* Vol. AP-24, No. 4, pp 533-537, July 1976.

[45] R.V. Row, 'On the Receiving Properties of a Small Horizontal Bare Circular Loop Antenna Buried in the Ground', *IEEE Trans. Antennas Propagat.,* Vol. AP-17, No. 5, pp 563-567, Sept. 1969.

[46] J. Galejs,'Input Resistance of Horizontal Loops Above a Conducting Ground Plane', *Radio Sci.,* Vol. 6, No. 11, pp 1011-1013, Nov. 1971.

[47] J.R. Wait, 'Radiation Resistance of a Small Circular Loop in the presence of a Conducting Ground', *J. Appl. Phys.,* Vol. 24, No. 5, pp 546-549, May 1953.

[48] J.R. Wait, 'Radiation from a Small Loop Immersed in a Semi-infinite Conducting Medium', *Can. J. Phys.,* Vol. 37, No. 5, pp 672-674, May 1959.

[49] J.R. Wait, K.P. Spies, 'Low Frequency Impedance of a Circular Loop over a Conducting Ground', *Electron. Lttrs.,* Vol. 9, No. 15, pp 346-348, July 1973.

[50] J.R. Wait, K.P. Spies, 'Subsurface Electromagnetic Fields of a Circular Loop of Current Located Above Ground', *IEEE Trans. Antennas Propagat.,* Vol. AP-20, No. 4, pp 520-522, July, 1972.

[51] J.R. Wait, K.P. Spies, 'Electromagnetic Fields of a Small Loop Buried in a Stratified Earth', *IEEE Trans. Antennas Propagat.,* Vol. AP-19, No. 5, pp 717-718, Sept. 1971.

[52] B.A. Shvarts, A.M. Kaganskiy, 'The Near Field of Loop Antennas for Inductive Coupling and the Required Spacing Between Transmitting Antennas Operating in a Common Frequency Channel', *Telecomm. Radio Engg. Pt. 2 (USSR),* Vol. 29, No. 5, pp 68-74, May 1974.

[53] B.A. Shvarts, A.M. Kaginskiy, 'The Near Fields of Loop Antennas in the Coupling Zone', *Telecomm. Radio Engg. Pt. 2 (USSR),* Vol. 31, No. 1, pp 126, Jan. 1976.

[54] L.N. An, G.S. Smith, 'The Horizontal Circular Loop Antenna near a Planar Interface', *Radio Sci.,* Vol. 17, No. 3, pp 483-502, May-June 1982.

[55] D.C. Chang, 'Characteristics of a Horizontal Circular Loop Antenna over a Multi-layered Dissipative Half-Space', *IEEE Trans. Antennas Propagat.,* Vol. AP-21, No. 6, pp 871-874, Nov. 1973.

[56] S.C. Moorthy, 'Analysis of Thin Circular Loop Antennas over a Homogeneous Earth', *Bell Syst. Tech. J.,* Vol. 49, No. 6, pp 1215-1233, July 1970.

[57] L.E. Vogler, 'Input Impedance Approximations for Small Dipole and Loop Antennas near Ground', *Can. J. Phys.,* Vol. 48, No. 9, pp 1036-1039, May 1970.

[58] A. Shoamenesh, L. Shafai, 'Characteristics of Circular Loop Antennas above a Lossless Ground Plane', *IEEE Trans. Antennas Propagat.,* Vol. AP-29, No. 3, pp 528-529, May 1981.

[59] P.P. Pavlov, 'Electromagnetic Field and Input Resistance of a Loop with Infinitely Long Cylindrical Ferrite Core Placed in a Conducting Medium', *Radio Engg. Electron. Phys. (USSR),* Vol. 7, No. 3, pp 411-421, March 1962.

[60] M.A. Islam, 'A Theoretical Treatment of Low Frequency Loop Antennas with Permeable Cores', *IEEE Trans. Antennas Propagat.,* Vol. AP-11, No. 2, pp 162-169, March 1963.

[61] J.R. Wait, M.A. Islam, 'Comments on "A Theoretical Treatment of Low Frequency Loop Antennas with Permeable Cores"', *IEEE Trans. Antennas Propagat.,* Vol. AP-11, No. 5, pp 592, Sept. 1963.

[62] R.W.Burton, R.W.P. King, T.T. Wu, 'The Loop Antenna with a Cylindrical Core: Theory and Experiment', *IEEE Trans. Antennas Propagat.,* Vol. AP-31, No. 2, pp 225-231, March 1983.

[63] C.W. Horton, F.C. Caral, C.M. McKinney, 'On the Radiation Patterns of Dielectric Rod Antennas of Circular Cross Section - the TM_{11} mode', *J. Appl. Phys.,* Vol. 21, No. 12, pp 1279-1283, Dec. 1950.

[64] C.W. Horton, C.M. McKinney, 'An Experimental Investigation of the Dielectric Rod Antenna of Circular Cross Section Excited in the Dominant Mode', *J. Appl. Phys.,* Vol. 22, No. 10, pp 1246-1249, Oct. 1951.

[65] C.M. McKinney, 'An Experimental Investigation of the Dielectric Rod Antenna of Circular Cross Section Excited in Rotationally Symmetric Modes', *J. Appl. Phys.,* Vol. 23, No. 1, pp 11-13, Jan. 1952.

[66] J. Brown, J.O. Spector, 'The Radiating Properties of End-fire Aerials', *Proc. Inst. Elect. Engg.* Vol. 104B, No. 13, pp 27-34, Jan. 1957.

[67] J.W. Duncan, R.H. DuHamel, 'A Technique for Controlling the Radiation from Dielectric Rod Waveguides', *IRE Trans. Antennas Propagat.,* Vol. AP-5, No. 3, pp 284-289, July 1957.

[68] R.H. DuHamel, J.W. Duncan, 'Launching Efficiency of Wires and Slots for a Dielectric Rod Waveguide', *IRE Trans. Microwave Theory Tech.,* Vol. MTT-6, No. 3, pp 277-284, July, 1958.

[69] C.M. Angulo, W.S.C. Chang, 'The Excitation of a Dielectric Rod by a Circular Waveguide', *IRE Trans. Microwave Theory Tech.,* Vol. MTT-6, No. 4, pp 389-393, Oct. 1958.

[70] C.M. Angulo, W.S.C. Chang, 'A Variational Expression for the Terminal Admittance of a Semi-infinite Dielectric Rod', *IRE Trans. Antennas Propagat.,* Vol. AP-7, No. 7, pp 207-212, July 1959.

[71] J.W. Duncan, 'The Efficiency of Excitation of a Surface Wave on a Dielectric Cylinder', *IRE Trans. Microwave Theory Tech.,* Vol. MTT-7, No. 2, pp 257-268, April 1959.

[72] Ta Shing Chu, N.R. Kilcoyne, 'The Excitation of a Dielectric Rod Antenna by a Helix', *IRE Trans. Antennas Propagat.,* Vol. AP-9, No. 4, pp 416-417, July 1961.

[73] T.S.M. MacLean, D.J. Williams, 'The Broadband Dielectric Rod Aerial', *Radio Electron. Engineer (GB),* Vol. 30, No. 2, pp 99-104, Aug. 1965.

[74] D.G. Kiely, 'Factors Governing the Radiation Characteristics of Dielectric Tube Aerials', *Proc. Inst. Elect. Eng. Pt. 3,* Vol. 97, pp 311-320, Sept. 1950.

[75] J.R. James, 'Theoretical Investigation of Cylindrical Dielectric Rod Antennas', *Proc. Inst. Elect. Eng.,* Vol. 114, No. 3, pp 309-319, March 1967.

[76] J.B. Andersen, 'Radiation from Surface Wave Antennas', *Electron. Lttrs.,* Vol. 3, No. 6, pp 251, June 1967.

[77] J.R. James, 'Radiation from Surface Wave Antennas', *Electron. Lttrs.,* Vol. 3, No. 7, pp 344, July 1967.

[78] H. Kleinburg, 'Theoretical Investigation of Cylindrical Dielectric Rod Antenna', *Proc. Inst. Elect. Eng.,* Vol. 114, No. 11, pp 1651-1652, Nov. 1967.

[79] J.R. James, 'Theoretical Investigation of Cylindrical Dielectric Rod Antenna', *Proc. Inst. Elect. Eng.,* Vol. 114, No. 11, pp 1652-1653, Nov. 1967.

[80] J.R. Blakey, 'Calculation of Dielectric Rod Aerial Radiation Patterns', *Electron. Lttrs.,* Vol. 4, No. 3, pp 46-47, Feb. 1968.

[81] D.F. Hastings, 'Dielectric Rod Support Tuned by Including Metal Wires for Reduction of Scattering', *IEEE Trans. Antennas Propagat.,* Vol. AP-16, No. 3, pp 350-351, May 1968.

[82] V.C. Smits, 'Rear Gain Control of a Dielectric Rod Antenna', *Microwave J.,* Vol. 11, No. 12, pp 65, Dec. 1968.

[83] E.G. Neumann, 'Radiation Mechanism of Dielectric Rod and Yagi Aerials', *Electron. Lttrs.,* Vol. 6, No. 16, pp 528-530, Aug. 1970.

[84] A.D. Yaghjian, E.T. Kornhauser, 'A Modal Analysis of the Dielectric Rod Antenna Excited by the HE_{11} Mode', *IEEE Trans. Antennas Propagat.,* Vol. AP-20, No. 2, pp 122-128, March 1972.

[85] J.R. Blakey, 'Radiation Properties of Composite Dielectric Rod Aerials', *Electron. Lttrs.,* Vol. 9, No. 6, pp 146-147, March 1973.

[86] J.R. Blakey, 'A Scattering Theory Approach to the Prediction of Dielectric Rod Antenna Radiation Patterns; the TM_{11} Mode', *IEEE Trans. Antennas Propagat.,* Vol. AP-23, No. 4, pp 577-579, July 1975.

[87] K.C. Gupta, I.J. Bahl, 'Design Considerations for Leaky Wave Antennas', *Proc. Inst. Elect. Eng.,* Vol. 123, No. 12, pp 1302-1306, Dec. 1976.

[88] A. Ittipiboon, L. Shafai, E. Bridges, 'A Dielectric Rod Antenna as a High Efficiency Feed for Reflector Antennas', *Can. Elect. Engg. J.,* Vol. 6, No. 4, pp 10-13. Oct. 1981.

[89] Ye.N. Vasil'yev, Z.V. Sedel'nikova, A.R. Seregina, 'Non- symmetrical Excitation of a Dielectric Rod', *Radio Engg. Electron. Phys. (USSR),* Vol. 24, No. 4, pp 10-16, April 1979.

[90] A.A. Kishk, L. Shafai, 'Radiation Characteristics of the Short Dielectric Rod Antenna: A Numerical Approach', *IEEE Trans. Antennas Propagat.,* Vol. AP-35, No. 2, pp 139-146, Feb. 1987.

[91] W.M. Elsasser, 'Attenuation in a Dielectric Circular Rod' *J. Appl. Phys.,* Vol. 20, pp 1193-1196, Dec. 1949

[92] C.H. Chandler, 'An Investigation of Dielectric Rods as Waveguide', *J. Appl. Phys.,* Vol. 20, pp 1188-1192, Dec. 1949.

[93] S.A. Schelkenoff, *Electromagnetic Waves,* Van Nostrand, New York, 1943.

[94] R.E. Collin, *Field Theory of Guided Waves,* McGraw Hill, New York, 1960.

[95] J.R. Wait, *Electromagnetic Theory,* Harper and Row, New York, 1985.

[96] P.J.B. Clarricoats, 'Propagation along Bounded and Unbounded Dielectric Rods; I: Propagation along an Unbounded Dielectric Rod', *Proc. Inst. Elect. Eng.,* Mono. 409E, Vol. 108C, pp 170-176, Oct. 1960.

[97] E.F. Gillespie, 'Power Flow and Negative Wave Impedance in the Dielectric Rod Waveguide', *Proc. Inst. Elect. Eng.,* Mono. 362E, Vol. 107C, pp 198-201, Sept. 1960.

[98] G. Biernson, D.J. Kinsley, 'Generalized Plots of Mode Patterns in a Cylindrical Waveguide Applied to Retinal Cones', *IEEE Trans. Microwave Theory Tech.,* Vol. MTT-13, No. 3, pp 345-356, May 1965.

[99] G. Biernson, D.J. Kinsley, 'Discrepancies in Dielectric Waveguide Mode Cutoff Conditions', *IEEE Trans. Microwave Theory Tech.,* Vol. MTT-13, No. 13, pp 884-885, Nov. 1965.

[100] P.J.R. Laybourn, 'Group Velocity Dielectric Waveguide Modes', *Electron. Lttrs.,* Vol. 4, No. 13, pp 507-509, Nov. 1968.

[101] A.W. Snyder, 'Continuous Mode Spectrum of a Dielectric Circular Rod', *IEEE Trans. Microwave Theory Tech.,* Vol. MTT-19, No. 8, pp 720-727, Aug. 1971.

[102] G.L. Yip, 'Launching Efficiency of the HE_{11} Surface Wave Mode on a Dielectric Rod', *IEEE Trans. Microwave Theory Tech.,* Vol. MTT-18, No. 12, pp 1033-1041, Dec. 1970.

[103] G.L. Yip, 'Launching Efficiency of the HE_{11} Surface Wave Mode on a Dielectric Tube', *IEEE Trans. Microwave Theory Tech.,* Vol. MTT-22, No. 1, pp 6-14, Jan. 1974.

[104] J. Arnbak, 'Leaky Waves on a Dielectric Rod', *Electron. Lttrs.,* Vol. 5, No. 3, pp 41-42, Feb. 1969.

[105] J.R. James, 'Leaky Waves of a Dielectric Rod', *Electron. Lttrs.,* Vol. 5, No. 11, pp 252-254, May 1969.

[106] G.I. Veselov, S.B. Rayevskiy, 'Complex Modes of a Circular Dielectric Waveguide', *Radio Engg. Electron. Phys. (USSR),* Vol. 28, No. 2, pp 13-19, Feb. 1983.

[107] G.I. Veselov, S.B. Rayevskiy, 'The Spectrum of Complex Modes in a Circular Dielectric Waveguide', *Telecomm. Radio Engg. Pt.2 (USSR),* Vol. 38, No. 2, pp 103-106, Feb. 1983.

[108] D.D. King, S.P. Schlesinger, 'Losses in Dielectric Image Lines', *IRE Trans. Microwave Theory Tech.,* Vol. MTT-5, No. 1, pp 31-35, Jan. 1957.

[109] S.P. Schlesinger, D.D. King, 'Dielectric Image Lines', *IRE Trans. Microwave Theory Tech.,* Vol. MTT-6, No. 3, pp 291-299, July 1958.

[110] D.S. Jones, *Acoustic and Electromagnetic Waves*, Oxford University Press, New York, 1986.

[111] R.F. Harrington, *Time Harmonic Electromagnetic Fields*, McGraw Hill, New York, 1961.

[112] J.R. Wait, *Electromagnetic Radiation from Cylindrical Structures*, Pergamon Press, New York, 1959.

[113] T. Tamir, A.A. Oliner, 'Guided Complex Waves, Part 1. Fields at an Interface', *Proc. Inst. Elect. Eng.,* Vol. 110, No. 2, pp 310-324, Feb. 1963.

[114] T. Tamir, A.A. Oliner, 'Guided complex waves, Part 2. Relation to Radiation Patterns', *Proc. Inst. Elect. Eng.,* Vol. 110, No. 2, pp 325-334, Feb. 1963.

[115] M. Abramowitz, I. Stegun, *Handbook of Mathematical Functions*, Dover Publications, New York, 1965.

[116] R.C. Johnson, H. Jasik, (Ed.) *Antenna Engineering Handbook*, McGraw Hill, New York, 1984.

[117] W.D. Rawle, L. Shafai, 'The Radiation Characteristics of Azimuthal Modes on an Infinitely Long Dielectric Circular Cylinder', *ANTEM '88 Proceedings*, Winnipeg, Manitoba, Aug. 1988.

[118] W.D. Rawle, L. Shafai, 'Field Amplitude Distributions for Hybrid Mode Surface Waves Propagating Along an Infinitely Long Dielectric Circular Cylinder', *1989 URSI Radio Science Meeting*, San Jose, Californian, pp 114, June 1989.

[119] W.D. Rawle, L. Shafai, 'The Near Zone Electromagnetic Fields of a Loop Antenna situated on an Infinitely Long Dielectric Circular Cylinder', *Proceedings of the Canadian Conference on Electrical and Computer Engineering*, Montreal , Quebec, pp 915-917, Sept. 1989.

[120] W.D. Rawle, 'On the Electromagnetic Characteristics of Loop Antennas Embedded in Cylindrically Stratified Media', *Ocean Wave Mechanics, Fluid Dynamics, and Mathematical Modelling*, M. Rahman (Ed.), Computational Mechanics Publications, Southampton, pp 523-531, 1990.

[121] W.D. Rawle, L. Shafai, 'The Electromagnetic Characteristics of Loop Antennas Positioned Coaxially in Cylindrically Stratified Media', *1990 URSI Radio Science Meeting*, Dallas, Texas, pp 165, 1990.

[122] W.D. Rawle, L. Shafai, 'Modal Current Distributions on Loop Antennas in Cylindrically Stratified Media', *ANTEM '90 Proceedings*, Winnipeg, Manitoba, pp 191-199, Aug. 1990.

[123] W.D. Rawle, L. Shafai, 'The Loop Antenna on an Infinitely Long Dielectric Circular Cylinder; A Report on the Calculation of Modal Parameters', *Department of Electrical and Computer Engineering, University of Manitoba, Technical Report TR90-01*, Sept. 1990.

[124] C.T. Tai, *Dyadic Green's Functions in Electromagnetic Theory*, Intext Education Publishers, London, 1971.

APPENDIX A

Large Argument Approximation for the Modal Impedance Integral

From (3.21), the modal impedance integral is as follows:

$$\mathcal{Z}_m = \frac{1}{\kappa_m} \int_{-\infty}^{\infty} \left[B_m^h(\lambda)\Omega_{11} - B_m^e(\lambda)\Omega_{12} \right] d\lambda$$

where, for $|\lambda| > k_i$, the terms which make up $B_m^e(\lambda)$, $B_m^h(\lambda)$, Ω_{11}, and Ω_{12} contain modified Bessel functions $\mathrm{I}_m(\bullet)$ and $\mathrm{K}_m(\bullet)$. Note that the term $\frac{1}{\kappa_m}$ which appears in front of the integral sign in the above expression cancels the κ_m term which appears in the expressions for $B_m^h(\lambda)$ and $B_m^e(\lambda)$.

Large argument approximations for the modified Bessel functions are now substituted into the equation for $\mathcal{Z}_m$. These approximations are as follows and may be found in the literature [115].

$$\begin{aligned} \mathrm{I}_n(x) &\approx \frac{e^x}{\sqrt{2\pi x}} \\ \mathrm{K}_n(x) &\approx \sqrt{\frac{\pi}{2x}} e^{-x} \end{aligned}$$

After extensive reduction, a general large argument approximation for the integrand may be obtained as follows:

$$\mathcal{I}(\lambda) \approx \frac{\omega\mu_o}{\sqrt{\rho a}} \left[\frac{-ja}{2} + \frac{jm^2}{(\epsilon_r + 1)k_o^2\rho} \right] \frac{e^{-\lambda(\rho - a)}}{\lambda}$$

The tail contribution may now be written:

$$\mathcal{Z}_{m,\,tail} = \mathcal{T} \int_z^\infty \frac{e^{-\lambda(\rho-a)}}{\lambda} d\lambda$$

where

$$\mathcal{T} = \frac{\omega\mu_o}{\sqrt{\rho a}} \left[\frac{-ja}{2} + \frac{jm^2}{(\epsilon_r + 1)k_o^2 \rho} \right]$$

and z is some arbitrarily large value of λ. The integral involved in the tail contribution is the well known exponential integral. Tabulated values for this function appear in the literature [115].

APPENDIX B

Development of Far Field Equations

The tangential field components for the external region, Region II, are as follows:

$$E_{z_{II}} = \sum_{m=-\infty}^{\infty} e^{-jm\phi} \int_{-\infty}^{\infty} B_m^e(\lambda)\Omega_{18} e^{-j\lambda z} d\lambda$$

$$H_{z_{II}} = \sum_{m=-\infty}^{\infty} e^{-jm\phi} \int_{-\infty}^{\infty} B_m^h(\lambda)\Omega_{18} e^{-j\lambda z} d\lambda$$

$$E_{\phi_{II}} = \sum_{m=-\infty}^{\infty} e^{-jm\phi} \int_{-\infty}^{\infty} \left[B_m^h(\lambda)\Omega_{11} - B_m^e(\lambda)\Omega_{12}\right] e^{-j\lambda z} d\lambda$$

$$H_{\phi_{II}} = \sum_{m=-\infty}^{\infty} e^{-jm\phi} \int_{-\infty}^{\infty} \left[B_m^e(\lambda)\Omega_{15} - B_m^h(\lambda)\Omega_{16}\right] e^{-j\lambda z} d\lambda$$

where $B_m^e(\lambda)$, $B_m^h(\lambda)$, Ω_{11}, Ω_{12}, Ω_{15}, Ω_{16}, and Ω_{18} are given in (3.17).

From these equations, the far field equations are developed using the method of steepest descent. In using this technique, it is advantageous to substitute the variable $\lambda = k_o \cos\alpha$. This substitution maps the two sheeted Riemann surface domain for λ into strips of width 2π in the α domain. Figure B.01 illustrates the mapping of λ into α and shows the transformed integration contour.

To illustrate the application of the steepest descent technique method, the development of the far field equation for $E_{\theta_{II}}$ will be reviewed in detail.

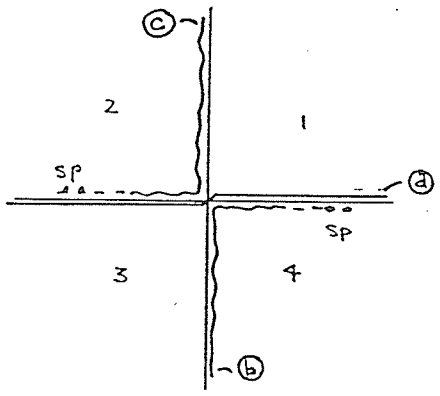

λ *plane – lower sheet*

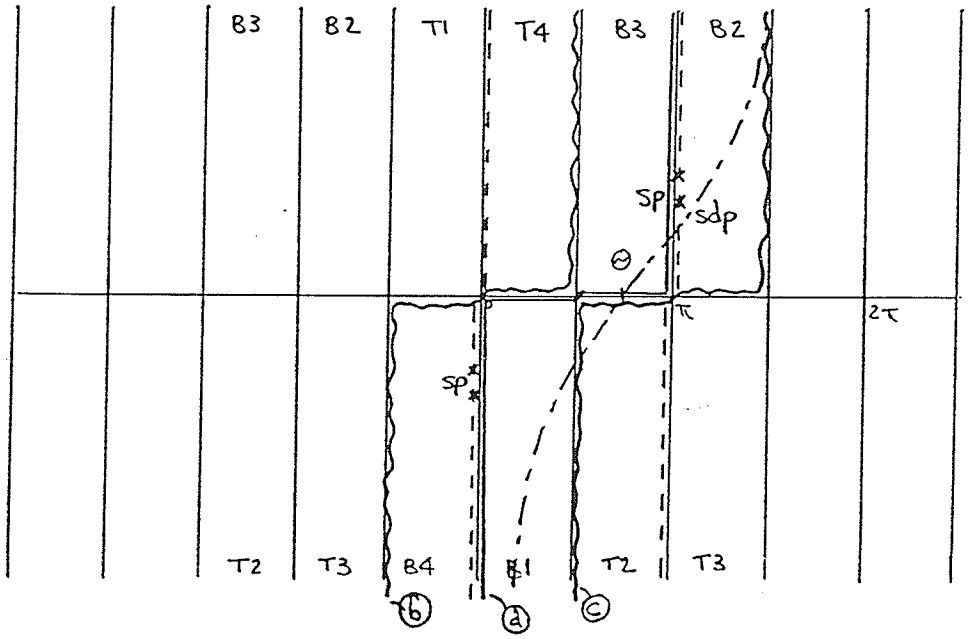

α *plane*

Figure B.01 Contour Mapping for Far Field Evaluation

Substituting $\lambda = k_o \cos\alpha$ into $E_{z_{II}}$, $d\lambda = -k_o \sin\alpha d\alpha$, and $\sqrt{k_o^2 - \lambda^2} = k_o \sin\alpha$:

$$E_{z_{II}} = \sum_{m=-\infty}^{\infty} e^{-jm\phi} \int_{-j\infty}^{\pi+j\infty} (k_o \sin\alpha)^2 B_m^e(k_o \cos\alpha) \times H_m^{(2)}(k_o \sin\alpha\rho) e^{-jk_o \cos\alpha z} k_o \sin\alpha d\alpha$$

The large argument approximation for the Hankel function [115] is substituted into the above equation:

$$E_{z_{II}} = \sum_{m=-\infty}^{\infty} e^{-jm\phi} \int_{-j\infty}^{\pi+j\infty} (k_o \sin\alpha)^2 B_m^e(k_o \cos\alpha) \times \sqrt{\frac{2}{\pi k_o \sin\alpha\rho}} e^{-j(k_o[\sin\alpha\rho + \cos\alpha z] - [m+\frac{1}{2}]\frac{\pi}{2})} k_o \sin\alpha d\alpha$$

Next, the cylindrical co-ordinates are transformed to spherical co-ordinates on the right hand side; $\rho = R\sin\theta$ and $z = R\cos\theta$. The exponential term becomes:

$$-j(k_o R[\sin\alpha \sin\theta + \cos\alpha \cos\theta] - [m + \frac{1}{2}]\frac{\pi}{2})$$

then

$$-j(k_o R\cos(\alpha - \theta) - [m + \frac{1}{2}]\frac{\pi}{2})$$

Substituting the spherical co-ordinates into the right hand side, and also moving the last $k_o \sin\alpha$, which appears next to $d\alpha$, under the square root sign yields:

$$E_{z_{II}} = \sum_{m=-\infty}^{\infty} e^{-jm\phi} \int_{-j\infty}^{\pi+j\infty} (k_o \sin\alpha)^2 B_m^e(k_o \cos\alpha) \times \sqrt{\frac{2k_o \sin\alpha}{\pi R \sin\theta}} e^{-jk_o R\cos(\alpha-\theta)} e^{j[m+\frac{1}{2}]\frac{\pi}{2}} d\alpha$$

At this point, the only approximation invoked has been the large argument approximation for the Hankel function. The steepest descent technique will now be employed.

Consider the exponential term $e^{-jk_oR\cos(\alpha-\theta)}$, α being the integration variable. R is taken to be a very large number. As α varies along the integration contour, the exponential term will change rapidly except in the region $\alpha = \theta$, the saddle point. Under the method of steepest descent [124], the exponent $-j\cos(\alpha-\theta)$ is expanded in a Taylor series about θ. Let the complex variable $\alpha - \theta = se^{j\gamma}$, $\alpha = se^{j\gamma} + \theta$, $d\alpha = e^{j\gamma}ds$. Using the first three terms of the Taylor series:

$$\begin{aligned} f(s) &= f(0) + s\frac{df}{ds}\bigg|_{s=0} + \frac{s^2}{2}\frac{d^2f}{ds^2}\bigg|_{s=0} \\ -j\cos(se^{j\gamma}) &= -j + j\frac{s^2}{2}e^{j2\gamma} \\ &= -j + j\frac{s^2}{2}(\cos 2\gamma + j\sin 2\gamma) \\ &= -\frac{s^2}{2}\sin 2\gamma - j(1 - \frac{s^2}{2}\cos 2\gamma) \end{aligned}$$

The steepest descent contour is taken along a line in the complex plane where the imaginary part of this series representation is constant. In this instance, $Im[-j\cos(se^{j\gamma})]$ is constant along the line $\gamma = +\frac{\pi}{4}$ in accordance with the direction of the contour taken above. Therefore, $-j\cos(se^{j\gamma})|_{\gamma=\frac{\pi}{4}} = -j - \frac{s^2}{2}$. This substitution for $-j\cos(\alpha-\theta)$ is applied to the equation for $E_{z_{II}}$. Additionally, all parts of the integrand except this exponential term indicated are considered *slowly varying* and are simply evaluated at $\alpha = \theta$. Therefore:

$$\begin{aligned} E_{z_{II}} &= \sum_{m=-\infty}^{\infty} e^{-jm\phi}(k_o\sin\theta)^2 B_m^e(k_o\cos\theta)\sqrt{\frac{2k_o\sin\theta}{\pi R\sin\theta}}e^{j(m+\frac{1}{2})\frac{\pi}{2}}e^{j\frac{\pi}{4}}\int_{-\infty}^{\infty} e^{k_oR(-j-\frac{s^2}{2})}ds \\ &= \sum_{m=-\infty}^{\infty} e^{-jm\phi}k_o^2\sin^2\theta B_m^e(k_o\cos\theta)\sqrt{\frac{2k_o}{\pi R}}e^{j[(m+1)\frac{\pi}{2}-k_oR]}\int_{-\infty}^{\infty} e^{-k_oR\frac{s^2}{2}}ds \end{aligned}$$

Note that the limits are now $\pm\infty$ for s, the magnitude of the complex variable.

Next consider:

$$\int_{-\infty}^{\infty} e^{-k_o R\frac{s^2}{2}} ds$$

Make the substitution $s = \sqrt{\frac{2}{k_o R}}$, $k_o^2 R\frac{s^2}{2} = t^2$, $ds = \sqrt{\frac{2}{k_o R}}dt$. the integral becomes:

$$\sqrt{\frac{2}{k_o R}}\int_{-\infty}^{\infty} e^{-t^2} dt$$

This is Laplace's integral and it has a tabulated value of $\sqrt{\pi}$. After some algebraic simplifications:

$$E_{z_{II}} = \sum_{m=-\infty}^{\infty} k_o^2 \sin^2\theta B_m^e(k_o\cos\theta)\frac{2}{R}e^{j[(m+1)\frac{\pi}{2}-m\phi-k_oR]}$$

To present this equation in terms of spherical co-ordinate field components:

$$\hat{a}_z = -\sin\theta\hat{a}_\theta, \quad \hat{a}_\theta = \frac{-\hat{a}_z}{\sin\theta}$$

Therefore:

$$E_{\theta_{II}} = -\sum_{m=-\infty}^{\infty} k_o^2 \sin\theta B_m^e(k_o\cos\theta)\frac{2}{R}e^{j[(m+1)\frac{\pi}{2}-m\phi-k_oR]}$$

Removing the terms not dependant upon m from underneath the summation, the final result is obtained:

$$E_{\theta_{II}} = \frac{-j2k_o^2\sin\theta e^{-jk_oR}}{R}\sum_{m=-\infty}^{\infty} B_m^e(k_o\cos\theta)e^{-jm(\phi-\frac{\pi}{2})}$$

Similarly:

$$H_{\theta_{II}} = \frac{-j2k_o^2\sin\theta e^{-jk_oR}}{R}\sum_{m=-\infty}^{\infty} B_m^h(k_o\cos\theta)e^{-jm(\phi-\frac{\pi}{2})}$$

For the azimuthal co-ordinates, after substitution of $\lambda = k_o\cos\alpha$ and the large argument approximation for the Hankel function:

$$E_{\phi_{II}} = \sum_{m=-\infty}^{\infty} e^{-jm\phi}\int_{-j\infty}^{\pi+j\infty}\left[B_m^h(k_o\cos\alpha)\Xi_1 - B_m^e(k_o\cos\alpha)\Xi_2\right]\times \sqrt{\frac{2}{\pi k_o\sin\alpha\rho}}e^{-jk_o(\sin\alpha\rho+\cos\alpha\rho)}k_o\sin\alpha d\alpha$$

where:

$$\begin{aligned}\Xi_1 &= \frac{j\omega\mu_o}{2}k_o\sin\alpha\left[e^{j(m-\frac{1}{2})\frac{\pi}{2}} - e^{j(m+\frac{3}{2})\frac{\pi}{2}}\right]\\ \Xi_2 &= \frac{m}{\rho}k_o\cos\alpha e^{j(m+\frac{1}{2})\frac{\pi}{2}}\end{aligned}$$

Substitute $\rho = R\sin\theta,\ z = R\cos\theta$ to obtain the exponent $-jk_oR\cos(\alpha-\theta)$. Follow the operations indicated in the development for $E_{z_{II}}$ upon $e^{-jk_oR\cos(\alpha-\theta)}$ to obtain the following:

$$E_{\phi_{II}} = \sum_{m=-\infty}^{\infty} e^{-jm\phi}\left[B_m^h(k_o\cos\theta)\Xi_3 - B_m^e(k_o\cos\theta)\Xi_4\right]\sqrt{\frac{2k_o}{\pi R}}e^{j(\frac{\pi}{4}-k_oR)}\int_{-\infty}^{\infty} e^{-k_oR\frac{s^2}{2}}ds$$

where

$$\begin{aligned}\Xi_3 &= \frac{j\omega\mu_o}{2}k_o\sin\theta\left[e^{j(m-\frac{1}{2})\frac{\pi}{2}} - e^{j(m+\frac{3}{2})\frac{\pi}{2}}\right]\\ \Xi_4 &= \frac{mk_o\cos\theta}{R\sin\theta}e^{j(m+\frac{1}{2})\frac{\pi}{2}}\end{aligned}$$

Employing Laplace's integral:

$$E_{\phi_{II}} = \sum_{m=-\infty}^{\infty}\left[B_m^h(k_o\cos\theta)\Xi_3 - B_m^e(k_o\cos\theta)\Xi_4\right]\frac{2}{R}e^{j(\frac{\pi}{4}-k_oR-m\phi)}$$

The term $\left[e^{j(m-\frac{1}{2})\frac{\pi}{2}} - e^{j(m+\frac{3}{2})\frac{\pi}{2}}\right]$, which is found in Ξ_3, may be simplified to $2e^{j(m\frac{\pi}{2}-\frac{\pi}{4})}$. The term $e^{j(m+\frac{1}{2})\frac{\pi}{2}}$, which is found in Ξ_4, may be simplified to $e^{j(m\frac{\pi}{2}+\frac{\pi}{4})}$.

A re-arrangement of terms yields:

$$\begin{aligned}E_{\phi_{II}} = \sum_{m=-\infty}^{\infty}\Big[&j\omega\mu_oB_m^h(k_o\cos\theta)k_o\sin\theta -\\ &\frac{jmk_o\cos\theta}{R\sin\theta}B_m^e(k_o\cos\theta)\Big]\frac{2}{R}e^{j(m\frac{\pi}{2}-k_oR-m\phi)}\end{aligned}$$

Removing terms which are independant of m from under the summation yields:

$$E_{\phi_{II}} = \frac{j2k_oe^{-jk_oR}}{R}\sum_{m=-\infty}^{\infty}\left[\omega\mu_oB_m^h(k_o\cos\theta)\sin\theta - \frac{mk_o\cos\theta}{R\sin\theta}B_m^e(k_o\cos\theta)\right]e^{-jm(\phi-\frac{\pi}{2})}$$

Similarly:

$$H_{\phi_{II}} = \frac{-j2k_o e^{-jk_o R}}{R} \sum_{m=-\infty}^{\infty} \left[\omega \epsilon_o B_m^e(k_o \cos\theta) \sin\theta + \frac{m k_o \cos\theta}{R \sin\theta} B_m^h(k_o \cos\theta) \right] e^{-jm(\phi - \frac{\pi}{2})}$$